



**Universidade de
Aveiro**
2021

Departamento de Engenharia de Materiais e
Cerâmica

**Patrícia Gaspar de
Oliveira**

**Fabrico de uma Plataforma de Microcápsulas de
Levedura para Regeneração do Tecido Ósseo**

**Fabrication of a Yeast Microcapsule Platform for
Bone Tissue Regeneration**



**Universidade de
Aveiro**
2021

Departamento de Engenharia de Materiais e
Cerâmica

**Patrícia Gaspar de
Oliveira**

**Fabrico de uma Plataforma de Microcápsulas de
Levedura para Regeneração do Tecido Ósseo**

**Fabrication of a Yeast Microcapsule Platform for
Bone Tissue Regeneration**

Dissertação apresentada à Universidade de Aveiro para cumprimento dos requisitos necessários à obtenção do grau de Mestre em Materiais e Dispositivos Biomédicos, realizada sob a orientação científica da Doutora Elisabete Coelho, Investigadora do Departamento de Química da Universidade de Aveiro, e do Doutor Vítor Gaspar, Investigador Júnior do Departamento de Química da Universidade de Aveiro

o júri

presidente

Professora Doutora Maria Helena Figueira Vaz Fernandes
Professora Associada, Universidade de Aveiro

arguente

Doutora Sofia Antunes Costa Lima
Investigadora Auxiliar, REQUIMTE-LAQV, Departamento de Química
Aplicada da Faculdade de Farmácia, Universidade do Porto

orientador

Doutora Elisabete Verde Martins Coelho
Investigadora Doutorada (nível 1), Universidade de Aveiro

coorientador

Doutor Vítor Manuel Abreu Gaspar
Investigador Doutorado (nível 1), Universidade de Aveiro

agradecimentos

Aos meus orientadores, Doutora Elisabete Coelho e Doutor Vítor Gaspar, agradeço por todos os ensinamentos, orientação, disponibilidade e ajuda ao longo deste ano que tiveram um impacto determinante para a realização deste trabalho.

A todos os meus colegas do grupo LAQV REQUIMTE e COMPASS, em especial à Rita Bastos, Rui Almeida e Pedro Lavrador por toda disponibilidade, partilha de conhecimentos, prontidão para o esclarecimento das minhas dúvidas e ajuda no laboratório.

Ao Doutor Ildefonso Marín pela disponibilidade, pela ajuda prestada na obtenção dos espectros RMN em estado sólido e por mostrar sempre um espírito de entreaajuda.

Agradeço também a todos os meus colegas do laboratório Tomaz pelo apoio que me deram e por garantirem a flexibilidade horária necessária para a efetivação desta dissertação.

Agradeço também a todos os meus amigos por toda a amizade, por acreditarem em mim e por, mesmo longe, me transmitirem sempre palavras de apoio e motivação durante o desenvolvimento deste trabalho.

Um especial agradecimento aos meus pais, irmã, avós e ao Ricardo pela paciência e por toda a força que me deram para continuar. Foram fundamentais para a realização e conclusão de mais uma etapa na minha vida.

Ao projeto Yeast4FoodMed (POCI-01-045-FEDER-030936) financiado por FEDER, através COMPETE2020 – Programa Operacional Competitividade e Internalização (POCI) e por FCT/MCT.

À unidade de investigação LAQV-REQUIMTE (FCT UIDB/50006/2020) pelo financiamento nacional (OE).

Muito obrigada a todos.

palavras-chave

levedura excedentária, *Saccharomyces pastorianus*, microcápsulas de leveduras, modificação química, hidrogéis fotoreticuláveis

resumo

O osso é o sistema de suporte mecânico do corpo humano, constituindo também uma proteção dos órgãos internos e um reservatório de minerais. Durante a vida, o tecido ósseo permanece em constante remodelação e tem capacidade de regenerar pequenas lesões. No entanto, em situações de fraturas ósseas críticas e/ou doenças crônicas, a regeneração óssea endógena é bastante limitada, resultando geralmente na não-união dos fragmentos ósseos, e na perda da função tecidual. Tendo em conta que o aumento da esperança média de vida, é acompanhado por um aumento da incidência de defeitos ósseos, torna-se urgente o desenvolvimento de biomateriais que possam entregar fármacos pró-osteogénicos, ou que tenham a capacidade de instruir a diferenciação de células estaminais adultas em células progenitoras do osso. Neste sentido, os hidrogéis têm sido cada vez mais explorados como plataforma tri-dimensional (3D) para suporte e entrega de células estaminais nos tecidos ósseos, devido à sua permeabilidade e semelhanças com a matriz extracelular (ECM). No entanto, devido à sua elevada permeabilidade, os hidrogéis apresentam uma fraca capacidade para entrega de fármacos. As microcápsulas de leveduras (YMCAPs) têm sido mencionadas como alternativas com potencial para encapsular, transportar e entregar agentes terapêuticos de uma forma específica e localizada. Estas microcápsulas podem ser obtidas através da reutilização das leveduras descartadas pela indústria cervejeira.

Nesta dissertação, pretende-se obter YMCAPs a partir da levedura excedentária *Saccharomyces pastorianus* e promover a sua inclusão num hidrogel 3D através de um processo de fotoreticulação. Para isso, a parede celular da levedura foi isolada por autólise térmica, obtendo-se YMCAPs_Aut (diâmetro: 3 - 7.5 µm; potencial zeta: -13.9 mV) compostas por 38 % de proteínas e 41 % de carboidratos (essencialmente mananas e β-glucanas). Nas YMCAPs_Aut, as β-glucanas são constituídas por resíduos de glucose em ligação (1→4), (1→3) e (1→6), na proporção de 50.2, 13.5 e 2.5 mol %, respetivamente. As ligações (1→4) estão divididas em (α1→4) e (β1→4). As mananas presentes nas YMCAPs_Aut são constituídas por resíduos de manose em ligação (1→2), (1→3) e (1→6), na proporção de 3, 1.4 e 0.2 mol %, respetivamente. Por extração alcalina com KOH 4M, as manoproteínas foram solubilizadas, expondo as β-glucanas na superfície da microcápsula, obtendo-se YMCAPs_4M (diâmetro: 3 - 7.5 µm; potencial zeta: 0.25 mV) compostas por 34 % de proteínas e 54 % de carboidratos (essencialmente β-glucanas). Nas YMCAPs_4M, as β-glucanas são constituídas por resíduos de glucose em ligação (1→4), (1→3) e (1→6), na proporção de 52.8, 20.0 e 2.7 mol %, respetivamente. As ligações (1→4) estão também divididas em (α1→4) e (β1→4). As YMCAPs foram posteriormente utilizadas para o desenvolvimento de uma plataforma fotoreticulável. Para isso, as YMCAPs foram modificadas quimicamente com grupos metacrilato ou com grupos norborneno. Com uma superfície quimicamente modificada, as YMCAPs foram covalentemente reticuladas com gelatina-metacrilada (GelMA), formando uma plataforma 3D multi-YMCAPs/GelMA, onde as YMCAPs atuam como unidades estruturais/funcionais, e a gelatina como estrutura 3D para adesão celular. A análise das ligações glicosídicas e espectroscopia de FTIR e RMN confirmou a síntese de YMCAPs funcionalizadas com os diferentes grupos químicos. O hidrogel híbrido fabricado foi posteriormente aplicado para a encapsulação de células estaminais humanas derivadas do tecido adiposo (hASCs). Estudos de viabilidade celular *in vitro* revelaram a biocompatibilidade das YMCAPs quando administradas diretamente ou incluídas dentro da matriz 3D contendo células estaminais.

Adicionalmente, o potencial desta plataforma híbrida hidrogel/cápsulas funcionar como um sistema de libertação de fármacos foi explorado. As YMCAPs demonstraram ser um veículo eficaz para a encapsulação de fármacos hidrofóbicos, conforme observado utilizando uma molécula fluorescente (i.e., vermelho de nilo) e com o uso de carvacrol, monoterpénóide antiosteoclastogénico, como meio de encapsulação da dexametasona.

Os resultados obtidos evidenciam a possível utilização destas plataformas híbridas como um sistema de entrega de células estaminais e moléculas bioinstrutivas para aplicação na regeneração óssea.

keywords

brewer's spent yeast, *Saccharomyces pastorianus*, yeast microcapsules, chemical modification, photocrosslinkable hydrogels

abstract

Bone is considered a mechanical support system of the human body, which imparts protection for internal organs, being also a reservoir of minerals. During life, bone tissue remains in constant remodelling and has the capacity to regenerate small lesions. Nevertheless, in situations of critical bone fractures and/or chronic diseases, endogenous bone regeneration is limited and generally results in non-union of the fracture fragments and in loss of tissue function. Bearing in mind that the improvement in life-expectancy is accompanied with a higher incidence of bone defects, it is urgent the development of biomaterials, which can deliver pro-osteogenic drugs or be able to instruct the differentiation of adult stem cells into progenitor bone cells. Given this, hydrogels have been increasingly explored as a tri-dimensional (3D) platform for support and delivery of stem cells to bone tissues, due to their permeability and similarities to the extracellular matrix (ECM). However, as a result of their high permeability, hydrogels have a low capacity for drug delivery. Yeast microcapsules (YMCAPs) have been mentioned as alternatives with the potential to encapsulate, transport and deliver therapeutic agents in a specific and localized manner. These microcapsules can be obtained through the reuse of spent yeasts discarded as a by-product of brewing industry.

In this dissertation, it was aimed to obtain YMCAPs from the brewer's spent yeast *Saccharomyces pastorianus* and promote their inclusion into a 3D hydrogel, through a photocrosslinking process. For that, the yeast's cell wall was isolated through thermal autolysis, obtaining YMCAP_Aut (diameter: 3 - 7.5 μm ; zeta potential: -13.9 mV) composed of 38 % of proteins and 41 % of carbohydrates (essentially, mannans and β -glucans). The β -glucans present in YMCAPs_Aut are constituted by glucose residues with (1 \rightarrow 4), (1 \rightarrow 3) and (1 \rightarrow 6) linkages in a proportion of 50.2, 13.5 and 2.5 mol %, respectively. The (1 \rightarrow 4) linkages are divided in (α 1 \rightarrow 4) and (β 1 \rightarrow 4). The mannans present in YMCAPs_Aut are constituted by mannose residues with (1 \rightarrow 2), (1 \rightarrow 3) and (1 \rightarrow 6) linkages in a proportion of 3, 1.4 and 0.2 mol %, respectively. Through alkaline extraction using 4M KOH, the mannoproteins were solubilized and β -glucans were exposed in the microcapsule surface, obtaining YMCAPs_4M (diameter: 3 - 7.5 μm ; zeta potential: 0.25 mV) composed of 34 % proteins and 54 % carbohydrates (essentially, β -glucans). The β -glucans present in YMCAPs_4M are constituted by glucose residues with (1 \rightarrow 4), (1 \rightarrow 3) and (1 \rightarrow 6) linkages in a proportion of 52.8, 20.0 and 2.7 mol %, respectively. The (1 \rightarrow 4) linkages are also divided in (α 1 \rightarrow 4) and (β 1 \rightarrow 4). YMCAPs were subsequently used for the development of a photocrosslinkable multi-YMCAPs platform. For this, YMCAPs were chemically modified with methacrylate groups or with norbornene groups. With a chemically modified surface, YMCAPs were covalently crosslinked to methacrylated gelatin (GelMA), forming a 3D multi-YMCAPs/GelMA platform with YMCAPs acting as structural/functional units, and with gelatin acting as a 3D structure for cell adhesion. Glycosidic analysis and FTIR and NMR spectroscopic confirmed the successful synthesis of functionalized YMCAPs with the different chemical groups. After, the fabricated hybrid hydrogel was applied to human adipose stem cells (hASCs) encapsulation. *In vitro* viability studies revealed the biocompatibility of YMCAPs when directly administered or included within the 3D matrix containing stem cells.

Moreover, the potential of this hybrid hydrogel/YMCAPs platform to act as drug delivery system was explored. YMCAPs demonstrated to be an effective vehicle for hydrophobic drugs encapsulation, as observed with the use of a fluorescent molecule (e.g., Nile red) and with the use of carvacrol, antiosteoclastogenic monoterpene, as a medium of encapsulation of dexamethasone.

Overall, the results highlight the possible use of these hybrid platform as a delivery system of stem cells and bioinstructive molecules for bone regeneration application.

Contents

List of figures	iii
List of tables	iv
1. Introduction.....	- 7 -
1.1. Bone tissue.....	- 8 -
1.1.1. Bone repair	- 9 -
1.2. Current strategies in bone tissue engineering	- 11 -
1.2.1. Hydrogels.....	- 13 -
1.2.2. Yeasts of the genus <i>Saccharomyces</i>	- 18 -
1.3. Glucans with reported bone tissue applications.....	- 24 -
1.3.1. Structure-activity relationship.....	- 26 -
2. Aims.....	- 35 -
2.1. Aims	- 36 -
3. Materials and Methods	- 37 -
3.1. Materials	- 38 -
3.2. Yeast microcapsules (YMCAPs) isolation, purification and characterization	- 38 -
3.2.1. YMCAPs isolation.....	- 38 -
3.2.2. YMCAPs characterization.....	- 40 -
3.3. YMCAPs surface chemical modification and characterization.....	- 46 -
3.3.1. Chemical synthesis of modified YMCAPs with carbic anhydride.....	- 46 -
3.3.2. Chemical synthesis of modified YMCAPs with methacrylic anhydride.....	- 46 -
3.3.3. Characterization of the YMCAPs chemical modification	- 47 -
3.4. Multi-YMCAPs/GelMA photocrosslinkable platform generation and characterization.....	- 48 -
3.4.1. Multi-YMCAPs/GelMA platform formulation	- 48 -
3.4.2. Multi-YMCAPs/GelMA platform characterization	- 50 -
3.5. Cell-laden multi-YMCAPs/GelMA platform.....	- 51 -
3.6. <i>In vitro</i> studies.....	- 51 -
3.6.1. AlamarBlue™ Assay – Cytotoxicity evaluation	- 51 -
3.7. YMCAPs drug encapsulation	- 52 -
3.7.1. Drug encapsulation and encapsulation efficiency	- 52 -
3.7.2. Drug release profile	- 54 -
3.8. Data analysis	- 54 -
4. Results and Discussion.....	- 55 -
4.1. YMCAPs characterization	- 56 -

4.1.1.	Morphology, particle size and zeta potential	- 56 -
4.1.2.	Structural analysis.....	- 57 -
4.2.	YMCAPs_Aut modification with norbornene and methacrylic moieties	- 64 -
4.2.1.	Fourier-transformed infrared spectroscopy	- 65 -
4.2.2.	Solid-state nuclear magnetic resonance spectroscopy	- 67 -
4.2.3.	Glycosidic linkage analysis	- 69 -
4.3.	Multi-YMCAPs/GelMA photocrosslinkable hybrid hydrogel platform.....	- 71 -
4.3.1.	Multi-YMCAPs/GelMA platform physical characterization	- 71 -
4.3.2.	Cytotoxicity evaluation	- 76 -
4.4.	Drug encapsulation and drug release profile.....	- 78 -
5.	Conclusion and Future Perspectives	- 82 -
5.1.	Conclusion and future perspectives.....	- 83 -
6.	References	- 85 -

List of figures

Figure 1: Bones' structural organization. (Adapted from Lavrador et al., 2018) ⁵	- 8 -
Figure 2: Schematic representation of normal fracture healing phases – inflammation, repair, and remodelling. (Adapted from Muire et al., 2020) ¹⁷	- 11 -
Figure 3: A) Microscope image of BM-MSCs-loaded GelMA. B) Histomorphometrical analysis indicating new bone volume (%); C) Van Gieson's Picro–Fuchsin staining with visible new bone formation (NB) and osteoid marker with arrows - scale bar = 200 μ m. (Adapted from Zhao et al., 2016) ⁴⁰	- 15 -
Figure 4: A) Representation of the chemical crosslinking of GelMA with photo-crosslinkable OGP under UV irradiation. B) ALP staining images (7 days after stimulation of osteogenic differentiation) and Alizarin red staining images (21 days after stimulation of osteogenic differentiation); C) Reconstruction of the defect site of distal femoral (μ -CT); D) BMD and BV/TV quantified by μ -CT. * $p < 0.05$, *** $p < 0.001$ compared with GelMA group, ### $p < 0.001$ compared with the GelMA/OGP group. (Adapted from Qiao et al., 2020) ³⁴	- 16 -
Figure 5: Representation of the multivalent crosslinking to forming a polymerized methacrylate with clusters of acrylated biophosphate (Ac-BP) plus Mg^{2+} nanoparticles (Ac-BP-Mg NPs). (Adapted from Zhang et al., 2017) ⁴⁹	- 18 -
Figure 6: Representation of yeast cell wall structure. (Adapted from Cabib and Arroyo 2013) ⁶⁸	- 21 -
Figure 7: Schematic representation of YMCAPs isolation procedure.	- 38 -
Figure 8: Schematic representation of the reduction of D-glucose to its corresponding D-glucitol, followed by an acetylation step with the production of D-glucitol hexaacetate that could be analysed by gas-phase chromatography.....	- 41 -
Figure 9: Representation of the preparation of (β 1 \rightarrow 3)-linked glucan partially methylated alditol acetates. ...	- 43 -
Figure 10: Schematic representation of glycine derivatization, including butylation of the carboxylic acid and acylation of the amine group.	- 45 -
Figure 11: Schematic representation of the chemical route used to obtain YMCAPs_Aut with incorporated norbornene groups.....	- 46 -
Figure 12: Schematic representation of the chemical route used to obtain YMCAPs_Aut with incorporated methacrylate groups.	- 46 -
Figure 13: Schematic representation of GelMA-c-YMCAPs_Aut hybrid platform generation.	- 49 -
Figure 14: The chemical principle of AlamarBlue™ cell viability assay.....	- 52 -
Figure 15: Widefield fluorescence microscopy micrographs of autofluorescent YMCAPs_Aut (A and B) and YMCAPs_4M (C and D).	- 56 -
Figure 16: Dispersion of YMCAPs in PBS. A) YMCAPs_Aut; B) YMCAPs_4M.	- 65 -
Figure 17: ATR-FTIR spectra of YMCAPs_Aut isolated from <i>Saccharomyces pastorianus</i> pre- and post-modification with norbornene and methacrylate groups in the 4000-400 cm^{-1} range. The red wavenumbers are the peaks assigned to the chemical modifications in YMCAPs.	- 66 -
Figure 18: Solid state CP-MAS NMR spectrum of A) unmodified and norbornene modified YMCAPs_Aut and respective subtractive spectrum; B) unmodified and methacrylated YMCAPs_Aut and respective subtractive spectrum.....	- 68 -
Figure 19: GelMA hybrid hydrogels prepared with 1 and 5 % (w/v) of YMCAPs_Aut, respectively.	- 71 -

Figure 20: Water content ratio of GelMA/YMCAPs_Aut and GelMA-c-YMCAPs_Aut. Data is represented as mean \pm standard deviation (n=3). **p* < 0.05..... - 72 -

Figure 21: Swelling ratio of GelMA/YMCAPs_Aut and GelMA-c-YMCAPs_Aut after immersion in PBS, at 37°C for 4, 24 and 48 h. Data is represented as mean \pm standard deviation (n=3). - 73 -

Figure 22: Mass loss profile of GelMA/YMCAPs_Aut and GelMA-c-YMCAPs_Aut immersed in PBS at 37°C for 28 days. Data is represented as mean \pm standard deviation (n=3). - 74 -

Figure 23: Compressive stress-strain curves and Young’s modulus representation of GelMA/YMCAPs_Aut and GelMA-c-YMCAPs_Aut. Data is represented as mean \pm standard deviation (n=3). **p* < 0.05 - 76 -

Figure 24: Stand-alone YMCAPs_Aut effect in hASCs cell viability. The cell viability is normalized with respect to the control (0 μ g/mL, 100 %). Data is represented as mean \pm standard deviation (n=4). **p* < 0.05 compare to the control group. - 77 -

Figure 25: hASCs cell viability within 3D multi-YMCAPs_Aut/GelMA platform constructs. Data is represented as mean \pm standard deviation (n=4). **p* < 0.05 - 78 -

Figure 26: Chemical structure of encapsulated drugs and respective molar mass and Ko/w values. - 78 -

Figure 27: Freeze-dried YMCAPs_Aut before (A) and after (B) Nile red encapsulation. Microscope fluorescence images of YMCAPs_Aut with encapsulated Nile red (C). - 79 -

Figure 28: A) Nile red-loaded YMCAPs_Aut and GelMA-c-YMCAPs_Aut_5% *in vitro* release profile, expressed as cumulative release (%). B) Time related differences in PBS colour solution associated to the Nile red release. Data is represented as mean \pm standard deviation (n=3). - 81 -

List of tables

Table 1: Yeast cell wall polysaccharides - 19 -

Table 2: Bone regeneration and bone-related disorders effects of β -glucans..... - 28 -

Table 3: Principal activity of β -glucans in bone regeneration and bone related disorders..... - 34 -

Table 4: Data from amino acids calibration curves (amino acid concentration, slope, R² and limit of quantification/detection). - 45 -

Table 5: Experimental conditions used for drug encapsulation in YMCAPs_Aut. - 53 -

Table 6: Carbohydrate analysis and yields from autolysis and 4M KOH extraction. - 57 -

Table 7: Glycosidic linkages composition (mol %) of the different fractions obtained during the YMCAPs isolation. - 60 -

Table 8: Protein content in YMCAPs and solubilized material determined based on % N and its conversion using the Kjeldahal factor (6.25). - 62 -

Table 9: Amino acids profile of YMCAPs_Aut and YMCAPs_4M. - 64 -

Table 10: Extension of chemical functionalization of YMCAPs_Aut with norbornene and methacrylic groups.- 69 -

Table 11: Glycosidic linkages composition (mol % and mg/g) of the different YMCAPs_Aut modified fractions. - 70 -

List of abbreviations

3D - tri-dimensional
Ala - alanine
ALP - alkaline phosphate
Asp - aspartic acid
ATR-FTIR - attenuated total reflectance Fourier transformed infrared
Bax - B-cell lymphoma 2 associated X protein
Bcl-2 - B-cell lymphoma 2
BD - branching degree
BMD - bone mineral density
BM-MSCs - bone marrow derived mesenchymal stem cells
BMP - bone morphogenic protein
BSY - brewer's spent yeast
BV/TV - bone tissue volume per tissue volume rate
Col1 - type I collagen
CP - cross polarization
CP-MAS - cross polarization magic angle spinning
CR3 - complement receptor 3
CS - chitosan
dPBS - Dulbecco's phosphate-buffered saline
DS - degree of substitution
ECM - extracellular matrix
EDC - 1-ethyl-3-(3-dimethylaminopropyl)carbodiimide hydrochloride
EE - encapsulation efficiency
ERK - extracellular-signal-regulated kinase
FDA - Food and Drug Administration
FGF-2 - fibroblast growth factor 2
GC-FID - gas-phase chromatography with flame ionization detector
GC-MS - gas chromatography couple to mass spectrometry
GelMA - methacrylated gelatin
Glc - glucose
GlcNAc - N-acetylglucosamine
Glu - glutamic acid
Gly - glycine
HA - hydroxyapatite
hASCs - human adipose stem cells
IFN- γ - interferon gamma
Ig - immunoglobulin
IGF - insulin-like growth factors
IL - interleukin
Ile - isoleucine
JNK - c-Jun N-terminal kinase
LC3B-I/LC3B-II - microtubule-associated protein 1/2 light chain 3B
Leu - leucine
Lys - lysine
Man - mannose
MAPK - mitogen-activated protein kinase
MC3T3-E1 - murine pre-osteoblasts
M-CSF - macrophage-colony stimulating factor
MG-63 - human osteosarcoma cell line
MMP - metalloproteinase
MSCs - mesenchymal stem cells

multiCP - multiple cross polarization
MW - molecular weight
NFATc1 - nuclear factor of activated T cell cytoplasmic 1
OCN - osteocalcin
OGP - osteogenic growth peptide
OH - hydroxyl group
OPG - osteoprotegerin
OPN - osteopontin
PAMPs - pathogen-associated molecular patterns
PBS - phosphate-buffered saline
PDGF-BB - platelet-derived growth factor with two B subunits
Phe - phenylalanine
PMAAs - partially methylated alditol acetates
Pro - proline
RANKL - receptor activator of nuclear factor kappa-B ligand
RGD - arginine-glycine-aspartic acid sequence
RT - room temperature
Runx2 - runt-related transcription factor 2
SANFH - steroid-induced avascular necrosis of the femoral head
ssNMR - solid-state nuclear magnetic resonance
TGF- β - transforming growth factor beta
Th17 - T helper 17 cells
TLR - toll-like receptor
TNF- α - tumor necrosis factor alpha
UV - ultraviolet
Val - valine
VEGF - vascular endothelial growth factor
YMCAPs - yeast microcapsules

1. Introduction

1.1. Bone tissue

Bone is a constituent of musculoskeletal system that act as a support structure and protective system for organs and bone marrow due to its rigidity and hardness¹. Physiologically, bone is involved in calcium metabolism², mineral homeostasis^{1,3}, acid-base balance⁴, and haematopoiesis^{1,3}. Moreover, it stores growth factors, cytokines, adipose tissue, and several essential ions such as calcium, phosphorus, magnesium, potassium, and zinc^{1,2}.

Bones are composite materials, with both an inorganic matrix (50-70 %) - containing calcium phosphates in the form of hydroxyapatite crystals (HA) that confers rigidity and strength to bones^{2,5} - and organic components (20-40 %) - essentially type I collagen (Col1) responsible for bone elasticity⁵. Bones are also composed of water (5-10 %), lipids (1-5 %) and cells (~10 %)^{1,5}.

Based on its macrostructural organization, bone tissue can be divided into cortical bone and trabecular bone (Figure 1). The cortical bone is a dense osseous tissue responsible for bone mechanical rigidity, with a porosity around 3-12 %⁶. It is found on the outer surface of the bone metaphysis and diaphysis, corresponding to 80 % of its total mass⁵. Collagen macromolecules and HA crystals are arranged in collagen fibers, which in turn, are organized in parallel layers with a thickness of 3-7 μm , termed lamellae^{6,7}. The bone lamellae are organized into concentric rings with a central channel (Havers canal) containing nerves and blood vessels, forming the functional unit of cortical bone - osteon or Havers System^{5,6}. The Haversian channels connect the medullary cavity and the external surface of the bone through the Volkmann channels. In the spaces between the bone lamellae, are located osteocytes that establish communication with each other through canaliculi with approximately 100-300 nm⁵. The remaining 20 % of osseous tissue correspond to trabecular bone mainly located at the ends of long bones (epiphyses) and predominantly associated with metabolic functions¹. Trabecular bone, also called cancellous bone, has a sponge-like morphology with high porosity (50-90 %) that consists of a network of bone trabeculae with connected lamellae whose cavities are filled with bone marrow^{1,5}.

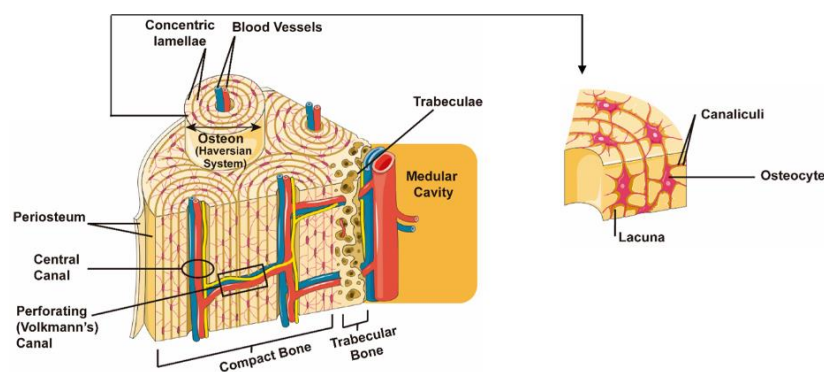


Figure 1: Bones' structural organization. (Adapted from Lavrador et al., 2018)⁵

Regarding cellular population of bone tissue, five distinctive cells may be pointed out: osteoprogenitor cells, osteoblasts, osteoclasts, osteocytes and bone lining cells. Osteoprogenitor cells, also called mesenchymal stem cells (MSCs) or stromal cells, are undifferentiated cells that may undergo osteoblastic differentiation – during the bone formation and remodelling⁷. Osteoblasts represents 4-6 % of the bone cell population¹, and are responsible for bone formation, more specifically for the synthesis of bone matrix organic and inorganic components^{7,8}. Osteocytes are osteoblasts-derived cells, located in bone lamellae lacunae that represent 90-95 % of the bone cell population¹. These cells are metabolic active, playing a key role in bone matrix maintenance⁷. Additionally, they are sensitive to mechanical stimuli, being sensitive to microfractures, an important feature to stimulate the bone remodelling process¹. Osteoclasts are multinuclear large cell (20-100 μm), involved in the reabsorption of organic and inorganic bone matrix with the formation of Howship lacunae in the bone tissue^{7,8}. Ultimately, bone lining cells are inactive cells that might be involved in calcium homeostasis⁹.

Bone is a dynamic organ that undergoes remodelling, a process that combines bone resorption and bone formation. The balance between bone resorption and formation enables: (i) the adaptation of bone to the mechanical stresses applied on a daily basis, (ii) the maintenance of bone mechanical properties, (iii) bone repair and (iv) mineral homeostasis¹⁰. Furthermore, bone has an intrinsic capacity to regenerate and generally heal micro and macrofractures without further complications². Nevertheless, with the increase in average life expectancy over time, there has been a higher incidence of bone pathologies that negatively affect the function of bone tissue and decrease bone quality, compromising the patient's quality of life⁵. Some of these pathologies are a consequence of an imbalance in bone remodelling process resulting in pathological conditions such as osteoporosis - which is associated with an increase in osteoclast activity accompanied by a decrease of osteoblast recruitment^{11,12} - and osteopetrosis, characterized by an abnormal increase in bone density that is related to the osteoclasts' inability to promote bone resorption^{11,13}. Bone disorders increase the risk of fracture, as in some high-energy trauma critical bone injuries, the intrinsic capacity of bone self-healing might be surpassed, subsequently resulting in non-united fractured fragments¹.

1.1.1. Bone repair

Bone repair is a complex physiological process for fracture healing composed of three distinct phases – inflammation, repair, and remodelling – that involves the simultaneous activity of immune and bone cells (Figure 2). Immediately after bone fracture, an inflammatory response is initiated

and comprises the development of a hematoma and the recruitment to the injury area of diverse immune cells including platelets, neutrophils, and M1 macrophages¹⁴. During the early stage of fracture healing, the hematoma environment and the tight action of immune cells results in fibrin thrombus formation, necrotic tissues clearance and inflammatory cytokines release (e.g., interleukin 1 (IL-1), IL-6, tumor necrosis factor alpha (TNF- α) and interferon gamma (IFN- γ)), which potentiate the proinflammatory environment¹⁴⁻¹⁷. The later stage of the inflammatory phase corresponds to the inflammation resolution where lymphocytes B modulate the balance between proinflammatory and anti-inflammatory signals by downregulation of proinflammatory cytokines release and increasing the production of IL-10^{14,17}. Regulatory T cells and T helper 17 cells (Th17) secrete IL-4 and IL-17, respectively, that have an anti-inflammatory action and stimulate osteoblastogenesis^{15,17}. Furthermore, M1 macrophages are polarized to M2 macrophages, a cell type that release anti-inflammatory cytokines (IL-4, IL-10 and IL-13) and growth factors - such as bone morphogenic proteins (BMP), transforming growth factor beta (TGF- β), fibroblast growth factor 2 (FGF-2) and vascular endothelial growth factor (VEGF) - that not only promote angiogenesis, but also the recruitment and differentiation of bone marrow MSCs (BM-MSCs) in chondrocytes and osteoblasts which prompt endochondral bone regeneration¹⁴⁻¹⁶. Lymphocytes T also increase receptor activator of nuclear factor kappa-B ligand (RANKL) and consequently, regulate osteoclastic activity, promoting the reabsorption of fibrin thrombus^{14,17}. With this microenvironment, the conditions for the repair phase are created. Hereafter, MSCs-derived chondrocytes are responsible for the formation of fibrocartilaginous callus, known as soft callus, that allows the joining of bone fragments^{2,14-17}. The soft callus formation is followed by chondrocytes hypertrophy and apoptosis resulting in callus mineralization, cartilage vascularization and osteogenesis initiation, where functional osteoblasts produce bone matrix leading to soft callus replacement by new woven bone (hard callus)¹⁴⁻¹⁷. The late stage of fracture healing (remodeling phase) is characterized by the replacement of the hard callus by lamellar bone with the medullary cavity in the center, and involves the joint action of osteoclasts (bone resorption) and osteoblasts (bone formation)^{2,14,16}. From here on, Th17 cells secrete IL-17, an interleukin that amplifies the expression of RANKL by bone lining cells stimulating osteoclastogenesis, thus activating osteoclasts to initiate resorption^{14,18}. Finally, with callus resorption, T and B lymphocytes are recruited to the remodeling site where the production of osteoprotegerin (OPG) - negative regulator of osteoclast activity -, and osteoblasts activity leads to new bone formation in the reabsorbed areas, restoring the bone architecture as well as its function^{14,17}.

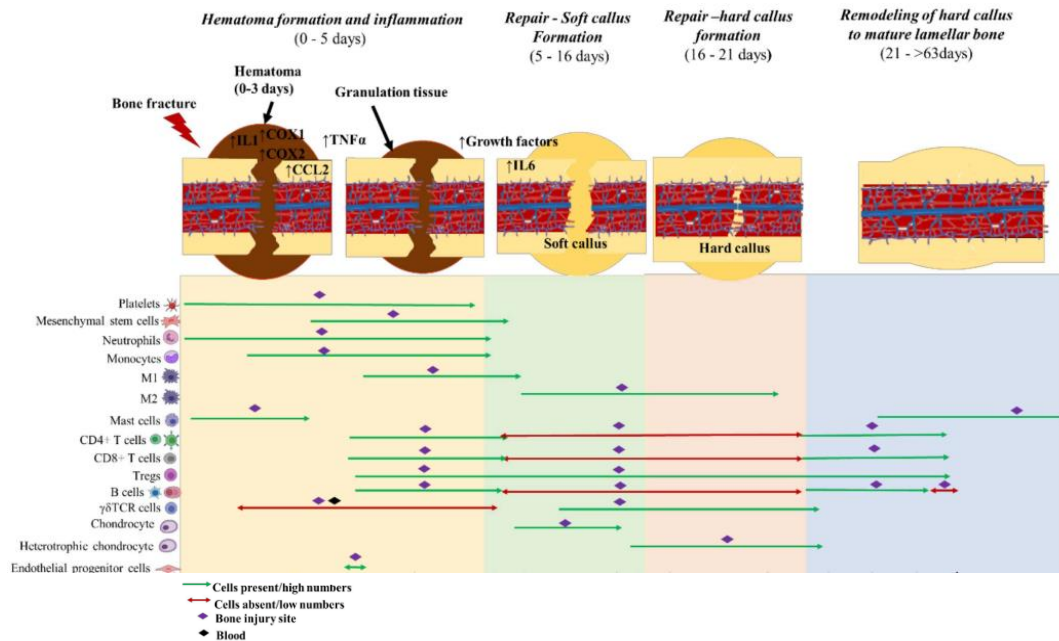


Figure 2: Schematic representation of normal fracture healing phases – inflammation, repair, and remodelling. (Adapted from Muire et al., 2020)¹⁷

1.2. Current strategies in bone tissue engineering

In addition to internal and external orthopaedic fixation of fractures, other methods for the reconstruction of bone defects have also been applied at a clinical level. These include bone grafts from the patient (autologous bone graft), from another individual of the same species (allografts) or from a different species (xenograft)¹. Due to the several limitations of these grafts including the shortage of donors, donor site morbidity and risk of disease transmission¹, intense research in regenerative medicine has been being done to enhance the repair and regeneration of bone tissues. With the intention to overcome the limitations of these biological-derived grafts, several bone-graft substitutes have been developed for bone tissue engineering applications, since the early 1960s¹⁹. The increase in bone biology knowledge and the developments in materials science, were accompanied with a progression in biomaterials design. In first generation of biomaterials, the materials were meant to be bioinert and thus, they did not induce a biological response and had a minimal interaction with the surrounding tissues. Contrarily, the second generation was characterized by the intentionally development of bioactive materials that were able to interact with the surrounding tissues and consequently stimulate tissue regeneration. The third generation of biomaterials are conceived with the aim to modulate the cellular behaviour through the

combination of materials with instructive molecules (drugs and/or biological compounds - e.g., growth factors) that improve the materials biological performance^{19,20}.

Scaffolds are one of the main components of tissue engineering, being temporary structures that possess an adequate architecture and provide a favourable environment to support new bone tissue formation. An ideal scaffold should fulfil specific requirements, which include: i) biocompatibility: support cell activity and induce a therapeutic responses without eliciting any toxic effects and adverse immune responses^{21,22}; ii) porosity (around 100 to 400 μm in diameter): provides space for cellular growth and proliferation, allows oxygen and nutrients supply and enables vascularization^{21,22}; iii) suitable mechanical properties: matching the bone tissue mechanical properties (e.g., strength and stiffness) for an adequate load transference and stress shielding avoidance^{21,22}; and iv) biodegradability: controlled degradation in a timescale matching to the new tissue formation^{21,22}.

The widely used biomaterials in the bone biomedical field include metals, ceramics, polymers and composite materials. The high mechanical performance of metals (e.g., titanium and its alloys) led to their exploration for bone tissue engineering²². However, the use of these materials in the biomedical field is limited by the toxic effects raised from the release of metallic ions and wear-induced particles debris, which consequently leads to adverse inflammatory responses²¹⁻²³. Ceramics may be inert or bioactive. The bioactive ceramics, such as calcium phosphates, HA and bioactive glass are of specific interest due to their capacity to form a bone-like apatite layer in their surface (bioactivity) when in contact with the biological environment, establishing a direct bond with bone tissue²³. Despite possessing an adequate Young's modulus for bone regeneration, ceramics application is limited by their low fracture toughness⁸ and brittleness²⁴. Natural polymers (e.g., alginate, collagen, etc) are known for their desirable biological properties, biodegradability and minimal immunological activity. Nonetheless, given their natural source, concerns arise from their composition variability. This limitation combined with their poor mechanical properties also impose a limitation for their application in bone tissue engineering^{21,23}. As an alternative, synthetic polymers (e.g., polycaprolactone, poly(glycolic acid), etc) have been under the scope for their ability to support the mechanical demands of load-bearing applications. However, their general lack of biological activity and slow hydrolytic degradation still needs to be surmounted²³. Composite materials used for bone regeneration generally comprises the combination of polymers (which confers elasticity and biocompatibility to the scaffold) and ceramic materials (which confers strength and stiffness to the scaffold), with the intention to take advantage of the beneficial properties of each material and, at the same time, overcoming their intrinsic limitations²¹.

Researchers have been continuously developing scaffolds to promote bone regeneration, however, an ideal scaffold combining appropriate biocompatibility, biological activity and mechanical properties is yet to be a reality²¹, and that is why drawing up strategies to improve the scaffolds stimulus activity of the bone repair is still a fundamental issue in medicine.

As mentioned, the later biomaterials generation is based on the creation of multifunctional scaffolds that not only act as structural support for bone tissue formation, but also as a vehicle for bioinstructive molecules delivery (including therapeutic drugs), to promote tissue healing and regeneration²⁵. A plethora of delivery systems have been studied for these applications and includes nanoparticles, liposomes, coatings and porous scaffolds and sponges²⁶. Among the different porous scaffolds already developed to act as drug delivery systems, hydrogels, due to their physical and biological properties, have shown interesting results for their application as osteogenic-inducing drugs loading system and consequent bone repair and regeneration^{27,28}. Furthermore, bioinspired and biomimetic YMCAPs delivery systems have been recently explored for a specific transport and delivery of bioactive molecules (DNA, siRNA, proteins, and drugs) to target regions, with a maximized therapeutic effect and reduced undesirable effects²⁹.

1.2.1. Hydrogels

Hydrogels are polymeric scaffolds that result from the crosslinking of hydrophilic/hydrophobic or amphiphilic biomaterials (e.g., polymeric chains, proteins, peptides, etc), resulting in the assembly of a 3D porous network rich in water. Generally, the significant hydrophilicity confers to the hydrogel the capability of water absorption, and consequently swelling, which in combination with its high permeability, allows the diffusion of nutrients, biomolecules and oxygen^{27,30,31}. At the same time, these appealing 3D scaffolds, can be assembled from bioactive materials, constituting an important supporting structure and analogue of the native ECM. Such, is considered a fundamental characteristic for cell adhesion, spreading and proliferation, consequently favouring new tissue formation^{27,30,31}. In fact, to data bioactive and biocompatible natural polymers (e.g., collagen, gelatin, chitosan, alginate, hyaluronic acid), have been favoured for the assembly of such platforms as opposite to the rather more inert synthetic alternatives (e.g., polycaprolactone, polylactic acid and poly lactic-co-glycolic acid). This might be explained by the similarities to the natural ECM which turn them highly biocompatible and bioactive, with low cytotoxicity and capable of recreating the osteogenic environment. As a result, the cell adhesion is facilitated, thus, potentiating the integration with surrounding tissues and reducing possible adverse inflammatory responses^{27,28,31}. All these characteristics are considered vital requirements for hydrogels

applications in the biomedical field, representing a promising strategy to be applied in bone regeneration.

Gelatin is widely used in bone tissue engineering since it is a hydrolytic degradation product of collagen, a major organic component of bone, having an adequate similarity to the bone ECM. Furthermore, the preparation methodology of gelatin from collagen enables the retention of proteolytic moieties and of several arginine-glycine-aspartic acid (RGD) sequences in the gelatin peptides backbone, which is essential for cell functions (adhesion, proliferation, and differentiation). The usefulness of gelatin with comparison to collagen is related to the higher peptide solubility and lower antigenicity, achieved through the heat denaturation³²⁻³⁴.

The hydrogels can be physically crosslinked, with the entanglement of the polymeric chains promoted through hydrogen bonding, electrostatic interactions, van der Waals interactions or hydrophobic interactions^{35,36}. The absence of covalent interactions makes the hydrogels reversible under certain external stimulus (e.g., pH, temperature, and ionic strength). On the other hand, in chemically crosslinking hydrogels, the diverse polymeric chains are covalently bonded, providing supplementary gel stability and mechanical properties³⁵⁻³⁷. For instance, although gelatin is capable of jellifying at low temperatures by physical crosslinking, this polymer is generally used in biomedical application after its chemical modification. Within the various possible chemical reactions, the ones with methacrylic and bio-orthogonal click reaction (e.g., norbornene) have been increasingly used for the synthesis of these hydrogels^{32,33}.

Besides being used as a 3D architecture templates for tissue repair and regeneration, the structural features of the hydrogels also afford them the potential to encapsulate biologics³⁸. Together with a localized delivery of the payloads, the use of hydrogels as a delivery system confers protection against degradation and immune system reactions to the loaded biomolecules/cells, enhancing their therapeutic effect³⁹. For instance, the entrapment of MSCs within the hydrogel is a promising approach in bone tissue engineering. Having bone defects as target, the cell delivery in a relevant timescale of bone regeneration, improves the desired cell function, supporting the MSCs proliferation and osteoblastogenic differentiation, which further enhances tissue restoration^{40,41}. Moreover, the hydrogels have the possibility to be directly injected into the defect site. Indeed, injectable hydrogels are gaining highly applicability to bone tissue engineering as a minimally invasive method for biological cargos delivery, with increase residence time of the cargos in the pathological site and moldability to the bone defect^{31,42,43}. The use of hydrogels protects the cells from the mechanical shear forces during the injection process that usually affects cell viability and function⁴⁰. In a rabbit femoral defect, the administration of BM-MSCs inside methacrylate gelatin

(GelMA) microspheres (165 μm), with a methacrylation degree of 75 %, result in an enhancement of bone formation, which is possible fundamentally due to the hydrogel features that confer protection to the encapsulated cells, together with stimulation of BM-MSCs proliferation, migration and osteogenic differentiation. This formulation not only improves bone architecture through the reduction of unmineralized osteoid, but also increases new bone volume at the femur (Figure 3), which is further enhanced with the synergetic effect of BMP-2 when simultaneously combined with BM-MSCs within the hydrogel mesh⁴⁰.

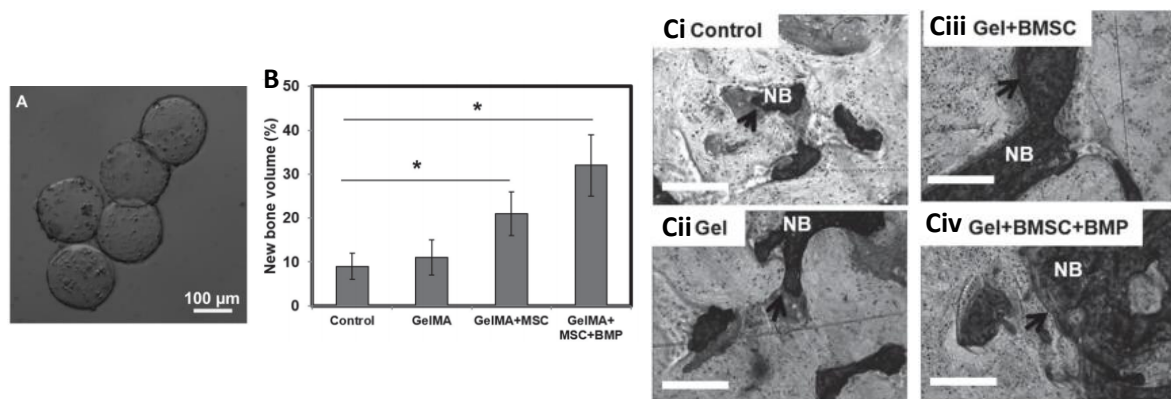


Figure 3: A) Microscope image of BM-MSCs-loaded GelMA. B) Histomorphometrical analysis indicating new bone volume (%); C) Van Gieson's Picro-Fuchsin staining with visible new bone formation (NB) and osteoid marker with arrows - scale bar = 200 μm . (Adapted from Zhao et al., 2016)⁴⁰

Furthermore, hydrogels are suitable for drug and protein local delivery, an approach that has shown evident osteogenic stimulation, both *in vitro*, with increase of osteogenic marker expression³⁴, and *in vivo*, with trabecular structure enhancement³⁴. However, bulk hydrogels generally suffer from a rapid release of the carrying molecules⁴⁴ and, therefore, some approaches as crosslinking degree adjustment and chemical crosslinking of the biomolecules may be interesting to obtain a slower and continuous drug release rate^{28,45}. In a recent study, photocrosslinkable osteogenic growth peptide (OGP) was incorporated in the GelMA hydrogel solution prior to ultraviolet (UV) irradiation, thus allowing the co-crosslinking of the peptide and the polymer chains during the hydrogel formation, obtaining GelMA-c-OGP (Figure 4A)³⁴. This system decreased the protein release kinetics while maintaining the osteogenic efficacy of the native molecule. The peptide sustained release accelerated bone formation when compared to GelMA and GelMA/OGP, which was evidenced by matrix mineralization associated with an increase in calcium content and in the expression of osteogenic-related markers (Figure 4B), namely alkaline

phosphate (ALP), BMP-2, osteocalcin (OCN) and osteopontin (OPN). *In vivo*, the potential of the scaffold for bone defect repair was emphasized. The treatment of Sprague-Dawley rats with a defect at the distal femur with GelMA-c-OGP improved bone quality in a greater amount compared to GelMA and GelMA/OGP groups, with the increase of bone mineral density (BMD), the amount of collagen fibers in cortical bone and the bone tissue volume per tissue volume rate (BV/TV) (Figure 4C)³⁴.

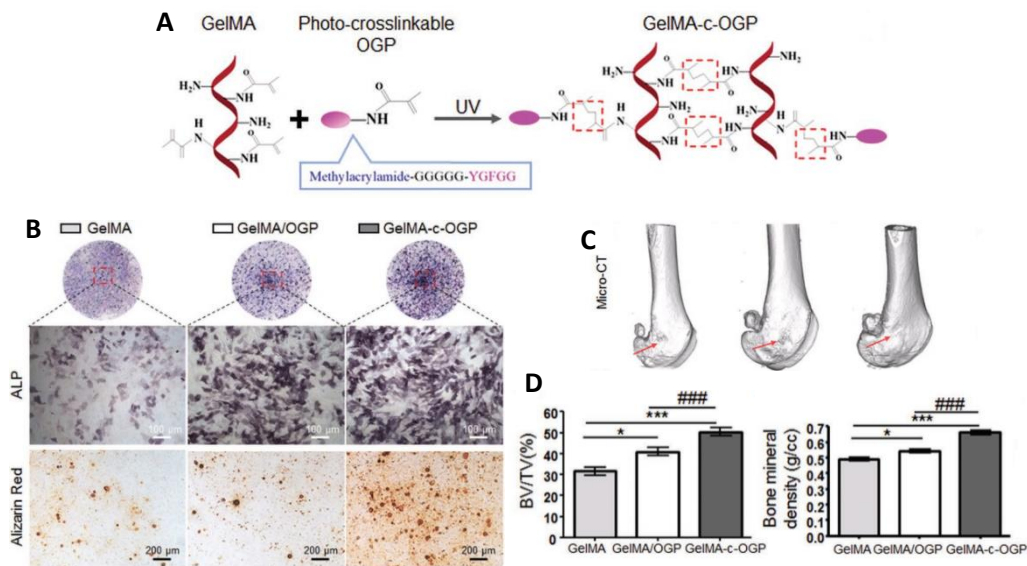


Figure 4: A) Representation of the chemical crosslinking of GelMA with photo-crosslinkable OGP under UV irradiation. B) ALP staining images (7 days after stimulation of osteogenic differentiation) and Alizarin red staining images (21 days after stimulation of osteogenic differentiation); C) Reconstruction of the defect site of distal femoral (μ -CT); D) BMD and BV/TV quantified by μ -CT. * $p < 0.05$, *** $p < 0.001$ compared with GelMA group, #### $p < 0.001$ compared with the GelMA/OGP group. (Adapted from Qiao et al., 2020)³⁴

Other limitation of bulk hydrogels is the intrinsic poor mechanical properties⁴⁶. Hence, in order to overcome bulk hydrogels limitations and improve the hydrogel properties and functionality, advances in the hydrogels-based scaffolds have been made. In this perspective, some appealing strategies include the incorporation of nano- and microparticles in the hydrogel mesh – composite hydrogels⁴⁷.

1.2.1.1. Composite hydrogels

Composite hydrogels refer to the incorporation of particles (nano- and micro- size) into the hydrogel network. Here, the hydrogel acts as a platform that retains the particles. The coupling of these two different materials in one scaffold allows the generation of new and unique properties

that are not present in the individual ones, minimising their intrinsic drawbacks^{44,47}. Due to the integration of particles that may absorb and support energy dissipation, the mechanical properties of these composite hydrogels can be modulated without changing the crosslinking degree^{48,49}. This was already demonstrated in a hybrid hydrogel of gelatin with gellan gum where microgels of gellan gum were used as a reinforcement of the weak mechanical properties of gelatin hydrogels, increasing the compressive modulus, failure stress and maximum strength (the latter 2.8 times higher compared to bulk gelatin hydrogels)⁵⁰.

Other benefits related to the development of these composite hydrogels include: i) the increase of drug loading capacity⁴⁴, ii) the stability of the encapsulated cargos⁵¹, iii) the possibility to tailor the drug release profiles, avoiding the initial burst release and increasing particles retention time^{44,51}, iv) the enhancement of drug bioavailability⁵¹ and v) the increase of its therapeutic efficiency⁵¹. In reliance on the above information, the use of these hybrid materials, with characteristics that are possible to modulate in order to create a favourable environment for tissue regeneration, enables the improvement of the materials' healing properties.

While the most common composite hydrogels applied in the biomedical field are nanoparticles-hydrogel hybrids, the incorporation of microparticles may also be possible⁵², demonstrating the versatility of this system. The incorporation of particles into the hydrogel may be achieved by distinct routes. The simplest approach comprises the suspension of prepared particles in a hydrogel-prepolymer solution, which enables the direct entrapment of particles during the polymerization of the hydrogel matrix^{47,48}. Additionally, the particles may also be modified with the introduction of functional groups on their surface to attribute them the capability to act as crosslinkers units, generating a hydrogel where chemical motifs of particles are covalently linked to multiple polymer chains^{47,48}. This approach improves the stability of the hydrogel mesh, as verified through the crosslinking reaction between biophosphanate-magnesium nanoparticles bearing acrylate groups with methacrylate hyaluronic acid, forming a composite hydrogel to support bone tissue regeneration with osteogenesis enhancement (Figure 5). The 3D scaffold with multivalent crosslinking domains has improved mechanical properties, including a higher Young's modulus and fracture compressive stress, with the latter being almost 3 times superior to bulk methacrylate hyaluronic acid⁴⁹.

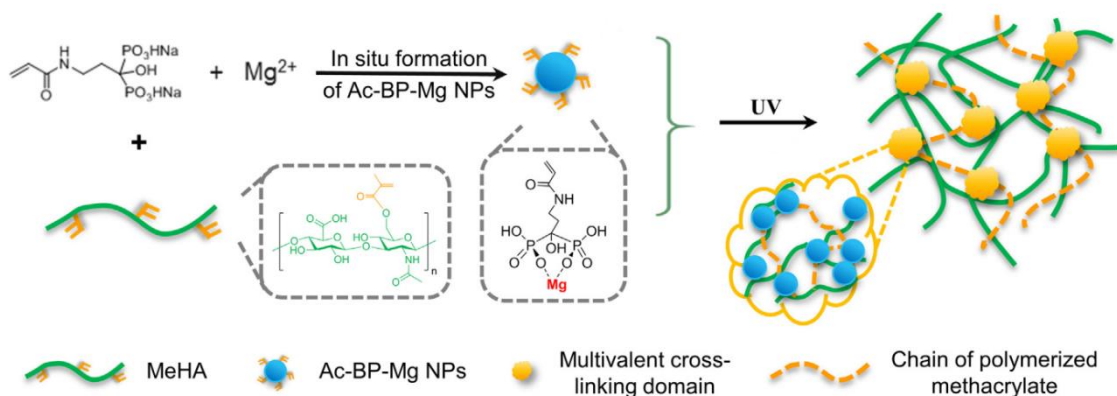


Figure 5: Representation of the multivalent crosslinking to forming a polymerized methacrylate with clusters of acrylated biophosphate (Ac-BP) plus Mg^{2+} nanoparticles (Ac-BP-Mg NPs). (Adapted from Zhang et al., 2017)⁴⁹

1.2.2. Yeasts of the genus *Saccharomyces*

Saccharomyces, a genus discovered in 1837, derives from the Greek term “sugar fungus” and represents a genus belonging to the Fungi kingdom, extensively applied in the baker and brewer industry and also have a number of biomedical applications^{53,54}. Yeasts are unicellular, with an ovoid or ellipsoid-like morphology, and a diameter around $5 \mu m$ ⁵⁵. These microorganisms can reproduce both asexually (budding) and sexually (ascospores) by coupling of two compatible yeasts⁵⁶.

Despite being eukaryotic microorganisms, yeasts are externally limited by a cell wall⁵³ with a thickness of 100 to 200 nm⁵⁷. This cell wall has a protective and supporting function, acting as a coating material that allows the preservation of the cell shape, providing mechanical support and controlling the internal osmotic pressure and the permeability of the cell⁵⁷. The available information on the constitution of yeast cell wall is mostly related to *Saccharomyces cerevisiae*. Nonetheless, the cell wall structure of *S. cerevisiae* and *Saccharomyces pastorianus* is similar, differing in the elasticity and in some properties of the polysaccharides, namely in the adhesive forces and in the rupture distance, which are superior in *S. cerevisiae*⁵⁸. The yeast cell wall is essentially composed of 85 % polysaccharides and 15 % proteins⁵⁹. Regarding the polysaccharide constitution, the cell wall consists of three main groups of polysaccharides: glucans (β -glucans and glycogen), type *N* and type *O* mannoproteins and, to a lesser extent, chitin (Table 1). These individual polysaccharides establish macromolecular complexes between them through covalent bonds that enables the formation of a biopolymer cell wall (Figure 6)^{60,61}.

Table 1: Yeast cell wall polysaccharides.

Polysaccharide	% in Cell Wall⁶²
Mannoproteins	35-40 %
β -glucans	50-60 %
Glycogen	1-23 %
Chitin	1-3 %

1.2.2.1. Yeast cell wall polysaccharides

1.2.2.1.1. Mannoproteins

Mannoproteins are glycosylated polypeptides essentially located on the outer surface of the cell wall, representing 35-40 % of its composition^{60,63}. These molecules are composed of proteins linked to mannose-carbohydrate chains and are involved in the modulation of cell permeability to macromolecules and in cell-cell recognition^{63,64}.

N-linked mannoproteins are mostly composed of carbohydrates (90 %) while the protein component represents only 10 % of total composition. The linkage between the protein and the polysaccharide domain is carried out through a glycation reaction between an *N*-acetylglucosamine (GlcNAc) and the amine group of the side chain of the asparagine amino acid. The polysaccharide domain is composed of a GlcNAc anchor trisaccharide linked to a backbone chain of 50 to 200 α 1 \rightarrow 6-linked mannose (Man) residues. This main chain is extensively branched with short (α 1 \rightarrow 2)-Man linked side chains that have (α 1 \rightarrow 3)-Man terminally linked⁶⁵.

In a lower proportion, type *O* mannoproteins are present, which are essentially composed of 50 % protein and 50 % carbohydrates. The linkage with the protein domain is established through the oxygen of the hydroxyl group (-OH) of the amino acids serine and threonine. These mannoproteins contain short oligosaccharide chains with 1 to 5 (α 1 \rightarrow 2)- and (α 1 \rightarrow 3)-linked mannosyl residues⁶⁵. The occurrence of phosphorylation in the mannose-carbohydrate chains, in the form of mannosylphosphate, alters the mannoproteins surface charge which is translated into an anionic behaviour^{60,63}.

1.2.2.1.2. Glucans

The yeast cell wall is mostly composed of glucans. These carbohydrates are essentially located in a more internal region, being responsible for cell wall elasticity and mechanical strength^{63,64}. Glucans correspond to chains of glucose (Glc) residues which, depending on the type of glycosidic linkage of the main chain and the branches they present, can be classified as (β 1 \rightarrow 3)-linked glucans, (β 1 \rightarrow 6)-linked glucans or glycogen⁶².

The inner layer of the cell wall of *S. cerevisiae* and similar yeasts is mainly composed of long-chain glucans with about 1500 Glc residues and a molecular weight of 240 kDa, linked by (β 1 \rightarrow 3) glycosidic bonds^{64,66}, that can be moderately branched with (β 1 \rightarrow 6)-Glc residues. Part of these (β 1 \rightarrow 3)-linked chains can interact in some points by hydrogen bonding, conferring them a 3D helical conformation^{63,64}. Aside from being covalently linked to mannoproteins via alkali-sensitive bonds or disulphide linkages, (β 1 \rightarrow 3)-linked glucans, through their non-reducing terminals, can be connected to the reducing terminal of GlcNAc via (β 1 \rightarrow 4) linkage^{63,66}. From the glucans present in the cell wall, 15 % correspond to (β 1 \rightarrow 6)-linked glucans⁶⁵, whose main chain consists of 100 to 200 (β 1 \rightarrow 6)-linked Glc residues, with a molecular weight of 24 kDa⁶⁴. This type of glucans, not only form bonds with (β 1 \rightarrow 3) glucans, but also with chitin, mannoproteins and glycogen^{66,67}. In addition to (β 1 \rightarrow 3) glucans and (β 1 \rightarrow 6) glucans, part of the β -glucans of brewer's spent yeast *S. pastorianus* consists of 30 % (β 1 \rightarrow 4)-linked Glc residues^{62,65}.

Glycogen is a (α 1 \rightarrow 4)-linked glucan with branching points of (α 1 \rightarrow 4,6)-Glc linkages at each 10 residues, representing 1-23 % of the yeast cell wall glucans⁶².

β -Glucans have already been applied in bone tissue engineering, which are described in detail in 1.3. section.

1.2.2.1.3. Chitin

In yeast belonging to *Saccharomyces* genus, chitin is the polysaccharide present in a smaller amount, corresponding to 1-3 % of the total polysaccharide content⁶², and it is found in the inner layer of the cell wall, close to the plasma membrane. Moreover, it is a GlcNAc polymer with around 100 to 190 (β 1 \rightarrow 4)-linked units^{63,66}. As previously mentioned, chitin chains can be linked to the non-reducing ends of (β 1 \rightarrow 3) glucans and (β 1 \rightarrow 6) glucans, via (β 1 \rightarrow 4)-linkages^{59,63}.

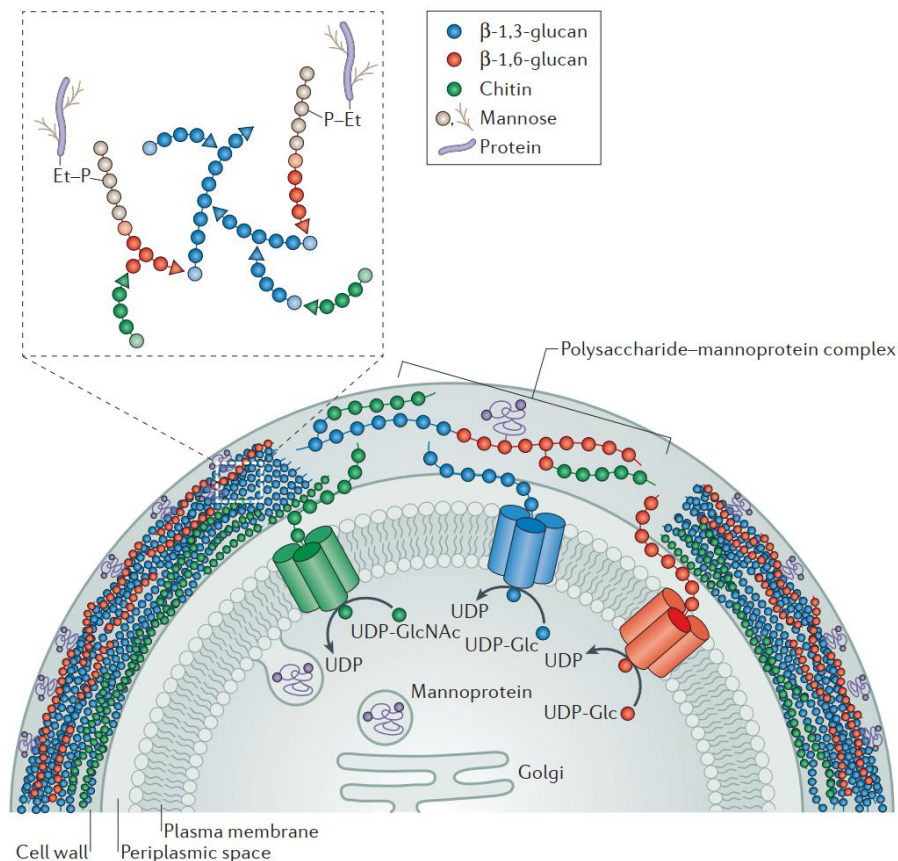


Figure 6: Representation of yeast cell wall structure. (Adapted from Cabib and Arroyo 2013)⁶⁸

1.2.2.2. Yeast cell wall modifications

The yeast cell wall plasticity is evident when considering the ability of yeasts to undergo structural modifications with polysaccharide composition changes, according to the extension of the stressful conditions they are exposed. Some of these modifications have already been described for *S. pastorianus*, a yeast commonly used in the brewer industry. This yeast, when submitted to alcoholic fermentation, due to the serial repatching process, have more branched and more phosphorylated mannoproteins, thus revealing a more hydrophilic and rigid structure⁶⁵. Dissimilar from yeasts of the initial inoculum, which are mostly composed of Glc units linked by (1→3) glycosidic bonds, yeasts resulting from the brewing process have a greater amount of (1→4)-linked Glc residues, which seems to result from an adaptation of this yeast to the fermentative stress⁶⁵. With the determination of the anomeric configuration of the glycosidic bond (1→4) enhanced in this brewer spent yeast, an increase of (α 1→4)-linked glucans along with (β 1→4)-linked glucans are verified⁶⁵. These modifications do not significantly alter the cell wall structure of *S. pastorianus*, and

their use may even be advantageous, which eventually may represent an opportunity to use this brewing industry by-product to obtain YMCAPs for applications in bone regeneration field where unique chemical modifications were performed biologically, induced by brewing stress conditions.

1.2.2.3. Yeast microcapsules

By submitting yeasts to a combination of chemical treatments with bases (e.g., 1M sodium hydroxide (NaOH)), acids (e.g., hydrochloric acid (HCl) at pH 4-5), and organic solvents (e.g., isopropanol and acetone) it is possible to remove the cytoplasmic content and preserve the yeast cell wall (water insoluble polysaccharides), thus obtaining biologically engineered YMCAPs⁵⁵. These are hollow and porous particles (pore size: ~600 nm) with an average diameter of 2-4 μm ^{49,69}. These yeast cell wall microcapsules consist of Glc polymers, essentially (β 1 \rightarrow 3)-linked glucans (80 %), and in a lower amount mannoproteins (<1 %) and chitin (2-4 %) ^{69,70}. The structural composition of YMCAPs render them suitable for drug encapsulation and delivery. The encapsulation is generally performed by natural diffusion, but other methods have already been applied as electrostatic adsorption⁷¹, slurry evaporation⁷² and dissolving-precipitating method⁷³. The incorporation of drugs in YMCAPs is commonly accompanied by a cover with a hydrogel of alginate and/or chitosan, to entrap the drug inside the microcapsule, allowing a slow and controlled release kinetics of the therapeutic agent⁷⁴. The release kinetics varies as a function of: i) the biomolecule molecular weight (MW) (higher MW have higher retention times)⁷⁵, ii) their solubility in the surrounding environment (higher solubility, higher release rate)⁷⁵, iii) the degree of branching associated with YMCAPs permeability (higher branching decrease the release rate)⁷⁵, iv) microcapsule porosity that may vary according to the ratio of (β 1 \rightarrow 3)/(β 1 \rightarrow 6)-glucans (higher porosity lead to a higher release rate)⁷⁶, and v) the presence of YMCAPs covering layer (cover decrease the payload burst release)⁷⁴.

Currently, YMCAPs stand out for their wide applicability in oral delivery. Oral delivery, compared to systemic delivery, has been considered the most desired form of administration owing to its convenience, higher compliance by the patient and easy modulation of the dose to be administered⁷¹. Notwithstanding, oral uptake has several limitations related to the low solubility, low permeability, sensitivity to P-glycoprotein (a protein related to resistance to various drugs), and gastrointestinal environment - low pH, enzymatic degradation^{29,77,78}. In view of this, yeasts can be used as a capsule for the incorporation of several bioactive compounds, protecting them from the gastrointestinal conditions and surmount several biological barriers to its absorption²⁹.

Furthermore, being β -glucans the major YMCAPs' constituent, side effects associated with the lack of specificity might also be overcome, since these carbohydrates are specifically recognized by

dectin-1 receptor and complement receptor 3 (CR3), which are present in certain types of cells of the immune system, including neutrophils, monocytes, dendritic cells, macrophages and intestinal M cells⁷⁷. Hence, when reaching the intestinal track, YMCAPs are internalized by intestinal M cells (found mainly in the lymphoid tissues of the mucosa, associated with Peyer's patch) and phagocytised by macrophages^{77,79}, being also accumulated in CD11c⁺ dendritic cells in subepithelial dome regions⁸⁰. This enables an efficient and specific transport of YMCAPs, through systemic circulation and lymphatic system, towards inflammable and tumour sites⁷⁹, whereby increasing the biocompatibility and biosafety of the administered drugs. The YMCAPs' transport by macrophages relies on the aforementioned receptors. Interestingly, treatment with dectin-1 and CR3 receptors inhibitors (anti-dectin-1 and anti-CR3 antibodies) result in hampering the engulfment of YMCAPs by macrophages⁷³. Regarding YMCAPs phagocytosis, it appears that the capacity of RAW 264.7 macrophages to internalize other particles is not affected nor its migration rate, which indicates a conservation of macrophages' physiological function⁷⁹. Moreover, higher branches of (β 1 \rightarrow 6)-linked glucans in YMCAPs, e.g., derived from mutant strain of *S. cerevisiae* R4 (branching frequency of 0.50) in particulate or soluble form, exhibit higher activity, reflected by a higher receptor affinity, being consequently phagocytised in a higher extent by human monocytes and neutrophils⁸¹. Furthermore, the YMCAPs surface modification may improve its uptake in the Payer's patch, for instance, polydopamine coating assigns a hydrophilic property and a negative charge to YMCAPs, which may be responsible for a 42 % enhancement of YMCAPs uptake by CD11c⁺ phagocytes⁸². This illustrates the possibility to tailor the YMCAPs surface according to the desire biological function, either in terms of composition of polysaccharides and its structure or in terms of chemistry by the introduction of functional groups, representing an opportunity for biomedical applications.

Additionally, the safety, lack of toxicity and resistance to digestive degradation (to a certain extent) of YMCAPs, supports its use in oral administration. YMCAPs are biodegradable and their disintegration may result from macrophages digestion (> 13 days)⁸³ and from exposure to gastrointestinal environment over prolonged periods of time (4 h exposure to simulated gastric fluid followed by 8 h exposure to simulated intestinal fluid resulted in lysis of part of YMCAPs-derived from *S. cerevisiae* SAF-Mannan, while some cell structures could still be observed)⁷¹. However, the degradation rate may differ according to the YMCAPs structural composition⁸⁴.

Considering the relevance of oral administration, it has been already reported the effectiveness of these yeast-derived microcapsules as carriers for nucleic acids⁸⁵, drugs⁷³, nanoparticles⁷⁷, liposomes⁷⁸, vaccines⁸⁶, and diagnostic agents⁸⁷. This application is possible since β -glucans particles are recognized by the U.S. Food and Drug Administration (FDA) as being generally safe. For bone

related diseases, YMCAPs were used as a diagnostic agent, with the development of a new approach for molecular imaging of inflamed regions, particularly for a situation of rheumatoid arthritis. For this purpose, fluorescent probes were encapsulated in glucan capsules which enable to verify the presence of marked macrophages in the lesion sites, owing to the microcapsules' phagocytosis by these immune cells. The images obtained allowed to make a distinction between progressive or remittent phase of the pathology in animal models with rheumatoid arthritis⁸⁷. More recently, a complexation of nanotubes with microRNA365 antagomir was performed and packed into YMCAPs for treating post-traumatic osteoarthritis pathogenesis. The complex recognition by macrophages in C57BL/6 mice with surgical destabilization of the medial meniscus, led to the suppression of microRNA365 with a consequent decrease in the inflammatory joint severity, thereby attenuating cartilage degradation (reduction of inflammatory cytokines – IL-1 β , IL-6, TNF- α ; reduction of degrading enzymes – metalloproteinase 13 (MMP-13); with a parallel upregulation of type II collagen, an anabolic cartilage marker)⁷¹.

The abovementioned studies indicate the future potential of these cargos as a new solution for the diagnosis and treatment of several diseases in which macrophages are involved, such as arthritis, osteoporosis, cancer, and bone fractures. Although research related to YMCAPs application in the biomedical field has mainly focused on their oral administration, other forms of application, as injection, may be explored. Moreover, the vast potential of YMCAPs can be further improved by surface chemical modifications, possible due to the elevated number of -OH groups in the monosaccharide units, in the near future. Indeed, a chemical conjugation of A/G protein to YMCAPs via 1-ethyl-3-(3-dimethylaminopropyl)carbodiimide hydrochloride (EDC) linker was already performed⁸⁸, proving that YMCAPs can be tailored to different purposes, thus creating new opportunities in the biomedical field.

1.3. Glucans with reported bone tissue applications

The vital role of immune system in bone cells behaviour and in the proper regulation of osteogenesis/osteoclastogenesis explains the emergence of the osteoimmunomodulation concept⁸⁹. Some biomaterials are capable of modulating the recruitment and the response of immune cells, affecting the macrophages' activity, the release of inflammatory cytokines and bone formation/bone resorption stimulating-factors^{15,89}. All of these ultimately influence bone dynamics and its eventual upshot. Among the several participants in bone healing, macrophages are the main producers of osteogenic and angiogenic factors⁹⁰. The secretion of these factors is dependent on a transition from inflammatory phase to repair phase. Wherefore, modifying the immune

microenvironment, particularly by controlling the macrophages' polarization in order to stimulate the resolution of inflammation, is a promising approach to promote bone regeneration and repair^{89,91}.

Naturally occurring β -glucans have known immunomodulatory activity, possible on account of its conserved structure which is common to several fungi and bacteria - pathogen-associated molecular patterns (PAMPs), which allows them to be recognized by immune cells⁹². Due to the relationship between (β 1 \rightarrow 3)-D-glucans and immunity, especially immune cells that are directly involved in bone remodeling and repair, their action on bone tissue could be a promising area for β -glucans application (Table 2). At bone level, the mechanism of glucans' action remains unknown, though its effect might occur indirectly by modulation of immune response with mediator's secretion or directly by interaction with bone cells and their precursors, stimulating its proliferation and differentiation.

Being β -glucans such important immunomodulators, they may have a favorable role in some inflammatory diseases correlated with bone loss, including rheumatoid arthritis, osteoarthritis, and periodontitis. The alleviation of inflammatory effects could promote an increase of bone formation. Both rheumatoid arthritis and osteoarthritis are characterized by an intense inflammation with proinflammatory mediators that promote joint erosion, and thus lead to cartilage and bone destruction which markedly affects joint motion⁹³. A highly branched (0.25) (β 1 \rightarrow 3)-D-glucans, with side chains of (β 1 \rightarrow 6)-D-Glc from *Pleurotus ostreatus*, also known as pleuran, was administered orally over 28 days in rats with adjuvant arthritis, lowering the hind paw volume^{94,95}. Furthermore, the administration of β -glucan from *S. cerevisiae* reduce alveolar bone loss in periodontitis model⁹⁶⁻⁹⁸. Once more, this reduction may be related to modulation of immune system with a decrease of proinflammatory cytokines and to modulation of RANKL and its inhibitor expression⁹⁷.

A successful bone-implant integration depends on a balance between the inflammation, as a consequence of the immune response to biomaterials and/or the implantation process itself, and tissue regeneration (calcium and collagen deposition). This balance is modulated by immune cells, particularly by macrophages. Hence, the use of coating materials, especially polysaccharides with immunomodulatory activities, may be beneficial to osteointegration. Zymosan is a *S. cerevisiae* wall fragment with (β 1 \rightarrow 3)-D-glucans backbone and (β 1 \rightarrow 6)-Glc linked residues as side chains. This polysaccharide was chemically grafted onto titanium (Ti) implants' surface to directly interact with macrophages and trigger M2 polarization which is essential for the regeneration process⁹⁰. The results reveal that when used in a proper concentration, zymosan can activate both toll-like receptor 2 (TLR2) and dectin-1 receptors and subsequent signaling pathways, enhancing the expression of

prohealing factors, such as oncostatin M (osteogenic inductor), VEGF (proangiogenic factor), platelet-derived growth factor with two B subunits (PDGF-BB) (proliferative inductor) and IL-10 (immunosuppressive cytokine) by macrophages⁹⁰. In addition, through the direct interaction between the zymosan coating and macrophages, a pro-regenerative environment is created, stimulating osteoblast differentiation and new bone growth in implant-bone interface⁹⁰. However, there seems to be a thin line between benefits and negative outcomes of zymosan biological activity. Higher doses can be detrimental by promoting an uncontrollable inflammation⁹⁰ and increasing the production of free oxygen radicals which promotes tissue necrosis, pseudoarthritis and stimulates bone resorption, demonstrating an inhibitory action on fracture healing⁹⁹.

1.3.1. Structure-activity relationship

Attributable to the great structural variability of β -glucans, namely backbone, MW, branching degree (BD) and chain conformation, there has been an effort to understand in what manner the structure influences the polysaccharides' activity¹⁰⁰. Despite their influence, some contradictory results have been pointed out^{92,100}, suggesting that although each of these factors seems essential to the attribution of a given biological activity, its action may be related to the combination of several structural characteristics.

1.3.1.1. Molecular weight

Generally, high MW β -glucans show considerably higher activity, being able to induce immune responses more efficiently. In contrast, shorter β -glucans (< 10000 Da) are inactive or present lower immunostimulatory activity^{92,100,101}. The size dependent activity may be explained partially because the higher MW, increases the structure stability and binding sites that allow a greater affinity for cellular receptors⁹². However, some research demonstrated that regardless the polysaccharide's MW, the immunostimulant capacity, the antitumor and antioxidant activity may be identical or even superior for low MW polysaccharides^{102,103}.

Steroid-induced avascular necrosis of the femoral head (SANFH) may be a consequence of excessive and prolonged consumption of glucocorticoids, conditions that might facilitate the apoptosis of bone cells^{104,105}. Soluble plant derived (β 1 \rightarrow 3)-glucans with an average MW of 9550 Da have an osteonecrosis protective effect by reducing the undesirable repercussions of dexamethasone. These protective effects embrace not only a decrease of proapoptotic related factors (B-cell lymphoma 2 associated X protein (Bax) and caspase-3) followed by upregulation of the antiapoptotic factor B-cell lymphoma 2 (Bcl-2) expression, but also an increase of osteogenic

markers (ALP, BMP-2, Runx2, osterix, OCN), contributing to the synthesis of the bone main components (collagen and calcium)^{104,105}. A similar therapeutic effect was observed in a SANFH rabbit model using soluble (β 1 \rightarrow 3)-glucan with a high MW (78 kDa), where a 60 days treatment resulted in an improvement of bone health status with a reduced number of lacunae and a restored trabecular bone structure¹⁰⁶. Other low MW polysaccharide was used as a therapeutic drug to prevent osteoporosis. Hydrolyzed (β 1 \rightarrow 3)-glucans derived from the mushroom *Pleurotus sajor-caju* interacted with murine pre-osteoblasts (MC3T3-E1) promoting its proliferation through the acceleration of the transition G1/S phase, which results in the upregulation of osteogenic-related gene markers expression, namely ALP, Col1 and OCN through the modulation of Runx2 and BMP-2 expression and MAPK and Wnt- β -catenin signaling pathways, the major pathways involved in osteogenesis¹⁰⁷.

The interaction of curdlan, a linear (β 1 \rightarrow 3)-D-glucan, with dectin-1 receptor modulate the AP-signaling pathway through the reduction of c-Fos expression, affecting the nuclear factor of activated T cell cytoplasmic 1 (NFATc1) synthesis. Being NFATc1 a critical transcription factor for osteoclast differentiation, the inhibition of NFATc1 expression and its nucleus translocation is accompanied by the suppression of macrophage RAW 264.7 differentiation induced by RANKL¹⁰⁸.

As osteoclasts are derived from myeloid hematopoietic stem cells, these catabolic cells express on their surface TLRs. Therefore, the activation of these receptors by RANKL or macrophage colony-stimulating factor (M-CSF) affect osteoclast activity. In the absence of RANKL, the activation of TLRs induce osteoclastogenesis of osteoclast precursor, increasing bone resorption¹⁰⁹. The co-stimulation of osteoclast progenitor cells by RANKL and TLRs agonists suppress osteoclast differentiation¹⁰⁹. Based on this knowledge, bone resorption induced by inflammation, could be attributed to TLR signal transduction. Hence, taking advantage of the co-stimulation effect, some molecules as peptidoglycan can be considered a barrier to osteoclast formation, through the activation of TLRs in cells previously stimulated with RANKL¹⁰⁹. Low MW β -glucans, laminaritetraose (MW 666), laminarihexaose (MW 990), laminarioligosaccharides (MW 1153) and curdlan (MW 3000), were compared to evaluate their capability to abolish osteoclast differentiation in a co-culture of mouse osteoblasts and bone marrow macrophages¹¹⁰. From these, only low MW curdlan suppresses the formation of osteoclasts through the interaction with primary osteoblast (decrease the expression of RANKL) and with the TLR2/TLR6 complex (inhibit the differentiation of osteoclasts precursor cells)¹¹⁰. This result suggests that even low MW has an antiosteoclastogenic effect, however, a MW superior to 1153 may be required for bone resorption repression.

Table 2: Bone regeneration and bone-related disorders effects of β -glucans.

Source	Application	Cell line / Organism	Results/Action	Ref
Linear (β 1 \rightarrow 3)-glucan (curdlan) 12.5, 25, 50, 100 μ g/mL	Bone regeneration	Mouse bone marrow cells RAW264.7 cells expressing or not dectin-1	<ul style="list-style-type: none"> • Suppress osteoclast formation (except for RAW 264.7 cells not expressing dectin-1 where a significant inhibition was only observed in presence of curdlan 100 μg/mL) • \uparrow Syk degradation and suppress RANKL induced osteoclast formation • \downarrow actin rings • \downarrow c-FOS protein expression and NFATc1 mRNA expression/translocation to the nucleus • \downarrow tartrate-resistant acid phosphatase, Oc-stamp, Cathepsin K, MMP-9 mRNA expression (osteoclastogenic genes) 	108
Low MW curdlan (MW 3000) 0.001, 0.01, 0.1, 1, 10 μ g/mL	Bone regeneration	Murine primary osteoblastic cells Mouse bone marrow cells Mouse calvarial organ	<ul style="list-style-type: none"> • Suppress osteoclast formation (\downarrow RANKL mRNA expression; = OPG mRNA expression) • \downarrow levels of medium calcium • Repress bone resorption via TLR2/6 	110
Krill CS + HA+ 8 %wt Curdlan Krill CS + β -TCP+ 8 %wt Curdlan	Bone regeneration	Saos-2 MC3T3-E1	<ul style="list-style-type: none"> • Curdlan \uparrow cell adhesion • Curdlan \uparrow cell growth • Curdlan \uparrow cell proliferation 	111
Krill CS + HA+ 8 %wt Curdlan	Bone regeneration	hFOB 1.19	<ul style="list-style-type: none"> • Curdlan \uparrow scaffold porosity, elasticity, water uptake and swelling • Curdlan \downarrow compressive strength and Young's modulus • Curdlan \uparrow cell viability, cell adhesion and proliferation • \uparrow TNF-α (associated with osteogenic differentiation), Col1, ALP activity and calcium deposition • \downarrow IL-6 	105, 106
Krill CS + HA+ 8 %wt Curdlan	Bone regeneration	MC3T3-E1	<ul style="list-style-type: none"> • Curdlan \downarrow water contact angle • Curdlan \uparrow fibronectin and laminin adsorption • Curdlan \uparrow osteoblast proliferation 	114

Source	Application	Cell line / Organism	Results/Action	Ref
Linear ($\beta 1 \rightarrow 3$)-glucans from <i>Agrimonia pilosa</i> (MW 9550 Da) 0, 5, 10, 25, 50, 100 $\mu\text{g/mL}$	Avascular necrosis of femoral head	MC3T3-E1 pre-treated with dexamethasone	<ul style="list-style-type: none"> • \uparrow cell viability • \downarrow apoptotic cells (\uparrow Bcl-2 protein expression; \downarrow Bax, cytochrome c, caspase 3 protein expression) • \uparrow ALP deposition, \uparrow collagen secretion, \uparrow calcium nodules • \uparrow BMP-2, Runx2, osterix, OCN, Wnt3, β-catenin, c-Myc protein 	104,1 05
Linear ($\beta 1 \rightarrow 3$)-glucans from Safflower (MW 78 kDa) 25, 100, 200 mg/kg	Avascular necrosis of femoral head	Japanese white rabbits (daily oral administration, 60 days)	<ul style="list-style-type: none"> • \downarrow empty lacunae • \downarrow fat diameter / adipose cell number • \uparrow bone marrow cells • \downarrow apoptotic cells (\downarrow Bax, caspase 3 protein expression; \uparrow Bcl-2 protein expression) • \downarrow Hydroxyproline serum levels and \uparrow Hexosamine serum levels 	106
Linear mix linked ($\beta 1 \rightarrow 3$) ($\beta 1 \rightarrow 4$)-glucans from Barley + BMP-7 6.25, 25, 100 and 400 $\mu\text{g/mL}$	Bone regeneration	MC3T3-E1	<ul style="list-style-type: none"> • Only glucan: = cell proliferation • Only glucan: = ALP activity • The mineralization induced by BMP-7 is inhibited by ($\beta 1 \rightarrow 3$) ($\beta 1 \rightarrow 4$)-glucans from Barley 	115
Branched ($\beta 1 \rightarrow 3$) ($\beta 1 \rightarrow 6$)-glucans from <i>Pleurotus ostreatus</i> (pleuran) 2 mg/kg	Rheumatoid arthritis	Male Lewis rats with adjuvant arthritis (oral administration, daily for 28 days)	<ul style="list-style-type: none"> • \uparrow total antioxidant status, \downarrow lipid peroxidation, \downarrow hind paw volume • = gamma glutamyltransferase activity • \downarrow TNF-α, IL-1α, monocyte chemoattractant protein-1 • \uparrow IL-4 	94
Pleuran 1 mg/kg	Rheumatoid arthritis	Male Lewis rats (oral administration, every second day, 28 days)	<ul style="list-style-type: none"> • Only glucan: \downarrow hind paw volume, \downarrow arthrogram score • Only glucan: = serum albumin levels <ul style="list-style-type: none"> ▪ Glucan potentiates the action of methotrexate (a drug used for rheumatoid arthritis treatment) in a combined administration. 	95
Linear ($\beta 1 \rightarrow 3$)-glucans from <i>Pleurotus citrinopileatus</i> (MW > 50 kDa)	Bone regeneration	Murine bone marrow cells	<ul style="list-style-type: none"> • Inhibit osteoclast differentiation 	116

Source	Application	Cell line / Organism	Results/Action	Ref
Branched ($\beta 1 \rightarrow 3$) ($\beta 1 \rightarrow 6$)-glucans from <i>Lentinus edodes</i> (lentinan) + BMP-7 6.25, 25, 100 and 400 $\mu\text{g/mL}$	Bone regeneration	MC3T3-E1	<ul style="list-style-type: none"> • Only lentinan: = cell proliferation • Only lentinan (100-400 $\mu\text{g/mL}$): \uparrow ALP activity • Lentinan (25-400 $\mu\text{g/mL}$) + BMP-7: \uparrow ALP activity • Lentinan + BMP-7: Formation of mineralized bone matrix 	115
Lentinan	Osteosarcoma	MG-63	<ul style="list-style-type: none"> • 5-100 mg/mL: \downarrow cell viability • \downarrow cyclinD1 protein expression (\downarrow proliferation) • \uparrow apoptosis (\uparrow cleaved caspase-3 and cleaved caspase-9) • \uparrow autophagy (\uparrow LC3B-II/LC3B-I and Beclin-1 protein expression) • \uparrow miRNA-340 expression (tumor suppressor) • Inhibit MAPK/ERK pathway 	117
Branched ($\beta 1 \rightarrow 3$) ($\beta 1 \rightarrow 6$)-glucans from <i>Grifola frondosa</i> 300 mg/kg	Bone regeneration	Human mesenchymal stem cells ICR rats (oral administration, 27 days)	<ul style="list-style-type: none"> • \uparrow cell viability • \uparrow calcium deposition, Col1, ALP, Runx2, Bone sialoprotein, OPN, osterix mRNA expression • \uparrow IGFBP2, IGFBP6, IGFBP4 protein levels • \uparrow IgA, IgM, IgG serum levels 	118
Hydrolysates of branched ($\beta 1 \rightarrow 3$) ($\beta 1 \rightarrow 6$)-glucans from <i>Pleurotus sajor-caju</i> (0.001, 0.01, 0.1, 1, 10 $\mu\text{g/mL}$)	Osteoporosis	MC3T3-E1	<ul style="list-style-type: none"> • \uparrow proliferation (\uparrow cells on S phase) • \uparrow calcium deposition, ALP, Col1, OCN, Runx2 mRNA expression • 0.1 and 1.0 $\mu\text{g/mL}$: \uparrow BMP-2 mRNA expression • \uparrow BMP-2, Runx2 protein levels (BMP-2 signaling pathway) • \uparrow ERK1, ERK2, JNK1, JNK2 mRNA expression (MAPK signaling pathway) • \uparrow Wnt5a, Fzd4, β-catenin, LRP5 mRNA expression (Wnt/β-catenin signaling pathway) 	107
Branched ($\beta 1 \rightarrow 3$) ($\beta 1 \rightarrow 6$)-glucans from <i>Saccharomyces cerevisiae</i>	Periodontitis	Male Wistar rats (daily oral administration, 49 days)	<ul style="list-style-type: none"> • \downarrow bone loss • = TNF-α plasma levels • \uparrow TGF-1β and hypothalaminc-pituitary-adrenal axis-driven hormone corticosterone responses to lipopolysaccharide 	96

Source	Application	Cell line / Organism	Results/Action	Ref
Branched β -glucans from <i>S. cerevisiae</i> 30 mg/kg	Periodontitis	Male Wistar Albino rats (daily oral administration, 28 days)	<ul style="list-style-type: none"> • \downarrow alveolar bone loss (\downarrow RANKL mRNA expression and \uparrow OPG mRNA expression) • \uparrow cyclo-oxygenase mRNA expression • \downarrow TNF-α and IL-10 blood levels 	97,98
Branched (β 1 \rightarrow 3) (β 1 \rightarrow 6)- glucans from <i>S. cerevisiae</i> (zymosan) 100 mg/kg	Fracture healing	Male Wistar Albino rats (daily administration via injection, 5 days)	<ul style="list-style-type: none"> • Cartilaginous union • Incomplete bony union and bone resorption • Pseudoarthrosis • Undifferentiated mesenchymal cells 	99
Titanium coated with zymosan <i>in vivo</i> : 1.0 μ g mm $^{-2}$; 0.1 μ g mm $^{-2}$; 0.01 μ g mm $^{-2}$	Implant-bone integration	Murine bone marrow derived macrophages RAW-blue reporter cells MC3T3-E1 Female Wistar rats	<ul style="list-style-type: none"> • \uparrow oncostatin M, VEGF, PDGF-BB, IL-10, ALP and OCN; \downarrow TNF-α • Activated TLR2 and dectin-1 receptors • Zymosan coating did not affect osteoblasts adhesion • 0.01-0.1 μg mm$^{-2}$: No severe inflammation • 0.1 μg mm$^{-2}$: \uparrow active osteoblasts embedded in dense bone matrix • 0.1 μg mm$^{-2}$: \uparrow trabecular bone structure, bone volume, implant-bone contact • 0.1 μg mm$^{-2}$: = TNF-α, alanine aminotransferase, aspartate aminotransferase, leukocytes number (compared to normal untreated rats) • 1.0 μg mm$^{-2}$: severe inflammation 	90
Branched (β 1 \rightarrow 3) (β 1 \rightarrow 4) (β 1 \rightarrow 6)-glucans from distillery waste <i>S.</i> <i>cerevisiae</i> sludge	Osteoblast proliferation	MG-63	<ul style="list-style-type: none"> • 0.3-0.7 mg/mL: \uparrow osteoblast cell proliferation 	119

ALP: alkaline phosphatase; Bax: B-cell lymphoma 2 associated X protein; Bcl-2: B-cell lymphoma 2; BMP: bone morphogenic protein; Col1: type I collagen; CS: chitosan; ERK: extracellular-signal-regulated kinase; HA: hydroxyapatite; hFOB 1.19: human fetal osteoblastic cell line; Ig: immunoglobulin; IGFBP: insulin-like growth factor-binding protein; IL: interleukin; JNK: c-Jun N-terminal kinase; LC3B-I/LC3B-II: microtubule-associated protein 1/2 light chain 3B; MAPK: mitogen-activated protein kinase; MC3T3-E1: murine pre-osteoblasts; MG-63: human osteosarcoma cell line; MMP-9: metalloproteinase 9; NFATc1: nuclear factor of activated T cell cytoplasmic 1; OCN: osteocalcin; OPG: osteoprotegerin; PDGF-BB: platelet-derived growth factor with two B subunits; RANKL: receptor activator of nuclear factor kappa-B ligand; Runx2: runt-related transcription factor 2; Saos-2: human osteosarcoma cell line; TGF- β : transforming growth factor beta; TLR2/6: toll-like receptor 2/6; TNF- α : tumor necrose factor alpha; VEGF: vascular endothelial growth factor.

The inhibition of osteoclast activity was also observed using soluble ($\beta 1 \rightarrow 3$)-glucan branched with ($\beta 1 \rightarrow 6$)-glucan from *S. cerevisiae* with a MW of 12-16 kDa¹²⁰. Contrarily, in another study, the inhibition of RANKL-induced osteoclast differentiation was only possible when using soluble linear ($\beta 1 \rightarrow 3$)-glucan with a MW superior to 50 kDa¹¹⁶. The differences in these results may be related to the presence of ($\beta 1 \rightarrow 6$) side chains, which may enhance the activity of β -glucans with lower MW.

1.3.1.2. Degree of branching

Although some opposite results were identified, it is commonly admitted that a high degree of branching, mainly a BD between 0.2 (1 branch for every 5th backbone Glc residues) and 0.33 (1 branch for every 3rd backbone Glc residues), is an important contributing factor to β -glucans immunomodulatory activity^{92,100,101}. Highly branched ($\beta 1 \rightarrow 3$)-D-glucans, with side chains of ($\beta 1 \rightarrow 6$)-glucopyranoside are found in yeasts and mushrooms.

Distillery yeast sludge derived from fuel alcohol production were reused as a source of β -glucans. Alkali extraction with 0.5 M NaOH resulted in glucan particles with 69 % ($\beta 1 \rightarrow 3$)-, 4 % ($\beta 1 \rightarrow 4$)- and 5 % ($\beta 1 \rightarrow 6$)-linked glucans¹¹⁹. Regarding β -glucans extracted from distillery yeast sludge, no cytotoxic effect was observed. In fact, a stimulation of human osteosarcoma cell line (MG-63) proliferation was verified, an effect most notorious for concentration of 0.1-0.5 mg/mL¹¹⁹.

Branched ($\beta 1 \rightarrow 3$) ($\beta 1 \rightarrow 6$)-D-glucans extracted from *Grifola frondosa* in a concentration of 50 μ g/mL and 20-30 μ m size induce osteogenic commitment of human MSCs with higher calcium deposition as verified in Alizarin staining test, and higher osteoblastic markers gene expression levels (Runx2, ALP, OCN, Col1 among others), across the studied time points (7 and 14 days). The increase in the expression of essential genes for bone regeneration may be linked to the upregulation of insulin-like growth factors (IGF), namely IGFBP 2, 4 and 6. Additionally, when administrated *in vivo* every day for 27 days, it was found that the animals treated with 300 mg/kg of glucans extracted from *G. frondosa*, particularly with 10-20 μ m size, expressed higher amounts of immunoglobulin (Ig) with immunomodulatory properties as IgA, IgG and IgM, which further demonstrates that glucans have an immune-enhancing effect, evidencing their therapeutic action¹¹⁸.

Lentinan, a *Lentinus edodes* derived ($\beta 1 \rightarrow 6$)- branched ($\beta 1 \rightarrow 3$)-glucan, with a BD of 0.23-0.42, has an excellent antitumor activity. The addition of lentinan to MG-63 cells might lead to tumor suppression via upregulation of microRNA340. Aside from leading to the decrease of cell proliferation, this microRNA has a cellular destructive action either by apoptosis or autophagy¹¹⁷.

The strong immunomodulating and antitumor activity of lentinan may also be correlated with its triple-helix conformation¹²¹.

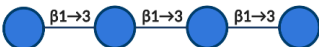
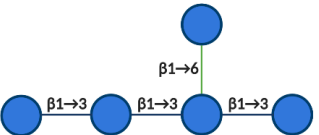
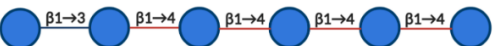
1.3.1.3. Conformation

Over and above, another known structural feature that influences the activity of β -glucans is conformation. It results from the different spatial organization of the polymer chains according to their lower energy state in a given solution¹²², which can assume a single-helix, triple-helix and random coil conformation. The different conformations are related to several factors including the glycosidic linkages established between the constituting sugars of the β -glucans' backbone and branches (if present), the polymer's MW and the hydrogen bonding between intra and/or inter-chains^{92,100}. There is some evidence suggesting that β -glucans with triple-helix conformation are biologically more active. Although not entirely understood, the higher interaction of triple-helix glucans with immune cells and probably with bone cells may be related to a higher stability and a higher receptor affinity when compared to single-helix conformers¹²¹. However, as for the other structural features, some reports indicate contradictory results, where single strand glucans showed a higher immunostimulatory activity¹²³. For instance, even though curdlan induces bone formation and reduces osteoclast activity, it possesses an unbranched structure and as previously discussed, its bioactivity seems to be independently of its MW. For this reason, conformation might be extremely relevant for receptor recognition. Curdlan, when heated to a temperature above 55°C tends to jellifying, assuming a triple-helix conformation¹²⁴. It was shown that the addition of curdlan (submitted to 90°C) to krill chitosan and HA scaffold might turn its surface more favorable for osteoblasts adhesion since this addition affects some of its physical properties, such as the increase of water uptake capability, wettability and swelling tendency - characteristics that enhance serum adhesion proteins adsorption (e.g., fibronectin and laminin). Adding to this, the presence of β -glucans seems to improve *in vitro* osteogenic differentiation via increasing TNF- α production by osteoblasts, highlighting the potential of curdlan application in impaired/delayed bone healing and regeneration¹¹¹⁻¹¹⁴.

The water-soluble linear mix linked (β 1 \rightarrow 4)(β 1 \rightarrow 3)-D-glucans from barley have a random coil configuration that tends to form aggregates in aqueous solution. The effect of glucans extracted from barley, *L. edodes* and *A. pullulans* SM-2001 in MC3T3-E1 culture was compared. Contrarily to other glucans, barley glucans impaired the mineralization process induced by BMP-7. This action may be related to the disordered conformation of glucans isolated from barley or to the mixture of (β 1 \rightarrow 4) and (β 1 \rightarrow 3) linkages in their backbone structure¹¹⁵.

An exhaustive study to elucidate the relationship of glucans structure-activity is extremely important so that its application at the clinical level becomes viable, since small structural differences may affect their biological performance. Comparing the structure of different glucans already evaluated for bone applications, it is difficult to define the ideal structure for its activity. Nevertheless, some structure key points can be identified: i) β -anomeric configuration seems to be essential for cell recognition; ii) a combination of high MW, the presence of branches and a triple helix conformation seems to potentiate β -glucans activity, since these parameters alone does not have a concise biological response. The principal glucans structures already used in bone tissue engineering and their principal activities in bone regeneration and bone related disorders are summarized in Table 3.

Table 3: Principal activity of β -glucans in bone regeneration and bone related disorders.

Glucans structure	Activity in bone regeneration and bone related disorders
 <p>Linear ($\beta 1 \rightarrow 3$)-glucan</p>	<p>Inhibit bone resorption:</p> <ul style="list-style-type: none"> • antiosteoclastogenic activity <p>Stimulate bone formation:</p> <ul style="list-style-type: none"> • promotion of osteogenic differentiation • activation of critical bone formation pathways • induction of mineralization • antiapoptotic activity
 <p>Branched ($\beta 1 \rightarrow 3$) ($\beta 1 \rightarrow 6$)-glucans</p>	<p>Antioxidant activity</p> <p>Anti-inflammatory activity</p> <p>Osteosarcoma suppressor</p> <p>Inhibit bone resorption:</p> <ul style="list-style-type: none"> • antiosteoclast activity <p>Stimulate bone formation:</p> <ul style="list-style-type: none"> • promotion of osteogenic differentiation • activation of critical bone formation pathways • induction of mineralization • increase trabecular bone structure • increase bone volume • osseointegration <p>Higher doses of zymosan:</p> <ul style="list-style-type: none"> • Severe inflammation • Bone resorption • Pseudoarthrosis • Cartilaginous union
 <p>Linear mix linked ($\beta 1 \rightarrow 3$) ($\beta 1 \rightarrow 4$)-glucans</p>	<p>Mineralization inhibition</p>

2. Aims

2.1. Aims

This thesis envisages the fabrication of a photocrosslinkable multi-YMCAPs/GelMA hydrogel hybrid as a platform for long-term, localized drug and MSCs delivery, in order to potentiate bone repair.

With the purpose of isolating YMCAPs from spent yeast discarded by the brewing industry, two different optimized bioprocesses are applied, so as to generate YMCAPs with distinct polysaccharide surface composition. The isolation of YMCAPs will be followed by a one-pot chemical modification to introduce norbornene or methacrylic crosslinking groups in YMCAPs surface biomolecules. With this chemical modification it is envisioned the fabrication of a hybrid platform through light-mediated covalent crosslinking between functionalized YMCAPs and GelMA biopolymer.

The drug encapsulation capacity of YMCAPs will also be evaluated with model compounds and with bioactive molecules with recognized bioinstructive, pro-osteogenic effects in MSCs.

Afterwards, the evaluation of this multi-YMCAPs/GelMA platform biological performance, specifically its cytotoxicity, will be accomplished in *in vitro* cultures.

The specific aims are the following:

- YMCAPs isolation and purification;
- YMCAPs chemical and structural characterization;
- YMCAPs surface chemical modification with norbornene or methacrylate chemistry groups and multi-YMCAPs/GelMA platform generation and characterization;
- Drug encapsulation and drug release profile evaluation;
- Incorporation of human adipose derived stem cells (*hASCs*) within multi-YMCAPs/GelMA platform;
- Assessment of *in vitro* *hASCs* viability to YMCAPs exposure;
- Assessment of *in vitro* *hASCs* viability within multi-YMCAPs/GelMA platform.

3. Materials and Methods

3.1. Materials

Spent yeast is a highly available material discarded by the brewing industry so, through a circular economy strategy, added-value may be attributed to them. *Saccharomyces pastorianus* with 6 fermentative cycles was used in this work, it was provided by brewery Super Bock Group (Porto, Portugal) in 2018.

3.2. Yeast microcapsules (YMCAPs) isolation, purification and characterization

Initially, from the samples provided by Super Bock Group (Porto, Portugal) the yeast was separated from the must. For this, the samples were washed with distilled water and centrifuged under the following conditions: 4704 g, 15 min, 4°C. This procedure was repeated 3 times. Part of the precipitate (initial yeast) was freeze-dried to determine the percentage of solids and moisture, according to the following equations:

$$\text{Solids (\%)} = \frac{\text{Dry weight}}{\text{Wet weight}}$$

$$\text{Moisture (\%)} = 100 - \text{solids (\%)}$$

3.2.1. YMCAPs isolation

YMCAPs were prepared from *S. pastorianus* through 2 different processes in order to obtain microcapsules with different polysaccharide composition on the surface. Firstly, the isolation of yeast cell wall from brewer's spent yeast was performed by thermal autolysis (60°C) resulting in YMCAPs containing highly phosphorylated mannoproteins as an external layer (YMCAPs_Aut)⁶⁵. Thereafter, YMCAPs previously isolated were submitted to an alkali extraction with 4M KOH to obtain YMCAPs with a low content of mannoproteins with β -glucans exposed on the surface (YMCAPs_4M) (Figure 7).

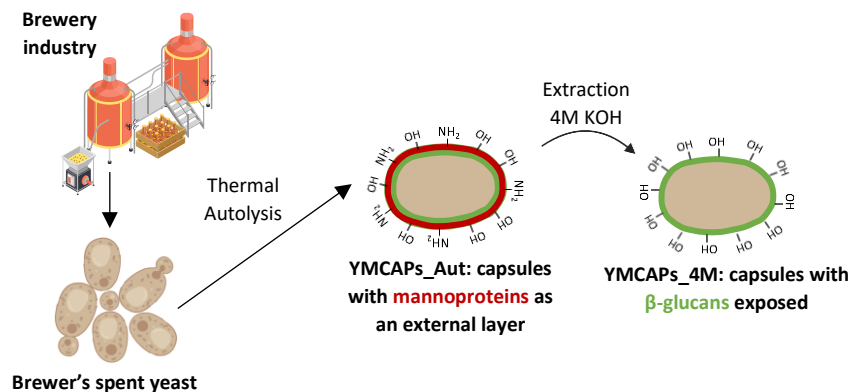


Figure 7: Schematic representation of YMCAPs isolation procedure.

3.2.1.1. Thermal autolysis

Autolysis is a natural lytic event where the endogenous yeast enzymes solubilize its intracellular content allowing the isolation of the yeast cell wall, without significant changes in their shape and structure¹²⁵.

The isolation of the yeast cell wall was achieved by submitting *S. pastorianus* to a 60°C bath for 2 h under constant magnetic stirring. At the end of this reaction, a heat shock was performed by placing the samples in a 100°C bath for 10 min, envisioning the inactivation of the enzymes responsible for the intercellular components' hydrolysis. Afterwards, the cytoplasmatic content (solubilized material) were physically separated from the insoluble autolysis residue (YMCAPs_Aut) by centrifugation at 4704 g, 4°C during 15 min. Both the soluble material and the residue were collected, frozen and freeze-dried.

3.2.1.2. Alkali extraction

In order to obtain YMCAPs_4M with lower content of mannoproteins and with β -glucans exposed on the microcapsule surface, 60 g of the thermal autolysis residue was submitted to an alkaline extraction with oxygen-free solution of 4M KOH + 20mM NaBH₄ during 2 h with stirring, at room temperature (RT), under a nitrogen atmosphere. Following the extraction, the soluble material (extracted material) was separated from the insoluble one (residue) by centrifugation at 4704 g, 0°C during 20 min. The separated residue and the extracted material were acidified with glacial acetic acid to pH 5. The chemical reaction between KOH with acetic acid results in potassium acetate formation, a salt that can be removed during dialysis using 12-14 kDa molecular weight cut-off cellulose membranes. Dialysis against water with a few drops of toluene and chloroform to prevent the proliferation of microorganisms, was carried out at 4°C with continuous stirring. The dialysate was replaced until the conductivity reached the conductivity of the distilled water. After dialysis, the material extracted during the 4M KOH extraction, and the obtained residue, were centrifuged under the following conditions: 25200 g, 4°C, 20 min. As a result, four different factions were separated: the soluble extracted material (sn 4M), the precipitated extracted material (pp 4M), the material that remains soluble in the dialysis membrane (sn FR 4M), isolating the final residue (YMCAPs_4M). The samples were frozen and freeze-dried.

3.2.2. YMCAPs characterization

3.2.2.1. Morphology and particle size

The morphology and particle size of the freeze-dried YMCAPs were visualized by widefield fluorescence microscopy (Axio Imager M2, Carl Zeiss, Germany), and the image processing was performed using Zeiss Zen v2.3 blue edition software. For fluorescence micrographs, an excitation and emission wavelength of 488 nm and 530 nm were used, respectively.

3.2.2.2. Zeta potential

YMCAPs suspensions were prepared by adding 1 mL of ion-exchanged water as a dispersing medium and left at RT during 24 h under stirring. The YMCAPs' zeta potential was measured by using a Malvern Zetasizer nano ZS equipment, at 25°C. For this, a zeta potential measurement cell (DTS 1070) was loaded with the prepared YMCAPs suspension and a voltage potential was applied to the cell gold electrodes, promoting the movement of the YMCAPs to the electrode of opposite charge. Data was acquired with 3 runs and the instruments was operated in automatic mode. Zeta potential was computed from the electroosmotic data and using the Smoluchowski equation.

3.2.2.3. Sugar analysis

The analysis of neutral sugars consists of three essential steps. The first step corresponds to hydrolysis under an acidic environment, which result in the separation of the different monosaccharides by the breakdown of the glycosidic bonds, thus promoting the polysaccharide depolymerization¹²⁶. Before hydrolysis, 200 μ L of 72 % H_2SO_4 was added to 1-2 mg of each sample and the reaction was carried out for 3 h at RT with occasional shaking. Then, with the addition of 2.2 mL of distilled water, the acid concentration was diluted to obtain 1M H_2SO_4 , which was followed by 5 min sonication to facilitate the polysaccharides' solubilization. To promote the polysaccharides' hydrolysis, the samples were incubated at 100°C in a heating block for 2.5 h. The tubes were cooled down in an ice bath. After hydrolysis, 200 μ L of the internal standard solution (2-deoxyglucose, 1 mg/mL) was added to each tube. Then, 1 mL of the hydrolysed sample was transferred to new culture tubes and neutralized with 200 μ L of 25 % NH_3 .

Afterwards, the hydrolysates were submitted to a reduction and subsequent acetylation to convert the sugars into alditol acetates that could be analysed by gas-phase chromatography (Figure 8). The reduction of monosaccharides in alditols allows the decreasing of the complexity of the chromatogram, since alditols only exist in the open form, giving rise to only one peak in the chromatogram per sugar¹²⁷. In addition, due to the polar nature of carbohydrates, an acetylation

step is required to derivatize the polar groups of alditols increasing their volatility¹²⁸. The reduction of neutral sugar released upon hydrolysis was performed by adding 100 μL of 15 % (m/v) NaBH_4 in 3M NH_3 to samples and incubating for 1h at 30°C. After, to eliminate BH_4^- ions in excess, 50 μL of glacial acetic acid was added twice. Then, 300 μL was transferred to *soviel* tubes and, in an ice bath, 450 μL of the catalysator 1-methylimidazole and 3 mL of acetic anhydride (acetylating agent) was added, mixed and incubated at 30°C in a heating block for 30 min. To remove the excess of acetic anhydride and to extract the resulting alditol acetates, 3 mL of distilled water and 2.5 mL of dichloromethane were added, respectively. After vigorous stirring, the separation of the two phases was achieved by centrifugation (1400 g, 30 s), being the aqueous phase subsequently removed by suction. This step of the liquid-liquid extraction was repeated. Afterwards, the organic phase was washed with 3 mL of distilled water, stirred, centrifuged and the aqueous phases was completely removed as previously described. Once more, the washing was repeated. After the washings, the organic solvent was evaporated in a centrifuge evaporator, and the samples were washed by two successive additions of 1 mL of acetone followed by its evaporation.

Finally, alditol acetates were analysed by gas-phase chromatography with flame ionization detector (GC-FID), on a Perkin Elmer – Clarus 400 chromatograph with a 30 m capillary column DB-225 (diameter: 0.25 mm, film thickness: 0.15 μm). For this, alditol acetates were diluted in 50 μL of anhydrous acetone and 2 μL of sample were injected into the GC column. The program used was: initial temperature 220°C standing for 7 min, followed by a rate of 5°C/min until 240°C. The injector temperature was set to 220°C and the temperature of the detector was set to 240°C. The flow rate of the carrier gas (H_2) was established at 1.7 mL/min. The identification of the chromatogram's peaks to the correspondent monosaccharide was based on comparison of the retention times of previously injected standards.

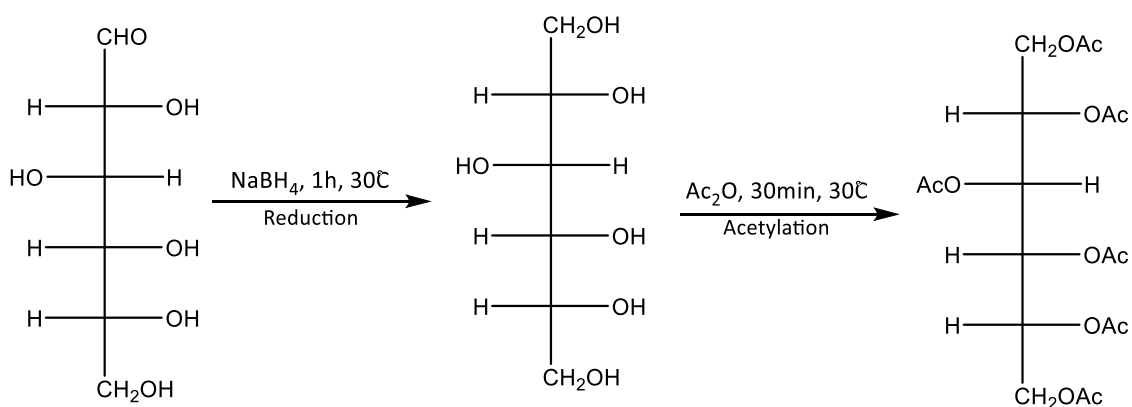


Figure 8: Schematic representation of the reduction of D-glucose to its corresponding D-glucitol, followed by an acetylation step with the production of D-glucitol hexaacetate that could be analysed by gas-phase chromatography.

3.2.2.4. Glycosidic linkages analysis

To elucidate the polysaccharides' structure, in particularly, the glycosidic linkages between their constituent sugar units, a methylation analysis was performed, with the production of partially methylated alditol acetates (PMAAs) (Figure 9).

Initially, 1-2 mg of the samples were dried overnight in a vacuum oven in the presence of phosphorous pentoxide (P_2O_5). Then, the samples were dissolved in dimethylsulfoxide (DMSO) for 24 h, at RT and under constant stirring. 40 mg of NaOH pellets powdered under argon atmosphere were added and the reactions were left under stirring, 30 min, at RT. The incorporation of a base allows the deprotonation of free hydroxyl groups (-OH) with the formation of alkoxide groups which, being good nucleophiles, facilitate the reaction with the methylating agent¹²⁹. After, for the methylation of the formed alkoxide groups, three successive additions of methyl iodide (CH_3I) (80 μ L) were performed with an appropriate syringe, and allowed to react for 20 min, with vigorous stirring between each addition. Methylated polysaccharides become less hydrophilic, therefore, to ensure their complete solubilization, 3 mL of a chloroform/methanol solution (1:1, v/v) were added. Then, the methylated samples were recovered by dialysis using membranes with a pore diameter of 12-14 kDa, against 50 % ethanol/water solution. The dialysate was collected and concentrated to dryness and the material was redissolved in DMSO and remethylated in order to ensure the methylation of all available positions (free -OH) in the polysaccharides. After repeating the dialysis and material concentration, the partially methylated polysaccharides (methyl esters) were hydrolysed with 500 μ L of 2M Tri-fluoroacetic acid (TFA) in a heating block at 121°C, with occasional stirring. After 1 h, the acid was evaporated in a speed vacuum concentrator to dryness. Then, 20 mg of sodium borodeuteride ($NaBD_4$) and 300 μ L of 2 M NH_3 were added and allowed to react for 1 h at 30°C in order to reduce the methylated monosaccharides in alditols. The use of $NaBD_4$ as a reducing agent, besides diminishing the chromatogram complexity, allows to later distinguish C_1 from C_6 , since the introduction of a deuterium atom in the C_1 position confers asymmetry to the molecule¹³⁰. After this period, the tubes were cooled in an ice bath and the excess $NaBD_4$ was neutralized by two additions of 50 μ L of glacial acetic acid. After reduction, to allow the separation of sugars by gas chromatography, the volatility of partially methylated alditols was increased through acetylation. For this, 450 μ L of the 1-methylimidazole and 3 mL of acetic anhydride were added. Acetylation occurs at the positions exposed by hydrolysis, namely at the carbon atoms involved in the glycosidic bonds¹³¹. The solution was incubated at 30°C in a heating block for 30 min. To decompose the excess of acetic anhydride, 3 mL of distilled water was added, and PMAAs were extracted by liquid-liquid extraction as abovementioned in sugar analysis section.

Finally, 0.5 μL of PMAAs diluted in 100 μL of anhydrous acetone were injected into the gas-chromatography-mass spectrometry (GC-MS) (Shimadzu GCMS-QP2010 Ultra) with an HT-5 capillary column. The injector operated in a split mode at 250°C. The column oven temperature was as follows: initial temperature (80°C); linear increase of 7.50°C/min up to 140°C maintaining this temperature for 5 min; then rises to 143.2°C at 0.2°C/min, followed by an increase rate of 12°C/min until 250°C. The flow rate of the carrier gas (helium) was 1.85 mL/min with a pressure of 124.1 kPa. The MS analysis was performed with an ion source temperature of 250°C, an electron impact mode at 70 eV and a scanning range of 50-700 m/z .

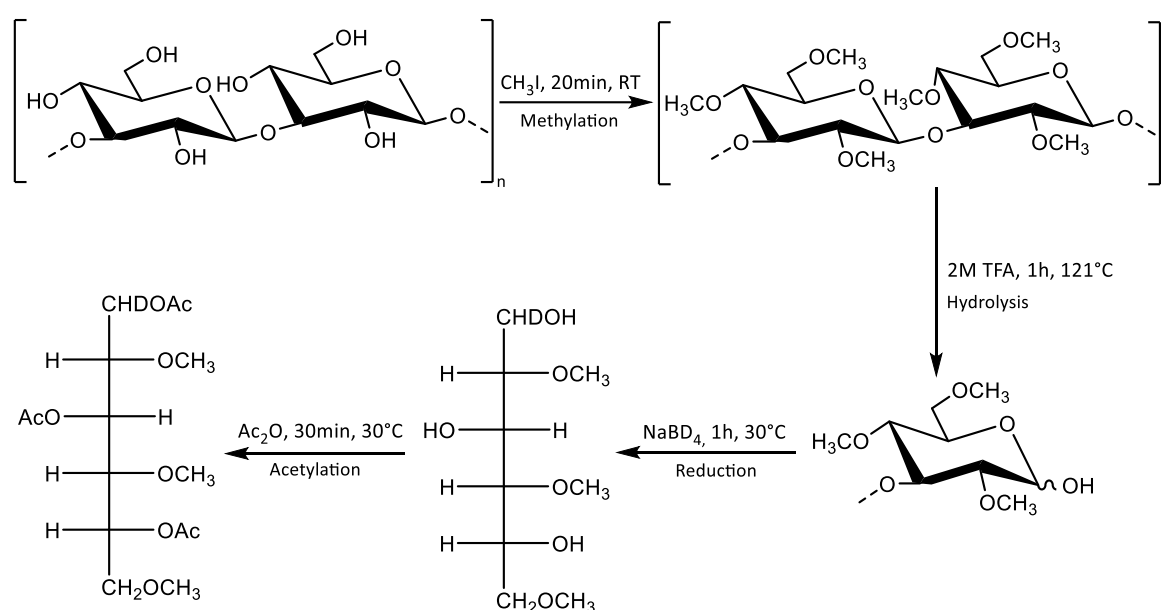


Figure 9: Representation of the preparation of (β1→3)-linked glucan partially methylated alditol acetates.

3.2.2.5. Protein content

3.2.2.5.1. Elemental analysis

The total protein content of the different microcapsules was evaluated by elemental analysis in order to determine the percentage of nitrogen (% N) present in the YMCAPs, using thermal conductivity as a detection method. The detection analysis parameters include combustion furnace temperature at 1075°C and after burner temperature of 850°C, using Truspec 630-200-200 equipment. The conversion of % N to the protein content was performed considering the Kjeldahl factor of 6.25.

3.2.2.5.2. Amino acid analysis

The amino acid composition analysis is a multi-step process that includes the protein's hydrolysis, followed by amino acids derivatization (Figure 10) and, finally, their chromatography analysis. To promote hydrolysis of the peptide bonds between the different amino acids, 1 mL of 6M HCl was added to 5 mg of sample, the mixtures were flushed with nitrogen gas and placed in an ultrasonic bath for 5 min (3 times). Maintaining the nitrogen atmosphere to minimize oxidation, the hydrolysis took place over 24 h at 110°C. After cooling the tubes, 500 µL of the internal standard norleucine (5.0 µmol/mL in 0.1 M HCl) was added. The samples were subsequently concentrated in a speed vacuum concentrator. After drying, the samples were redissolved in 1 mL of 0.1M HCl and filtered through a 0.45 µm filter to collect the free amino acids. The samples were once more concentrated to dryness. After hydrolysis, 200 µL of 3M HCl in isobutanol was added to the dry samples and left to react for 10 min at 120°C. At the end of this time, the samples were stirred and allowed to react for another 30 min at 120°C, where the carboxylic acid of the amino acids is butylated, forming butyl esters. After cooling the tubes to RT, the excess reagent was evaporated. Then, 200 µL of the antioxidant 3,5-di-tert-butyl-4-hydroxytoluene (BHT) in ethyl acetate (2 µg/mL) was added and further evaporated. The amino group of the amino acids was then acylated by adding 100 µL of heptafluorobutyric anhydride which reacted for 10 min at 150°C. The reagent in excess was also evaporated to dryness. Lastly, the resulting material was redissolved in 150 µL of ethyl acetate and immediately analysed by GC-MS (Shimadzu GCMS-QP2010 Ultra). The injector operated in a linear velocity mode at 250°C. The program of the column oven temperature was the following: the oven initial temperature was 70°C, increasing to 170°C with a rate of 2°C/min. Once the temperature reached 170°C, a second increase with a rate of 16°C/min up to 250°C was followed and temperature was then kept constant for 5 min. The flow rate of the carrier gas (helium) was 1.86 mL/min with a pressure of 120.0 kPa. The MS analysis was performed with an ion source temperature of 250°C, an electron impact mode at 70 eV and a scanning range of 50-700 *m/z*.

The determination of amino acids concentration in the samples was conducted according to the calibration curves prepared for the individual amino acids (Table 4). To achieve this, the amino acids were dissolved in 6M HCl, in which 500 µL of the internal standard norleucine (5.0 µmol/mL in 0.1M HCl) was added. Then, the derivatization (butylation of the carboxylic acid and acylation of the amine group) was proceeded in the same manner as described above. After dryness, the amino acid was also redissolved in 150 µL of ethyl acetate and analysed by GC-MS.

Table 4: Data from amino acids calibration curves (amino acid concentration, slope, R² and limit of quantification/detection).

	Minimum aa concentration (mg/mL)	Maximum aa concentration (mg/mL)	Slope	R ²	LOQ (mg/mL)	LOD (mg/mL)
Ala	0.025	0.4	1.7414	0.9995	0.005	0.002
Asp	0.05	0.5	2.2409	0.9998	0.002	0.001
Glu	0.05	0.5	2.0711	0.9989	0.007	0.002
Gly	0.05	0.6	1.901	0.9995	0.002	0.001
Ile	0.025	0.6	1.0004	0.9968	0.006	0.002
Leu	0.05	0.5	1.801	0.9992	0.004	0.001
Lys	0.05	0.7	2.2103	0.9983	0.005	0.002
Phe	0.05	0.4	2.4374	0.9988	0.005	0.002
Pro	0.05	0.3	1.805	0.9995	0.005	0.002
Val	0.025	0.75	1.6148	0.9987	0.005	0.001

aa: amino acid; Ala: alanine; Asp: aspartic acid; Glu: glutamic acid; Gly: glycine; Ile: isoleucine; Leu: leucine; Lys: lysine; Phe: phenylalanine; Pro: proline; Val: valine; LOQ: limit of quantification; LOD: limit of detection.

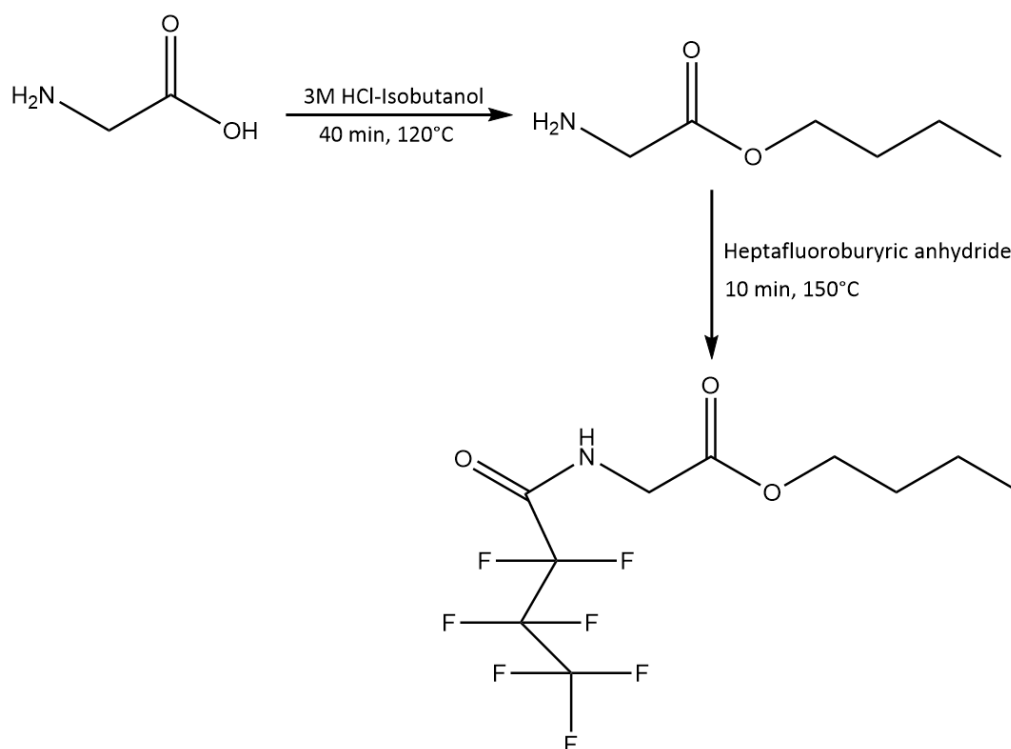


Figure 10: Schematic representation of glycine derivatization, including butylation of the carboxylic acid and acylation of the amine group.

3.3. YMCAPs surface chemical modification and characterization

3.3.1. Chemical synthesis of modified YMCAPs with carbic anhydride

To enable the formation of a YMCAPs platform through a chemical click reaction between the thiol group and the norbornene, the microcapsules were chemically modified with carbic anhydride to introduce the norbornene group, through anhydride-based reactions with -OH and amine groups of the YMCAPs polysaccharides and proteins (Figure 11). Dry DMSO, 10 mL, were added to 2 g of YMCAPs, followed by the addition of 2 mmol of carbic anhydride, reacting for 24 h at RT, under magnetic stirring. At the end of this time, the samples were washed 4 times with 40 mL of distilled water, by centrifugations in the following conditions: 25200 g, 20 min, RT. The modified microcapsules were collected, frozen and freeze-dried.

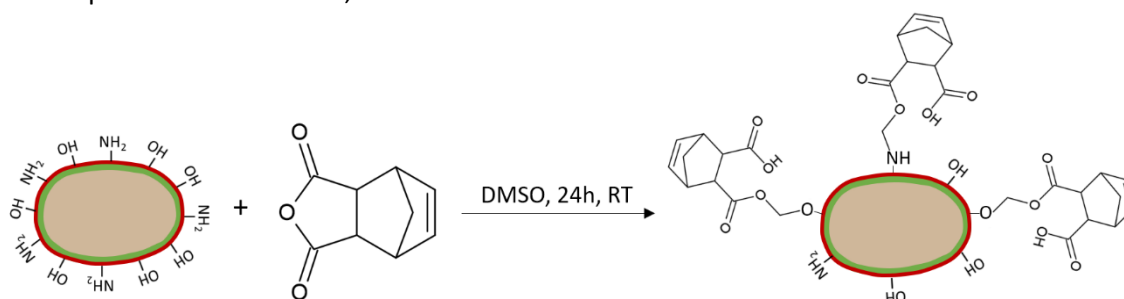


Figure 11: Schematic representation of the chemical route used to obtain YMCAPs_Aut with incorporated norbornene groups.

3.3.2. Chemical synthesis of modified YMCAPs with methacrylic anhydride

In addition to the modification with norbornene, the incorporation of methacrylate groups in YMCAPs, through anhydride-based reactions with -OH and amine groups (Figure 12), was also evaluated, envisioning the functionalization of YMCAPs for subsequent aggregation in larger scaffolds. YMCAPs, 2 g, were dissolved in 10 mL of phosphate-buffered saline solution (PBS). Then, 4 mmol of methacrylic anhydride was added to the samples and allowed to react at RT, under magnetic stirring. After 24 h, the reaction was stopped, and the samples were washed 4 times with 40 mL of distilled water and centrifuged (25200 g, 20 min, RT). The post-modification capsules were collected and freeze-dried.

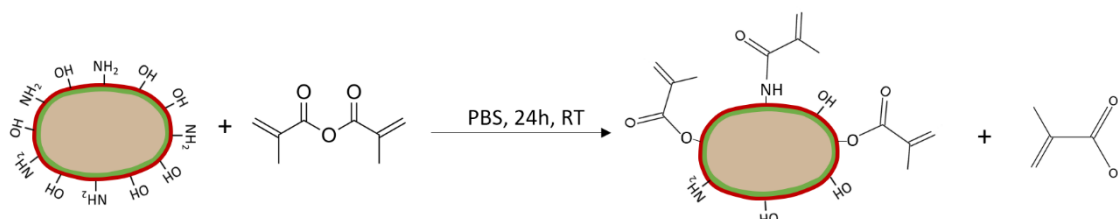


Figure 12: Schematic representation of the chemical route used to obtain YMCAPs_Aut with incorporated methacrylate groups.

3.3.3. Characterization of the YMCAPs chemical modification

3.3.3.1. Fourier-transform infrared spectroscopy

To evaluate the surface chemistry of the microcapsules and verify the presence of the norbornene and methacrylate on the modified samples, dried modified and non-modified YMCAPs were analysed via attenuated total reflectance Fourier transformed infrared (ATR-FTIR) spectrometry, using a Brüker Alpha FT-IR spectrometer. Spectra were recorded in the absorbance mode and the samples were scanned from 4000 to 400 cm^{-1} , at a resolution of 4 cm^{-1} , with a total of 256 scans. The obtained data was processed using OPUS software.

3.3.3.2. Solid-state nuclear magnetic resonance spectroscopy

Solid-state nuclear magnetic resonance (ssNMR) was also used to characterize the modified YMCAPs, through the observation of the spectral changes post-modification. The analysis was carried out on a 9.4 T magnetic field Bruker Avance III 400 spectrometer equipped with a double-resonance 4 mm Bruker MAS probe. Larmor frequencies of ^{13}C were 100.6 MHz. Two different experiments were performed: i) conventional cross-polarization (CP) - for observation of reacted norbornene/methacrylate bound resonances; ii) multiple cross-polarization (MultiCP) - for quantification of reacted norbornene/methacrylate groups.

CP measurements were performed using a delay time of 7.5 s and a contact time of 3.5 ms. The radiofrequency pulses of the carbon and proton channel were adjusted to 55 kHz and 75 kHz, respectively, with an increment rate of 30 %. Decoupling of ^1H spin during the acquisition was achieved using SPINAL-64 pulse sequence (power of 85 kHz; acquisition time of 0.05 s). The procedure comprised an accumulation of 10445 scans.

In multiCP, the experiment is decomposed in several CP blocks ($n=10$). Both RF pulses of ^{13}C and ^1H channels were adjusted to 55 kHz and 75 kHz, respectively, to meet the Hartmann-Hahn condition, with 10 % ramped-amplitude increment in the ^1H channel. The SPINAL-64 proton decoupling was employed at a power of 85 kHz. Other multiCP parameters include: 4.5 μs contact time, 7.5 s recycle delay, 2.5 s inter-CP-blocks and 10 kHz MAS frequency. The spectrums were recorded with 10445 scans.

3.3.3.2.1. Degree of substitution

For norbornene and methacrylate groups quantification the whole spectrum obtained from multiCP of unmodified YMCAPs (IntA) and modified YMCAPs (IntB) were integrated from 200 to 0 ppm. From the subtraction of the two spectrums, the integration area corresponding to the

chemical modification agent is determined. From this data, the carbon moles (CM) of norbornene/methacrylic were calculated according to the following equation:

$$\text{CM Norbornene/Methacrylic} = \frac{(\text{IntB} - \text{IntA}) \times (\text{CM protein} + \text{CM polysaccharide})}{\text{IntA}}$$

CM of protein and polysaccharide were obtained through elemental analysis

$$\text{Norbornene moles} = \frac{\text{CM norbornene}}{9} \quad \text{Methacrylic moles} = \frac{\text{CM of methacrylic}}{8}$$

The degree of substitution [DS (%)] was determined considering the norbornene and methacrylic moles determined from ssNMR and the total of -OH and NH₂ moles present in YMCAPs available for the chemical modification (-OH and NH₂ moles were estimated through the results of sugar and protein analysis).

3.3.3.3. Glycosidic linkages analysis

Changes in the glycoside linkages post-modification was evaluated with a view to identifying the modification positions in the polymer. The glycosidic linkages analysis was performed by methylation followed by polysaccharides' hydrolysis, reduction, and acetylation, as described in section 3.2.2.4.

3.4. Multi-YMCAPs/GelMA photocrosslinkable platform generation and characterization

3.4.1. Multi-YMCAPs/GelMA platform formulation

Considering the highest degree of substitution for methacrylate YMCAPs_Aut, the composite hydrogel, formed by YMCAPs and gelatin was only performed using YMCAPs_Aut chemically modified with methacrylic anhydride. Gelatin methacrylate, with a substitution degree of 75 %, was prepared by Monteiro et al., 2020¹³². Four distinct YMCAPs-hydrogels were prepared: i) 1 % (w/v) of non-modified YMCAPs (GelMA/YMCAPs_Aut_1%); ii) 5 % (w/v) of non-modified YMCAPs (GelMA/YMCAPs_Aut_5%); iii) 1 % (w/v) of modified YMCAPs (GelMA-c-YMCAPs_Aut_1%); and iv) 5 % (w/v) of modified YMCAPs (GelMA-c-YMCAPs_Aut_5%). The hydrogel precursor solution was prepared with 10 % (w/v) GelMA solution prepared with PBS and 0.15 % (w/v) of photoinitiator (lithium phenyl (2,4,6-Trimethylbenzoyl) phosphinate (LAP) prepared with PBS). The YMCAPs (1 % or 5 % (w/v)) were mixed with the polymeric solution prior to the network formation. The mixed solution was placed in a cylindrical PDMS molds (6 mm diameter, 2 mm height), and the

photocrosslinking via free radical chain polymerization was prompt by exposure to visible blue light (405 nm) with an incident light intensity of 8.17 mW/cm², during 5 min (Figure 13).

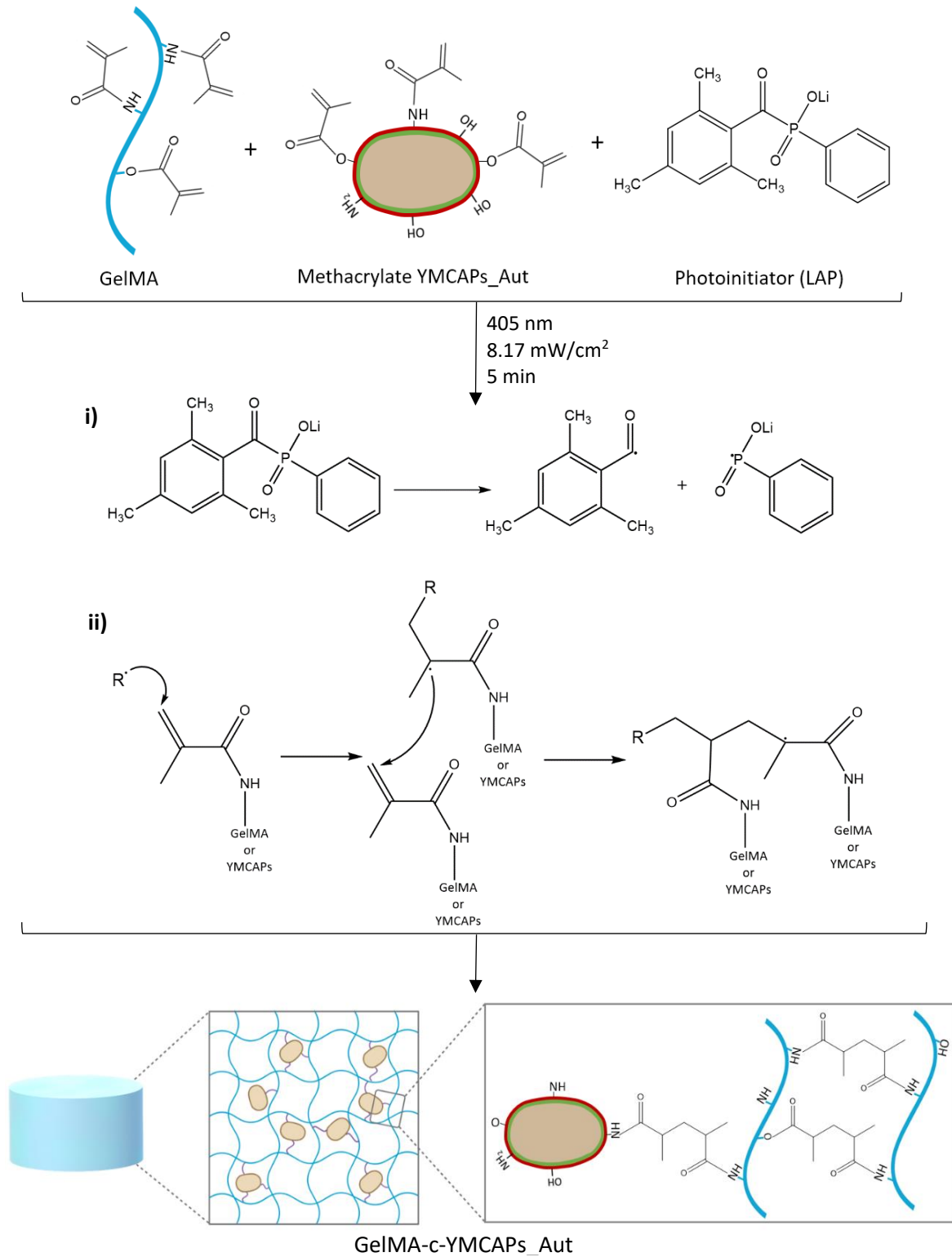


Figure 13: Schematic representation of GelMA-c-YMCAPs_Aut hybrid platform generation.

3.4.2. Multi-YMCAPs/GelMA platform characterization

3.4.2.1. Water Content

To evaluate YMCAPs-hydrogels water content, after the YMCAPs-hydrogels crosslinking, the surface moisture was removed with a filter paper and each formulation (n=3) was immediately weighted (W_i). The weight step was followed by freeze-drying to remove the water, and to obtain the dry weight (W_d). The water content was calculated according to the following formula:

$$\text{Water content (\%)} = \frac{W_i - W_d}{W_i} \times 100$$

3.4.2.2. Swelling behaviour

To characterize the swelling behaviour, the prepared 6 mm × 2 mm circular YMCAPs-hydrogels (n=3) were weighted immediately after crosslinking (W_i) and immersed in 15 mL PBS (pH 7.4) at 37°C. At different time points (4, 24 and 48 h), the wetted hydrogels were removed from the PBS, the excess of PBS on the surface was wiped off with a filter paper and the swollen weight (W_s) was recorded. The PBS absorption capacity was calculated according to the following formula:

$$\text{Swelling (\%)} = \frac{W_s - W_i}{W_i} \times 100$$

3.4.2.3. Mass loss

The mass loss of the prepared 6 mm × 2 mm circular YMCAPs-hydrogels (n=3) were evaluated through their immersion in 15 mL PBS (pH 7.4) at 37°C, for 28 days. For that, equilibrated hydrogels were weight (W_e). At different time points (3, 7, 14, 21 and 28 days), the hydrogels were removed from the PBS and after remotion of the excess of surface PBS with a filter paper, the weight of each specimen were obtained (W_f). The PBS was changed every week. The YMCAPs-hydrogels percentage loss was calculated according to the following formula:

$$\text{Mass loss (\%)} = \frac{W_e - W_f}{W_e} \times 100$$

3.4.2.4. Mechanical properties

Mechanical testing of the prepared YMCAPs-hydrogels (n=3) was conducted with a Instron Uniaxial mechanical test machine, using a 50 N load cell at RT. The specimens with 6 mm diameter and 2 mm thickness, were immersed in PBS for 24 h to swell and reach the equilibrium. The displacement ramp rate was set to 1 mm/min and a pre-load force of 1×10^{-3} N was applied. A

sensitivity of 30 % was used and the upper force limit was set to 45 N. The Young's modulus was calculated from the slope of the strain-stress curves in the linear region corresponding to 0-5 % strain.

3.5. Cell-laden multi-YMCAPs/GelMA platform

Initially, the adhesion domains that attach human adipose stem cells (*hASCs*) to the culture T-flask were disrupted by incubating the cells with TrypLE™ Express Enzyme detaching reagent for 5 min at 37°C with 5% CO₂ atmosphere. After the incubation period, the trypsinization efficiency was evaluated by observation of the detachment and loss of cell typical morphology, becoming increasingly rounded in appearance. Afterwards, the cells were separated from the ECM using a cell strainer (40 µm) and the trypsin reaction was stopped through the addition of culture medium, followed by a centrifugation step (300 g, 5 min at 25°C). The cells (pellet) were then resuspended in α-MEM culture medium, and the number of cells were counted using Trypan Blue solution (1:9 proportion of cells to Trypan Blue solution) in a Neubauer counting chamber. Trypan Blue is a negatively charged dye which is not incorporated into cells with an intact membrane due to the electrostatic repulsion, thus, only damaged cells are stained blue¹³³. Afterwards, under sterile conditions, precisely 1x10⁶ cells/mL were resuspended in the hydrogel precursor solution (10 % (w/v) GelMA prepared in Dulbecco's phosphate buffered saline (dPBS) containing the photoinitiator LAP [0.15 % (w/v)] also prepared in dPBS and 1 % or 5 % (w/v) methacrylate YMCAPs before light exposure. The hydrogel production was carried out in sterile conditions as abovementioned in section 3.4.1.

3.6. *In vitro* studies

3.6.1. AlamarBlue™ Assay – Cytotoxicity evaluation

The biocompatibility of YMCAPs and GelMA-c-YMCAPs were evaluated through a metabolic activity assay. For 2D condition, *hASC* cells were initially plated on plastic adherent 96-well plate at a density of 1 × 10⁴ cells/well (n=4) in α-MEM culture medium supplemented with 10 % (v/v) FBS and 1 % antibiotic-antimycotic mixture and maintained for 24 h at 37°C under a controlled humidified atmosphere of 5 % CO₂. Then, cells were incubated at different time points (24, 48 and 72 h) with YMCAPs, under 9 distinct concentrations (0, 25, 50, 75, 100, 250, 500, 750 and 1000 µg mL⁻¹). For 3D conditions, cell-laden GelMA-c-YMCAPs_Aut_1% and GelMA-c-YMCAPs_Aut_5% prepared according to 1.2 section, were analysed on days 1, 4 and 7 (n=4). To assess cell metabolic activity of both conditions, the AlamarBlue™ assay was performed. Following the incubation

period, the culture medium was replaced by α -MEM containing 10 % (v/v) AlamarBlue™ reagent. This reagent is composed of resazurin, a cell permeable blue weakly-fluorescent dye which, in contact with metabolic active cells, is reduced to a highly fluorescent pink-coloured resorufin (Figure 14). Thus, the conversion from resazurin to its reduced state is proportional to the number of viable cells and can be estimated according to the fluorescence intensity. After 4 h of incubation at 37°C, the medium was transferred to a black-clear bottom 96-well plate for the fluorescence intensity measurement. The fluorescence was detected at an excitation/emission wavelengths of 540/600 nm, using a Synergy HTX multimode microplate reader (BioTek Instruments).

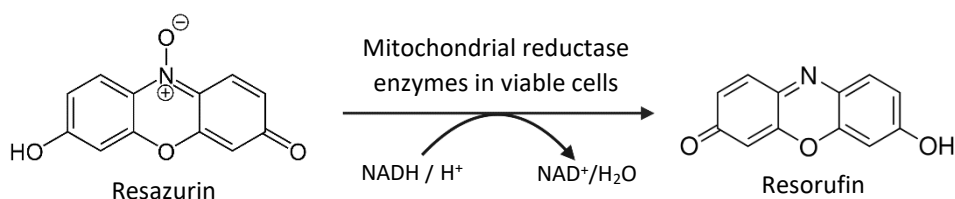


Figure 14: The chemical principle of AlamarBlue™ cell viability assay.

3.7. YMCAPs drug encapsulation

3.7.1. Drug encapsulation and encapsulation efficiency

Different compounds (naringin, naringenin, dexamethasone and Nile red) and several strategies were tested in order to evaluate the encapsulation capacity of YMCAPs_Aut. Every experiment evaluated for drug encapsulation are described in detail in Table 5. Briefly, for naringin encapsulation, different conditions were tested: i) stirring (magnetic stirring, orbital stirring and 360°); ii) with or without initial suspension of YMCAPs_Aut in water at 37°C for 24 h previously to the addition of drug; iii) encapsulation medium (10 % EtOH, 100 % EtOH, 100 % DMSO); iv) encapsulation time (4 h, 24 h); v) YMCAPs_Aut:naringin ratio; and vi) with or without freeze-drying after the encapsulation reaction.

For naringenin, dexamethasone and Nile red, 10 mg of YMCAPs were suspended in 1 mL of pure ethanol solution containing naringenin, dexamethasone or Nile red (500 $\mu\text{g}/\text{mL}$, 500 $\mu\text{g}/\text{mL}$, 250 $\mu\text{g}/\text{mL}$, respectively). The prepared suspensions were incubated overnight at RT, under magnetic stirring. After completion of the reaction, drug loaded YMCAPs_Aut were separated from the involving medium containing free drug by a combination of washings with distilled water and centrifugations at 25200 g for 15 min at RT.

For dexamethasone encapsulation a second encapsulation condition was tested: 500 $\mu\text{g}/\text{mL}$ of dexamethasone were mixed with YMCAPs_Aut with a minimum possible volume of carvacrol (40

μL) and let to react for 4 h at 37°C. The reaction was followed by supernatant separation and washings.

Table 5: Experimental conditions used for drug encapsulation in YMCAPs_Aut.

	Drug	YMCAPs (mg/mL)	Drug (mg/mL)	Media of encapsulation	Time (h)	Temperature (°C)	Stirring
1	Naringin	1	1	10 % EtOH	4	RT	360° vertical rotation
2	Naringin	1	1	10 % EtOH	24	RT	360° vertical rotation
3 ^{a,b}	Naringin	1	1	10 % EtOH	24	RT	Magnetic
4 ^a	Naringin	1	1	10 % EtOH	24	RT	Orbital
5 ^a	Naringin	10	1	100 % EtOH	24	RT	Magnetic
6 ^a	Naringin	10	1	100 % DMSO	24	RT	Magnetic
7	Naringenin	10	0.5	100 % EtOH	24	RT	Magnetic
8	Dexamethasone	10	0.5	100 % EtOH	24	RT	Magnetic
9	Nile red	10	0.250	100 % EtOH	24	RT	Magnetic
10	Dexamethasone	10	12.5	100 % Carvacrol	4	37	-

a. Initial suspension of YMCAPs at 37°C, during 24h. The initial suspension was followed by the addition of drug.

b. After the encapsulation reaction, the samples were freeze-dried

3.7.1.1. Encapsulation efficacy

The encapsulation efficiency [EE (%)] was calculated through the ratio of the amount of free drug in the supernatant after the reaction and the amount of drug added for the reaction.

$$EE (\%) = \frac{\text{Amount of drug added for the reaction} - \text{Remaining free drug}}{\text{Amount of drug added for the reaction}} \times 100$$

Naringin, naringenin and dexamethasone encapsulated in carvacrol after reaction were determined by UV-vis maximum absorbance measurement at a wavelength (λ) of 282 nm, 289 nm, and 240 nm, respectively, in a 96-well quartz microplate (Hellma Analytics). All measurements were performed in a multi-mode plate reader (Synergy HTX, Biotek Instruments).

Nile red was detected by fluorescence intensity measurement at excitation $\lambda=540/35$ nm and emission $\lambda=600/40$, in a black side and clear bottom microplate, using a Synergy HTX multimode microplate reader (BioTek Instruments).

For dexamethasone encapsulation evaluation, high performance liquid chromatography (HPLC) was performed. The UltiMate 3000 HPLC was equipped with a LiChrocart LiChrospher[®] reverse phase C18 column with 5 μm of pore size and a diameter of 250 mm \times 4 mm, using an isocratic mode with a mobile phase of methanol:water [60:40 (v/v)] filtered through 0.2 μm membrane filters. The program used consisted of: flow rate of the mobile phase was set to 1.0 mL/min; the assay was performed at 35°C; the injection volume was 30 μL ; UV detector at 240 nm.

For the encapsulated compounds, calibration curves were prepared using standard solutions (Dexamethasone – 2 to 100 μg ; $y=0.0254x + 0.0181$; $R^2: 0.9991$. Nile red – 0.1 to 100 μg ; $y=12159\ln(x) + 22009$; $R^2: 0.9835$) which were used to determine the concentration of the drugs.

3.7.2. Drug release profile

The *in vitro* release profile of Nile red from stand-alone YMCAPs and GelMA-c-YMCAPs_5% was analysed in 2 mL PBS (pH 7.4), at 37°C, with a stirring of 150 rpm in an orbital shaker (VWR[®] model 3500I), under dark. At pre-determined time points (1, 2, 3, 4, 24, 48, 72, 240 h), a sample consisting of 1 mL was withdrawn and replaced with 1 mL of fresh PBS. The removed samples were stored at -20°C and after 10 days, the release of Nile red was monitored via fluorescence changes, as performed in section 3.7.1.1. for EE determination.

3.8. Data analysis

The statistical analysis was performed by using the IBM SPSS statistics 26 software. At least 3 independent experiments ($n=3$) were used. Data were analysed by using one-way ANOVA followed by Tukey's post-hoc test. The data was tested for normal distribution (Shapiro-Wilk test) and homogeneity of variances (Levene test). A level of significance of $*p < 0.05$ was considered in all samples. The data were expressed as mean \pm standard deviation.

The data plots were constructed using GraphPad Prism 8.0.1 software (Trial version).

4. Results and Discussion

4.1. YMCAPs characterization

4.1.1. Morphology, particle size and zeta potential

The observation of the processed, naturally derived, YMCAPs by widefield fluorescence microscopy revealed a typical yeast spherical to ellipsoidal shape with a uniform particle size that varied from 3 to 7.5 μm in diameter (Figure 15). The zeta potential of the YMCAPs appears to be (-13.9 ± 0.239) mV for YMCAPs_Aut and (0.249 ± 0.0646) mV for YMCAPs_4M. Interestingly, the presence of mannoproteins led to an increase in the negative surface charge. This shift in zeta potential was expected since YMCAPs_Aut have highly phosphorylated mannoproteins on its surface, thus contributing to its negative charge⁶⁵.

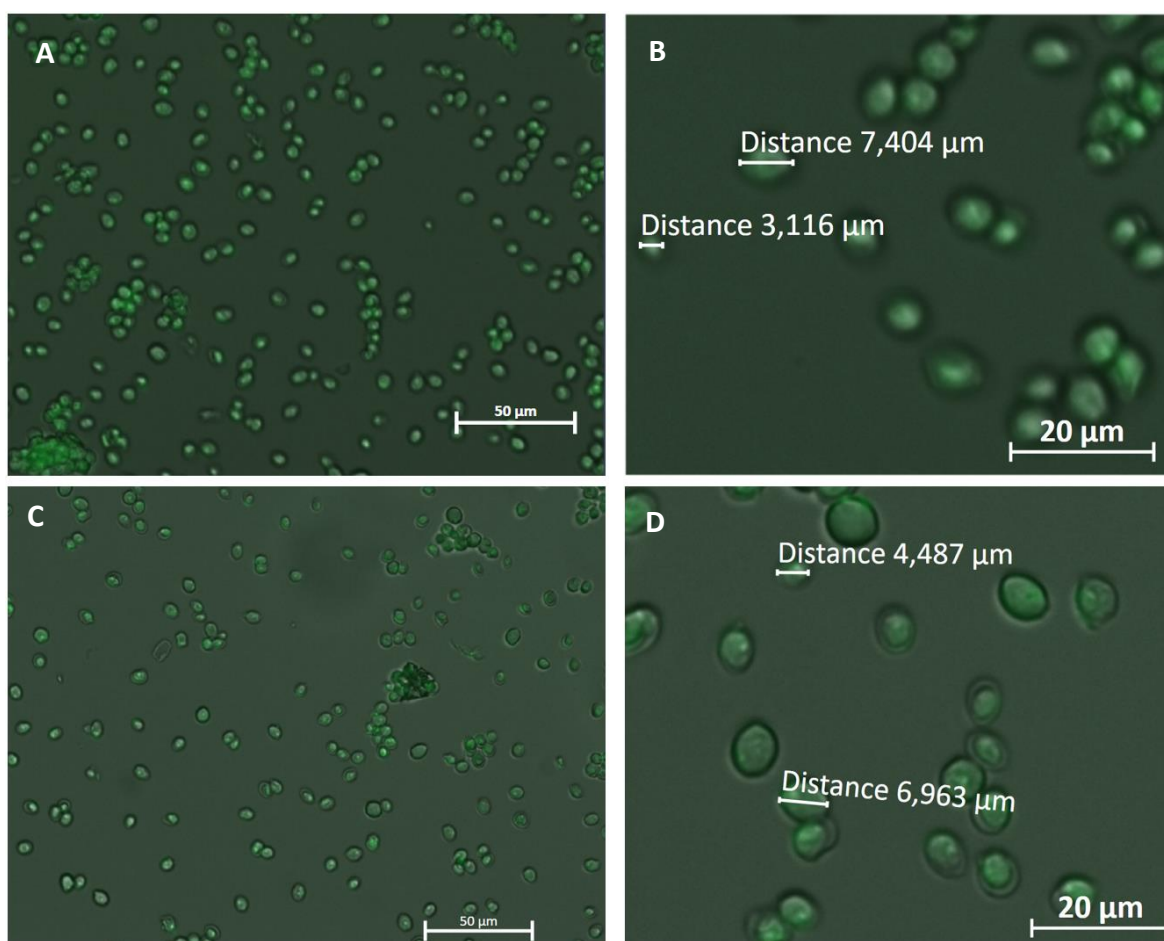


Figure 15: Widefield fluorescence microscopy micrographs of autofluorescent YMCAPs_Aut (A and B) and YMCAPs_4M (C and D).

4.1.2. Structural analysis

4.1.2.1. Neutral sugar analysis

With the purpose of obtaining drug microcarriers derived from the BSY *S. pastorianus*, the yeast cell wall isolation was promoted by a thermal and alkali treatment. The thermal treatment (autolysis) using a temperature superior to 45°C allows the solubilization of the cytoplasmatic content and the separation of the yeast cell wall (insoluble and denser) by centrifugation⁶⁷. The followed alkali treatment with 4M KOH was used to tailor the YMCAPs surface through the solubilization of the dense entangle mannoproteins while maintaining the inner layers of the yeast cell wall practically intact⁶⁷. The sugar composition and the amount of carbohydrates present in the initial yeast and in the obtained microcapsules were determined by neutral sugars analysis, the results of which are summarized in Table 6.

Table 6: Carbohydrate analysis and yields from autolysis and 4M KOH extraction.

Fraction	Yield (%) (w/w)	Carbohydrate (mol %)			Total carbohydrate (mg/g)
		Rib	Man	Glc	
BSY	-	4	23	73	328
YMCAPs_Aut	79.8	2	24	74	415
Sn Aut	0.1	44	30	26	98
sn 4M	9.5 (11.6)	-	51	49	566
pp 4M	8.5 (10.4)	-	7	93	268
sn FR 4M	1.7 (3.4)	-	11	89	661
YMCAPs_4M	18.5 (38.1)	-	4	96	536

Rib: ribose; Man: mannose; Glc: glucose; BSY: brewer's spent yeast. The yield values without brackets were calculated in function of BSY mass basis; The yield values in brackets were calculated in function of YMCAPs_Aut mass basis.

The initial yeast has a moisture content of 78 % and, therefore, a percentage of total solids of 22 %. With autolysis, a mass yield of about 0.1 % (w/w) of soluble material and 79.8 % (w/w) of insoluble material (YMCAPs_Aut) was achieved, containing 42 % of carbohydrates. Considering the mass yields calculated in function of BSY mass basis, the alkali extraction allowed a mass yield of 18 % (w/w) of soluble material (sum of yields of sn 4M and pp 4M) and 20 % (w/w) remained insoluble (sum of yields of YMCAPs_4M and sn FR 4M). However, from de insoluble material, a mass yield of 1.7 % (w/w) was obtained from the material that become soluble in water upon dialysis (sn FR 4M). From the solubilized material, a mass yield of 8.5 % (w/w) was obtained from the material that

precipitated upon dialysis (pp 4M). This process allowed the obtention of YMCAPs_4M with 54 % of carbohydrates. The alkali extraction with a strong base (4M KOH) achieved a higher mass yield of solubilized sugars compared to the other isolation process (autolysis), which indicates that the sugar solubilization was more extensive in this process. Similarly, a higher carbohydrate percentage was achieved in YMCAPs_4M in comparison to the thermal autolysis treatment (YMCAPs_Aut), which may indicate a higher protein content in the YMCAPs_Aut. Other studies, where a sequential extraction of yeast polysaccharides methodology (alcohol insoluble residues were submitted to a hot water extraction, followed by a sequential alkali extractions with 0.1M KOH, 1M KOH and 4M KOH), were more extensive in polysaccharide extraction together with proteins, releasing a final residue enriched in polysaccharides containing 68 % of carbohydrates⁶⁵.

According to the results of the sugar analysis, total carbohydrate content in BSY reaches 33 %, composed of 73 mol % Glc, 23 mol % Man, and 4 mol % Rib residues. The enrichment of *S. pastorianus* in Glc, followed by Man is corroborated by structural yeast cell wall characterization studies, in which glucans are described as Glc polymers, being the predominant polysaccharide in the yeast cell wall, and mannoproteins as protein-linked to mannose residues⁶².

The polysaccharides composition of YMCAPs is dependent on the methodology applied to their isolation. As a result, the produced YMCAPs possess perceptible surface composition differences. During the thermal autolysis, the increase of temperature induces a self-destructive action of the yeast which, under the used experimental conditions (temperature and reaction time), promotes the remotion of the cytoplasmatic content while keeping the structure of the cell wall intact, resulting in YMCAPs herein designated as YMCAPs_Aut. The remotion of the intracellular content (soluble material) may be inferred by the highly recovered of Rib (a sugar constituent of the ribonucleic acids) in the autolysis supernatant (44 mol %), compared to the autolysis residue (2 mol %). YMCAPs_Aut have in their structure 74 mol % of Glc residues and 24 mol % of Man residues, corresponding to 42 % of total carbohydrates. Although some Glc and Man residues were released and are present in the supernatant, the quantity of Glc and Man remains the same after autolysis, compared to BSY, demonstrating that there was no significant change in the structural composition of the yeast cell wall during its isolation and purification. Subsequently, the alkali treatment with 4M KOH result both in a soluble and insoluble fraction. Each of these fractions was then neutralized, dialyzed, and centrifuged, allowing the physical separation of a supernatant (sn 4M), a precipitate (pp 4M), a material that become soluble upon the dialysis step (sn FR 4M) and an insoluble final residue, also called YMCAPs_4M. This treatment enables the extraction of some polysaccharides, namely superficially located mannoproteins (51 mol % of Man residues become soluble) and

probably glycogen (49 mol % of Glc), leading to YMCAPs_4M with Glc residues (96 mol %) and 4 mol % of Man residues that remained retained, demonstrating the obtention of YMCAPs_4M with resistant β -glucans exposed.

4.1.2.2. Glycosidic linkages analysis

To characterize the type of glycosidic bonds that link the structural constituent monosaccharides, partial methylation of the YMCAPs polysaccharides was performed. In general, the sugar percentage obtained by neutral sugar analysis is comparable to the number of linkages involving Glc and Man residues (Table 7). The proportional maintenance of the carbohydrate composition supports the results derived from both analyses.

In both YMCAPs, there is a prevalence of (1 \rightarrow 4)-linked glucans, with a molar percentage of 50.2 % in the YMCAPs_Aut and 52.8 % in the YMCAPs_4M. The (1 \rightarrow 4)-linked glucans in YMCAPs_Aut are branched with 2.8 mol % of Glc residues linked by (1 \rightarrow 4,6) and 10.6 mol % of terminally linked Glc. Similarly, the YMCAPs_4M have 2.6 mol % of Glc residues linked by (1 \rightarrow 4,6) and 13.3 mol % of terminally linked Glc. The prevalence of Glc residues linked by (1 \rightarrow 4)-glycosidic bonds was previously identified in the *S. pastorianus* cell wall⁶⁵, where the anomeric configuration were 55 mol % of (α 1 \rightarrow 4) and 30 mol % of (β 1 \rightarrow 4)⁶².

The analysis of glycosidic bonds also revealed the presence of (1 \rightarrow 3)-linked glucans (13.5 mol % in YMCAPs_Aut and 20 mol % in YMCAPs_4M) and, in a minor quantity, of (1 \rightarrow 6)-linked glucans (2.5 mol % YMCAPs_Aut and 2.7 mol % in YMCAPs_4M). The higher mol % of Glc residues (1 \rightarrow 3)-linked in comparison with Glc residues (1 \rightarrow 6)-linked is in agreement with the yeast cell wall structural characteristics described in literature to the genus *Saccharomyces*^{62,65,66}. The (1 \rightarrow 3)-linked glucans present in the YMCAPs are slightly branched. It was only determined 0.2 mol % of (1 \rightarrow 3,4)-Glc in both microcapsules, 2.0 mol % and 2.3 mol % of (1 \rightarrow 3,6)-Glc in YMCAPs_Aut and YMCAPs_4M, respectively, and 0.1 mol % of (1 \rightarrow 3,4,6)-Glc in YMCAPs_Aut. The latter linkage reveals the presence of Glc residues with two branches. In addition, (1 \rightarrow 6)-linked glucans are highly branched molecules being the mol % of branches involving the (1 \rightarrow 6)-linked glucans higher than the mol % of linear (1 \rightarrow 6)-linked glucans, which is in accordance with what is portrayed in the literature⁶³. Furthermore, the conditions used during the alkali extraction were conducive to the non-destruction of the glucans structure, allowing a general maintenance of their type of linkages.

Table 7: Glycosidic linkages composition (mol %) of the different fractions obtained during the YMCAPs isolation.

Glycosidic Linkages	Brewer's spent yeast <i>Saccharomyces pastorianus</i>				
	YMCAPs_Aut	YMCAPs_4M	sn FR 4M	pp 4M	sn 4M
t-Glc	10.6	13.3	11.6	12.1	7.9
3-Glc	13.5	20.0	-	9.3	0.2
4-Glc	50.2	52.8	73.1	59.9	48.3
6-Glc	2.5	2.7	0.4	2.1	0.3
3,4-Glc	0.2	0.2	-	0.2	0.1
3,6-Glc	2.0	2.3	1.0	1.8	0.8
4,6-Glc	2.8	2.6	3.9	3.6	2.7
3,4,6-Glc	0.1	-	-	0.1	-
2,3,4,6-Glc	3.2	3.0	4.2	3.3	4.6
Total	85.1 (74)	97.0 (96)	94.2 (89)	92.3 (93)	64.9 (49)
t-Man	8.7	1.4	3.2	6.5	23.0
2-Man	3.0	0.4	1.0	0.8	6.6
3-Man	1.4	0.2	0.4	0.3	3.3
6-Man	0.2	0.1	-	0.1	0.3
2,3-Man	0.4	0.3	-	-	-
2,6-Man	0.8	-	-	0.3	1.1
3,6-Man	0.1	-	-	0.1	0.1
2,3,4,6-Man	0.7	0.4	1.2	0.4	0.5
Total	15.3 (24)	2.7 (4)	5.8 (11)	8.4 (7)	34.8 (51)
4-GlcNAc	0.4	0.4	-	0.1	0.3
Total	0.4 (n.d.)	0.4 (n.d.)	-	0.1 (n.d.)	0.3 (n.d.)

The values obtained in sugar analysis are presented between brackets

n.d. not determined in sugar analysis

Combining the published available information and the results of the glycosidic analysis, it can be assumed that the carbohydrate part of mannoproteins in YMCAPs_Aut is composed of a main chain of (1→6)-Man (0.2 mol %) with side chains of (1→2)-linked Man residues (3 mol %) that end in (1→3)-Man (1.4 mol %). Moreover, these microcapsules contain Man residues linked by (1→2,6)-, (1→2,3)-, and (1→3,6)- in a proportion of 0.8 mol %, 0.4 mol % and 0.1 mol %, respectively. Considering the occurrence of these glycosidic linkages and the total of Man in this fraction, the degree of branching of these highly branched mannoproteins in YMCAPs_Aut was determined to

be 8.5 %. The covalent bonds between mannoproteins and glucans are removed under an alkali environment in which mannans are soluble⁶⁷. In fact, after the alkali extraction, the mannoproteins content was reduced from 15 mol % (in YMCAPs_Aut) to 3 mol % (in YMCAPs_4M), which, once more, not only supports the removal of this alkali-soluble polysaccharide from the yeast cell wall, but also emphasizes the elevated number of Glc residues (97 mol %) and, in this regard, of glucans in YMCAPs_4M. The (1→2,6)-Man linkage in the sn 4M fraction is an indication of the occurrence of mannans solubilization, essentially at the type *N* mannoproteins level, since this branching residue is only present in this mannose-carbohydrate chains^{65,66}. Thereby, the 3 mol % of Man residues with fewer branches that remained in the YMCAPs after the treatment with 4M KOH, may correspond to mannoproteins that establish type *O* glycosidic bonds. These are mannoproteins with a short carbohydrate chain, distributed in an inner region, close to the cytoplasmatic membrane^{65,66}. In addition, the soluble material has 35 mol % of extracted mannoproteins, with a higher proportion of terminally linked Man (23 mol %) when compared to the Man branched residues, which may suggest a greater extraction of lower MW mannoproteins^{65,134}.

Furthermore, as a consequence of 4M KOH extraction, a higher mol % of glucans were found both in the soluble material (65 mol %) and in the pp 4M (93 mol %). Most of these glucans are (1→4)-linked glucans with (1→4,6)-Glc, a characteristic structure of glycogen, which might point that the alkali extraction provide the ideal conditions for the removal of intracellular and insoluble glycogen, that may not be extracted during the autolysis⁶². Glycogen is a polysaccharide particularly difficult to remove from the yeast cell wall, since this α -glucan is entrapped within the dense carbohydrate structure of the yeast cell wall, establishing linkages with β -glucans⁶⁷.

The material that remained insoluble after 4M KOH extraction was dialyzed, allowing to recover new polysaccharide fractions. Owing to this process, a fraction (sn FR 4M) enriched in glucans (94.2 mol %), in particular glucans with Glc residues linked by (1→4)-glycosidic bonds (73.1 mol %), terminally linked (11.6 mol %), and (1→4,6)-Glc (3.9 mol %) consistent with glycogen⁶². Also, the solubilization of Man polymers that persisted after the alkali extraction (6 mol %) was also observed, contributing to the reduction of this type of polysaccharide in the YMCAPs_4M.

It should also be noted that methylation analysis enabled the detection of reduced amounts of (1→4)-GlcNAc (≤ 0.4 mol %). The (1→4)-GlcNAc probably corresponds to chitin and/or to the type *N* mannoproteins, in which the linkage between the protein and the glycosylated part is established by two residues of (1→4)-GlcNAc¹³⁵.

The presence of glucitol acetate- (1→2,3,4,6)-Glc - and mannitol acetate - (1→2,3,4,6)-Man may be associated with sub-methylated of the highly branched cell wall polysaccharides. An inefficient

methylation may be related to the dense entangled cell wall structure that restrains the accessibility of the methylating agent to the yeast sugars.

4.1.2.3. Protein content and amino acid analysis

The YMCAPs protein content was determined by combining elemental analysis and amino acid analysis. According to the results described in Table 8, the nitrogen content determined by the elemental analysis corresponds to a protein concentration of 384 mg/g in YMCAPs_Aut and 340 mg/g in YMCAPs_4M. The protein may establish a complex with Man residues, in a form of mannoproteins. The decreasing on protein content in YMCAPs_4M after alkali extraction, accompanied with the protein recovered in the solubilized fractions (169 and 78 mg/g in sn 4M and sn FR 4M, respectively), further supports the removal of part of the densely branched network of mannoproteins present in the yeast cell wall. The concentration in YMCAPs_4M was reduced by 11.4 %, which corresponds to a decrease of 44 mg/g. Bearing in mind that the protein concentration was established with reference to % N, there is a potential upward bias in the estimated values, given the existence of nucleotides in YMCAPs_Aut, even in a lower percentage, in which nitrogen bases are also present (e.g., Rib residues). Furthermore, combining the results of sugar analysis and protein analysis, the extraction of Man residues was much more extensive compared to the protein extraction that are in accordance to the *N*-type mannoproteins extracted, with more than 90 % of carbohydrates and less than 10 % of protein⁶⁵.

Table 8: Protein content in YMCAPs and solubilized material determined based on % N and its conversion using the Kjeldahal factor (6.25).

	% N	Concentration (mg/g)
YMCAPs_Aut	6.1	384
YMCAPs_4M	5.4	340
sn 4M	2.7	169
sn FR 4M	1.2	78

Likewise, the sum of the detected amino acids determined through acid hydrolysis is in concordance with the protein concentration obtained from the elemental analysis. According to the literature, the most abundant amino acids in BSY include glutamic acid, aspartic acid, and lysine, while methionine and cysteine are the least abundant¹³⁶. The amino acid profile of YMCAPs_Aut

and YMCAPs_4M reveals that the predominant amino acids in both YMCAPs are asparagine/aspartic acid, glutamine/glutamic acid, and lysine, which is in conformity with the literature (Table 9). Contrarily, serine and threonine were only found in trace amounts. With 4M KOH extraction asparagine/aspartic acid, glutamine/glutamic acid, phenylalanine, and lysine were solubilized, thereby its concentration decreases in these YMCAPs surface.

Although cysteine, methionine, tyrosine, and tryptophan have already been identified in BSYs¹³⁶, they were not detected in YMCAPs. Some amino acids present instability during acid hydrolysis, undergoing transformations during this process. Although they are released from the peptide sequence by acid hydrolysis, some suffer partial or complete destruction. For instance, tyrosine is partially destroyed¹³⁷ and may undergo halogenation¹³⁸. The same destruction happens to serine and threonine, with a loss of approximately 5 to 10 %^{137,138}. Besides this, in this very acidic and high temperature environment, cysteine and tryptophan are destroyed and therefore they cannot be directly determined by acid hydrolysis^{137,138}. Performing hydrolysis under a nitrogen atmosphere is of extremely importance to minimize the degradation phenomena. In the case of an inefficient oxygen removal, methionine can be oxidized to methionine sulfoxide and methionine sulfone, impeding their detection. However, for other amino acids, the hydrolysis conditions (HCl 6M, 24 h at 110°C) may not be sufficient to cleave the peptide bonds and release them. Valine and isoleucine contain peptide bonds with very hydrophobic residues that are quite resistant to acid cleavage, especially in sequences as Ile-Ile, Val-Val, Ile-Val, thus the amounts obtained from these amino acids are often low^{137,138}. Asparagine and glutamine undergo deamination reactions, being converted into aspartic acid and glutamic acid and, therefore, are incorporated into the value of the respective acid, preventing their distinction and resulting in the overestimation of the acidic form^{137,138}. Taking into account the limitations of this methodology, the non-detection of some amino acids is expected, and the obtained values are considered an approximation to the real ones.

Table 9: Amino acids profile of YMCAPs_Aut and YMCAPs_4M.

	YMCAPs_Aut ($\mu\text{g}/\text{mg}$)	YMCAPs_4M ($\mu\text{g}/\text{mg}$)
Ala	6.74	9.36
Apx	70.56	62.18
Glx	66.61	48.63
Gly	12.60	15.10
Ile	33.26	37.33
Leu	32.13	29.58
Lys	78.71	62.52
Phe	43.28	32.73
Pro	23.29	28.06
Ser	t	t
Thr	t	t
Val	14.89	19.22
Total	382.08	344.71

Ala: alanine; Asx: asparagine/aspartic acid; Glx: glutamine/glutamic acid; Gly: glycine; Ile: isoleucine; Leu: leucine; Lys: lysine; Phe: phenylalanine; Pro: proline; Val: valine; t: trace.

4.2. YMCAPs_Aut modification with norbornene and methacrylic moieties

The functionalization of the YMCAPs surface with photocrosslinkable chemical groups were performed with the purpose to create a multi-YMCAPs/GelMA hybrid hydrogel platform, through the chemical reaction of modified YMCAPs with GelMA. The YMCAPs functionalization efficiency with carbic anhydride and methacrylic anhydride was investigated through FTIR, ssNMR and glycosidic linkage analysis. The chemical modification was only carried out for one type of YMCAPs – YMCAPs_Aut. The exclusion of YMCAPs_4M was based on material dispersion in PBS solution. YMCAPs_4M sedimented more quickly compared to YMCAPs_Aut (Figure 16), evidencing their poor dispersion in PBS, an unsuitable characteristic for the formation of a platform where it is intended to have a homogeneous distribution of YMCAPs in the hydrogel matrix. The differences observed might be related with YMCAPs zeta potential, since the material surface charge influences the stability of the suspension. The neutral charge of YMCAPs_4M enables interparticle interactions through van der Waals attractive forces, promoting their flocculation¹³⁹. On the other hand, YMCAPs_Aut with a lower zeta potential ($-13.9 \text{ mV} \pm 0.239 \text{ mV}$) seems to present a higher

suspension stability attributable to the higher electrostatic repulsive forces between YMCAPs, which is translated in a lower sedimentation rate¹³⁹. Thus, from now on, only the microcapsules resulting from the autolysis process were used.

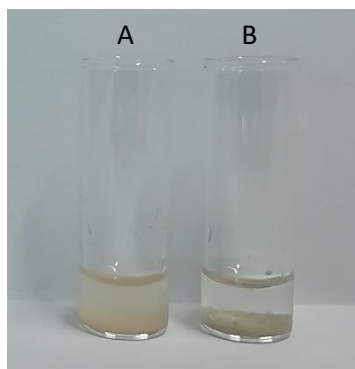


Figure 16: Dispersion of YMCAPs in PBS. A) YMCAPs_Aut; B) YMCAPs_4M.

4.2.1. Fourier-transformed infrared spectroscopy

The chemical modification of YMCAPs_Aut was confirmed by FTIR spectroscopy (Figure 17). The FTIR spectra of modified and unmodified YMCAPs display a broad peak above 3000 cm^{-1} corresponding to -OH stretching, essentially derived from the absorbed water¹⁴⁰. The 2920 and 2853 cm^{-1} peaks are assigned to CH_2 asymmetric stretching vibration of proteins and carbohydrates, respectively¹⁴¹. A signal of the protein component is observed at 1630 cm^{-1} – amide band I related to C=O stretching vibrations, and at 1522 cm^{-1} – amide band II related to N-H and C-N vibrations of the peptide bond^{142–144}. Also, it is observed a peak at 1455 cm^{-1} corresponding to asymmetric deformation of CH_3 and CH_2 in proteins and peptides^{142–144}. The peak observed at 1373 cm^{-1} may be attributable ($\beta 1\rightarrow 3$)-linkages from glucans⁷². Although the intracellular content of yeast was removed during the YMCAPs_Aut isolation and purification, it is possible to observe a peak appearing at 1236 cm^{-1} which corresponds to the asymmetric PO_2^- stretching vibration of free nucleotides, probably resulting from DNA and RNA degradation^{142,143}. The asymmetric PO_2^- stretching vibration in this region may also be attributable to the highly phosphorylated mannoproteins. Another peak can be found at 1078 cm^{-1} corresponding to symmetric P=O stretching vibration from phosphate, mainly related to phosphorylated mannoproteins and Rib sugar in RNA^{142,143,145}. Notwithstanding, the latter peak may also be attributable to ($\beta 1\rightarrow 3$)-glucans¹⁴⁶. According to literature, the absorption region of carbohydrates, including β -glucans and mannans, extends from ~ 1200 to 780 cm^{-1} ^{142–144}. In the obtained spectrum, the characteristic peaks assigned to C-O, C-OH and C-O-C stretching of yeast cell wall polysaccharides appear around 1148

cm^{-1} and 1019 cm^{-1} ^{72,142–144}. The mixed region between $920\text{--}780 \text{ cm}^{-1}$ comprises the glucans and mannans absorption and respective β - and α -glycosidic vibrations and pyranose ring vibrations^{142,143,146}.

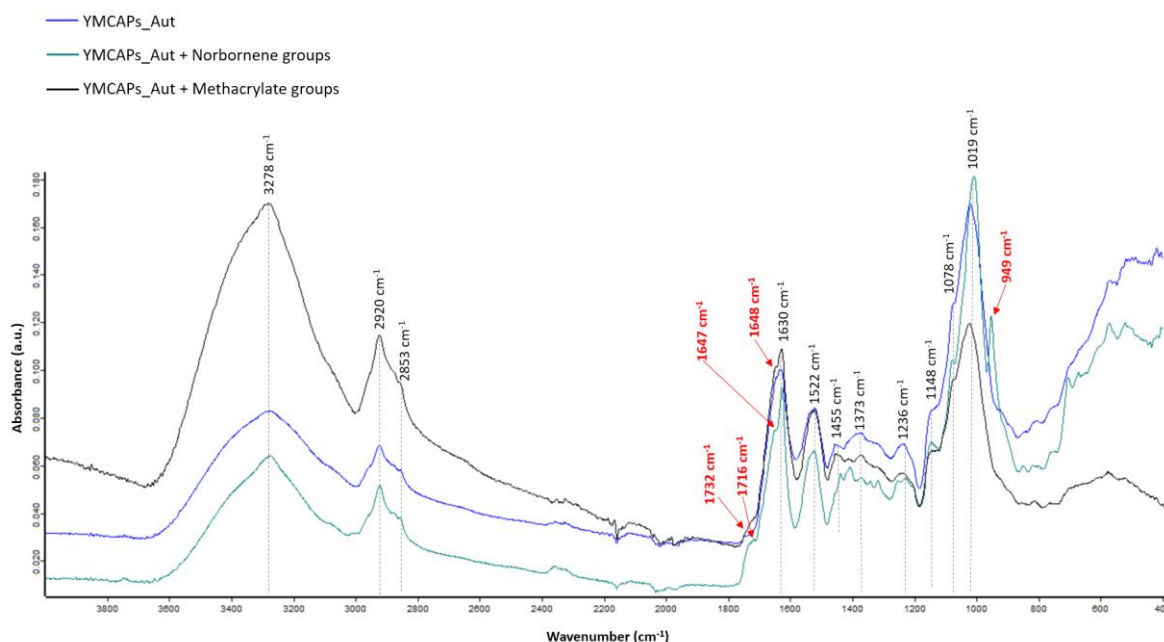


Figure 17: ATR-FTIR spectra of YMCAPs_Aut isolated from *Saccharomyces pastorianus* pre- and post-modification with norbornene and methacrylate groups in the $4000\text{--}400 \text{ cm}^{-1}$ range. The red wavenumbers are the peaks assigned to the chemical modifications in YMCAPs.

After modification, new bands are expected to appear in the wavenumber spectral region between ~ 1800 to 900 cm^{-1} . In the case of the YMCAPs_Aut treated with carbic anhydride, a small peak arises at 1716 cm^{-1} indicative of the ester bond established between the carbic anhydride and YMCAPs_Aut via an esterification reaction¹⁴⁷. Moreover, an additional 1647 cm^{-1} peak corresponding to alkene bonds from the norbornene group appears in the spectra¹⁴⁸. The new peak appearing in 949 cm^{-1} region might be related to mannans' modification, as other studies refer mannans' specific peaks appearing at ~ 911 and 972 cm^{-1} ¹⁴⁶. Regarding methacrylation of YMCAPs_Aut, new small shoulder peaks appear at 1648 cm^{-1} representing the C=C stretching in methacrylate moiety, and at 1732 cm^{-1} manifesting the carbonyl group (C=O) stretching¹⁴⁹. The presence of these new peaks confirms the YMCAPs_Aut chemical modification and, consequently, the incorporation of sites for chemical interaction essential for the platform formation.

4.2.2. Solid-state nuclear magnetic resonance spectroscopy

The successful modification of YMCAPs_Aut was also confirmed by ssNMR. In cross-polarization/magic angle spinning (CP-MAS) spectrum of YMCAPs_Aut, protein and carbohydrate regions may be exploited. Protein regions appear around 180 to 120 ppm and 50 to 0 ppm. In the carbohydrate region between 110 ppm to 60 ppm, C_1 (100 ppm), C_4 (85 ppm), C_2/C_3 (80 to 70 ppm) and C_6 (60 ppm) resonances of the sugar rings can be distinguished¹⁵⁰.

As shown in B-A spectrum of Figure 18A, several additional resonance peaks appear, arising from the incorporated norbornene group in YMCAPs_Aut surface. Upon reaction with carbic anhydride, a peak emerged at 170 ppm, which is assigned to the carbon of the anhydride carbonyl group¹⁵¹. The peak visible at 135 ppm is attributable to the alkene bond in the norbornene group¹⁵¹. At around 50 ppm, some differences can be found, corresponding to the bridge protons, bridgehead carbons and C-H bond of the carbic group¹⁵¹. Furthermore, the difference between CP-MAS spectrum of YMCAPs_Aut and CP-MAS spectrum of YMCAPs_Aut + Norbornene reveals possible Glc and Man carbons, probably in the C_2 , C_3 , C_4 and C_6 , and protein residues bonded to norbornene. C_6 of sugars have a higher susceptibility to react with norbornene. However, as observed in CP-MAS spectrum, the modification also occurred in the other sugar carbons (C_2 , C_3 , C_4) available for the chemical modification.

In the case of methacrylated sample, the B-A spectrum shows the appearance of additional resonance peaks of the methacrylic, providing evidence of modification (Figure 18B). The peak around 170 ppm is attributable to C=O of the anhydride group¹⁵². At 130 and 140 ppm the carbon signals of C=C double bond are present¹⁵². In addition, the peak at 20 ppm corresponds to the CH₃ of methacrylic anhydride¹⁵². Once more, the differences between the two spectrums, indicate possible protein and carbohydrate residues (C_1 , C_2 , C_3 , C_4 and C_6) bonded to methacrylic anhydride.

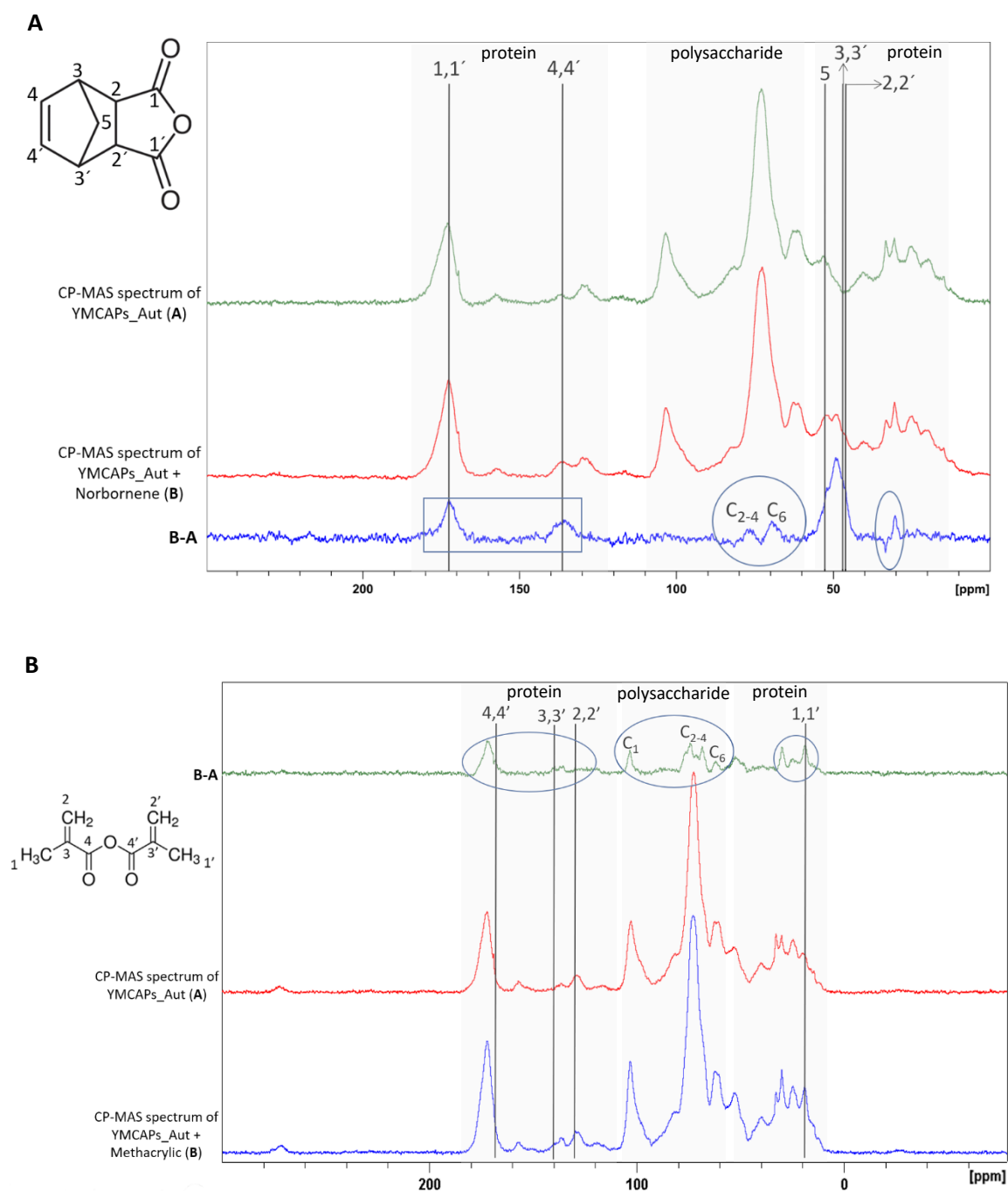


Figure 18: Solid state CP-MAS NMR spectrum of A) unmodified and norbornene modified YMCAPs_Aut and respective subtractive spectrum; B) unmodified and methacrylated YMCAPs_Aut and respective subtractive spectrum.

Through the integration of the resonance peaks in the CP-MAS quantitative spectrum from $\delta=200$ to 0 ppm, it is possible to quantify the number of norbornene or methacrylic moles in the YMCAPs_Aut (Table 10). Accordingly, 0.461 mmol of norbornene per gram of YMCAPs_Aut were

quantified, which correspond to a yield of 44 % and to a DS of 8.6 %. Notably, the reaction with methacrylic anhydride were considerably more extensive with a yield of 73 %, which represent the presence of 1.425 mmol of methacrylate groups per gram of YMCAPs_Aut and a DS of 26.4 %. It is noteworthy that future optimizations of carbic anhydride and methacrylic anhydride amount used for the modification reaction may improve considerably the DS, and possibly, the extension of modification might be controlled.

Table 10: Extension of chemical functionalization of YMCAPs_Aut with norbornene and methacrylic groups.

	mmols per gram	Yield (%)	Degree of substitution (%)
Norbornene	0.461	43.5	8.6
Methacrylate	1.425	73.1	26.4

4.2.3. Glycosidic linkage analysis

Glycosidic linkage analysis allows the comparison between the YMCAPs_Aut and chemically modified YMCAPs_Aut for the identification of specific binding sites of the functional groups in YMCAPs_Aut carbohydrates (Table 11).

Considering the autolysis residue modified with carbic anhydride, it is observed that the chemically modified sample suffers a decrease in (1→3)-linked glucans and (1→6)-linked glucans from 56.1 mg/g to 44.4 mg/g and 10.6 mg/g to 4.4 mg/g, respectively. The reduction of (1→3)-Glc is accompanied by an increase of (1→2,3,4,6)-Glc branches, suggesting the presence of the norbornene group in C₂, C₄ and C₆ of Glc residues. Similarly, the reduction of (1→6)-Glc, combined with the increase of (1→2,3,4,6)-Glc branches, also indicates a change in C₂, C₃ and C₄. Furthermore, the difference in C₂ is further detected by the occurrence (1→2,4)-linked glucans, which is believed to appears after chemical modification of C₂ in (1→4)-glucans. These results are in agreement with those obtained by ssNMR, where an increase of peak intensity, due to norbornene binding to C₂₋₆ sugar carbons, was observed. On the other hand, it is possible to verify an increase of (1→4)-Glc from 209 mg/g to 237 mg/g, which may arise from the modification in the Glc terminals that were declined post-modification.

With respect to the YMCAPs_Aut modified with methacrylic anhydride, it is possible to identify differences in the terminally linked Glc, with a reduction from 43.9 mg/g to 40.0 mg/g, in parallel with an enhancement of linear (1→3)- and (1→4)-linkages, from 56.1 mg/g to 58.9 mg/g and 208.8 mg/g to 220.1 mg/g, respectively. The change in the absolute number of these linkages may result

from the modification in C₁, which was also observed in ssNMR spectrum. In addition, the decrease of (1→6)-Glc, accompanied by an increase in the (1→3,4,6)-Glc branch, indicates the presence of methacrylate moieties in C₃ and C₄. Similar to YMCAPs_Aut modified with carbic anhydride, some modification occurs in C₂ revealed with the appearance of (1→2,4)-linked glucans.

Table 11: Glycosidic linkages composition (mol % and mg/g) of the different YMCAPs_Aut modified fractions.

Glycosidic Linkages	Chemically modified BSY <i>Saccharomyces pastorianus</i>		
	YMCAPs_Aut	YMCAPs_Aut + Carbic Anhydride	YMCAPs_Aut + Methacrylic Anhydride
t-Glc	10.6 (43.9)	8.9 (39.5)	9.2 (40.9)
3-Glc	13.5 (56.1)	10.0 (44.4)	13.3 (58.9)
4-Glc	50.2 (208.8)	53.4 (237.1)	49.5 (220.1)
6-Glc	2.5 (10.6)	1.0 (4.4)	2.1 (9.4)
3,4-Glc	0.2 (0.8)	0.2 (0.8)	0.1 (0.5)
3,6-Glc	2.0 (8.3)	1.5 (6.7)	1.8 (8.0)
2,4-Glc	-	0.1 (0.5)	0.1 (0.6)
4,6-Glc	2.8 (14.1)	2.7 (12.2)	2.6 (11.6)
3,4,6-Glc	0.1 (0.4)	0.1 (0.3)	0.1 (0.5)
2,3,4,6-Glc	3.2 (13.3)	4.1 (18.3)	2.1 (9.2)
Total	85.1 (356.3)	81.9 (364.1)	80.9 (359.6)
t-Man	8.7 (36.5)	10.7 (47.3)	10.8 (47.8)
2-Man	3.0 (12.6)	3.4 (15.0)	3.8 (16.8)
3-Man	1.4 (5.7)	1.9 (8.4)	1.9 (8.4)
6-Man	0.2 (0.9)	0.2 (0.8)	0.2 (1.0)
2,3-Man	0.4 (1.8)	0.3 (1.5)	0.8 (3.4)
2,6-Man	0.8 (3.2)	0.8 (3.5)	0.9 (4.0)
3,6-Man	0.1 (0.3)	0.1 (0.3)	0.1 (0.4)
2,3,4,6-Man	0.7 (2.9)	0.3 (1.3)	0.5 (2.1)
Total	15.3 (63.9)	17.6 (78.1)	18.9 (83.8)
4-GlcNAc	0.4	0.5	0.3
Total	0.4	0.5	0.3

The values in brackets correspond to the mass balance (mg/g)

Despite the modifications in Glc linkages being tenuous, they coincide with the carbohydrate modifications detected by ssNMR. Nonetheless, the results suggest that the modification occurred

essentially in the mannoproteins, more specifically in the protein domain. As mentioned previously, the YMCAPs_Aut have a dense structure so, the most available regions for the chemical modification are those located in the most superficial layer. In this regard, the YMCAPs_Aut functionalization was successful, being marked with a relatively high binding to NH₂ groups.

4.3. Multi-YMCAPs/GelMA photocrosslinkable hybrid hydrogel platform

Taking into account that chemical modification had a greater extension in the presence of methacrylic anhydride, the formation of a multi-YMCAPs_Aut/GelMA hybrid hydrogel platform, consisting of YMCAPs_Aut incorporated in GelMA hydrogel matrix, was performed using only YMCAPs_Aut functionalized with methacrylate groups. The carbon double bonds introduced in YMCAPs_Aut enable their photocrosslinking with GelMA via free radical polymerization in the presence of a photoinitiator (LAP), resulting in the formation of a 3D hybrid hydrogel⁵¹. Upon blue light exposure, the photon absorption result in LAP cleavage with free radical formation that, by interaction with methacrylate groups present on YMCAPs_Aut and GelMA, initiate the chain polymerization, which propagates within or between polymer chains, resulting in covalent crosslinking³².

YMCAPs_Aut platform disks (GelMA/YMCAPs_Aut and GelMA-c-YMCAPs_Aut) were prepared with 6 mm diameter × 2 mm height (Figure 19). The effects of different percentages of YMCAPs_Aut [1 and 5 % (w/v)] and the influence of YMCAPs_Aut chemical modification in the physical properties of the scaffolds (swelling, water content, degradation rate and Young's modulus) were evaluated.

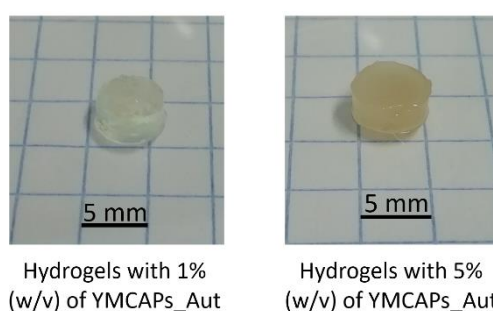


Figure 19: GelMA hybrid hydrogels prepared with 1 and 5 % (w/v) of YMCAPs_Aut, respectively.

4.3.1. Multi-YMCAPs/GelMA platform physical characterization

The prepared hybrid hydrogels are all high-water content biomaterials, an essential feature for upkeeping cellular viability. The water content was determined to be above 80 %, ranging from (84

± 1.7) % in GelMA-c-YMCAPs_Aut_5% to (92 ± 0.4) % in GelMA-c-YMCAPs_Aut_1% (Figure 20). The lower extremity (hydrogels with lower water content) is represented by scaffolds with higher YMCAPs_Aut percentage, while in the higher extremity are the hydrogels with lower YMCAPs_Aut percentage.

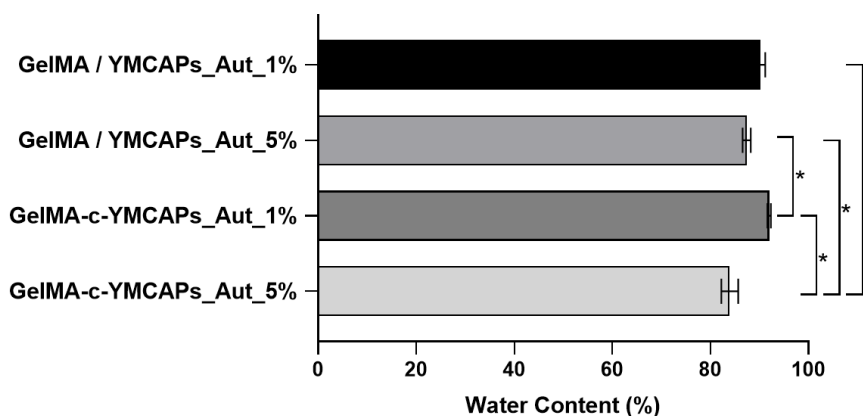


Figure 20: Water content ratio of GelMA/YMCAPs_Aut and GelMA-c-YMCAPs_Aut. Data is represented as mean \pm standard deviation (n=3). * $p < 0.05$

Additional water uptake capacity after crosslinking is an important hydrogel feature that may affect the gas exchange, nutrients diffusion, hydrogel surface, mechanical properties and thus, the healing process^{153–155}. After 48 h, the hydrogel reached an equilibrium, with a maximum mass increase of (20.2 ± 2.6) %, in the case of GelMA/YMCAPs_Aut_1%, indicating a lower swelling ratio of the prepared hybrid hydrogels. According to the data reported in Figure 21, the swelling ratio decreases with the increase in the hydrogel matrix of the YMCAPs_Aut percentage from (13.7 ± 2.8) % to (4.4 ± 1.8) % in GelMA-c-YMCAPs_Aut, in 24 h. Similarly, the incorporation of chemically modified YMCAPs_Aut diminishes the swelling capability, which may be attributed to the increase of crosslinking points, and consequent reduction of polymer chains mobility¹⁵⁶.

From 4 h to 24 h, the reduction of GelMA/YMCAPs_Aut_5% swelling ratio may be indicative of initial mass loss of this hydrogel.

Overall, the combination of a higher yeast capsules concentration [5 % (w/v)] and photocrosslinkable YMCAPs_Aut, densify the crosslinking structure, which may improve the stiffness of the hydrogel^{153,157}, thus leading to a substantial reduction of PBS absorption capacity (4.4 ± 1.8) %. Analogous results were obtained by photopolymerization of GelMA with poly (ethylene glycol) diacrylate¹⁵⁷. This change in swelling is relevant for biomedical applications, since a greater swelling is generally associated with both a weakening of hydrogels matrix and a fluid-

mediated pressure increase under the area aimed to be regenerated. As a result, this can be a stimulus for additional inflammation, and must be further characterized with *in vivo* assays^{157,158}.

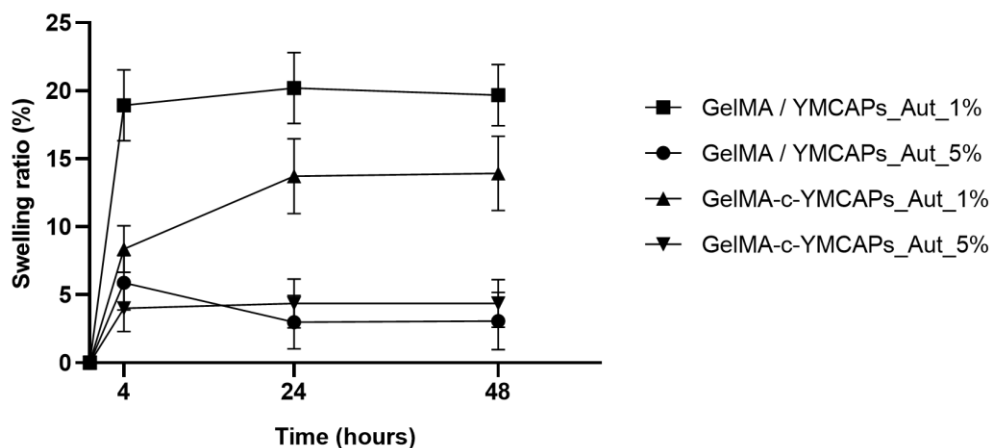


Figure 21: Swelling ratio of GelMA/YMCAPs_Aut and GelMA-c-YMCAPs_Aut after immersion in PBS, at 37°C for 4, 24 and 48 h. Data is represented as mean \pm standard deviation (n=3).

The degradation behaviour is an essential parameter that affects the cell and YMCAPs_Aut delivery in the biological environment, and consequently, the drug release and osseointegration. After 28 days immersed in PBS at 37°C, the mass loss of GelMA/YMCAPs_Aut_1%, GelMA-c-YMCAPs_Aut_1% and GelMA-c-YMCAPs_Aut_5% occurred in a similar way, being the remained weight percentages (88.3 ± 2.7 %), (85.5 ± 1.7 %) and (86.7 ± 3.1 %), respectively (Figure 22). Regarding GelMA/YMCAPs_Aut, the increase of YMCAPs_Aut content is associated with a faster degradation rate of the hydrogel. The mass loss of GelMA/YMCAPs_Aut_5% was perceptible after 3 days, reaching 75 % of decomposition after 28 days. The accelerated degradation of this hybrid hydrogel might be related to the higher instability, prompted by the elevated volume of YMCAPs_Aut in the hydrogel matrix and by the weak interaction forces between GelMA and YMCAPs_Aut. The polymer matrix/YMCAPs_Aut (w/w) ratio seems to be inappropriate to adequate maintenance of its initial structure, leading to a quick disintegration. This trend was reversed with the improvement of molecular interactions through the chemical modification of YMCAPs_Aut. Indeed, the results indicate that the degradation may be controlled through the introduction of co-crosslinking GelMA and YMCAPs_Aut. In such circumstances, the use of YMCAPs_Aut not only hold by the GelMA hydrogel, but as an integral part and as a participant in the hydrogel polymerization, reinforce their structure and delay the extensive degradability.

Nonetheless, it is important to take into account that in a *in vivo* environment, hydrogels degradation is dependent on several biological factors, including the presence of other cell types,

biological fluids, etc. Besides keeping the RGD domains present in the collagen, gelatin also preserves degradation moieties in its polymer chains. In a proper repair environment, MMPs (e.g., collagenases and gelatinases) are present and exert a proteolytic activity in various stages of the regeneration process^{159,160}. By a way of illustration, the hydrogel mass loss evaluation of 10 % GelMA (with a DS of 87.8 %) mediated by collagenases activity demonstrated a relatively fast hydrogel degradation, with a mass loss of 38 % within 24 h¹⁶¹. Whereby, *in vivo*, the activity of these enzymes will affect the degradation rate of the GelMA matrix, and consequently, the release of YMCAPs_Aut will be faster. In the bone defect area, the released YMCAPs_Aut will be exposed to: i) macrophages that may internalize the YMCAPs particles and potentiate their degradation; and ii) acid environment resulting from the bone cells activity, that may induce the degradation of mannoproteins and glycogen, due to α linkages susceptibility to acid hydrolysis.

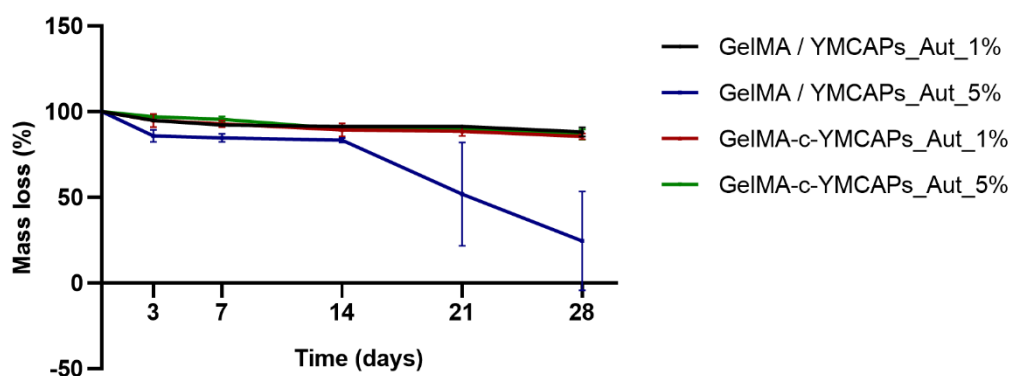


Figure 22: Mass loss profile of GelMA/YMCAPs_Aut and GelMA-c-YMCAPs_Aut immersed in PBS at 37°C for 28 days. Data is represented as mean \pm standard deviation (n=3).

To evaluate the mechanical performance of the prepared hydrogels, a compressive test was carried out. The incorporation of particles within the hydrogel matrix generally supports the dissipation of the loading energy, improving the scaffolds' stress-strain behaviour^{48,49}. The mechanical properties may be modulated with the adjustment of the particles' concentration, being the rise of particles concentration translated into a positive increase of elastic modulus⁴⁸, from (18.2 ± 0.6) % in GelMA-c-YMCAPs_Aut_1% to (24.1 ± 2.4) % in GelMA-c-YMCAPs_Aut_5% (Figure 23). Similar results were obtained combining GelMA with HA, where hydrogel Young's modulus was improved in a HA concentration dependent manner, reaching 24 kPa, which corresponds to a 11 kPa increase compared to bulk GelMA hydrogel¹⁶².

Furthermore, the chemical modification allows the obtention of mechanically more resistant hydrogels. A positive correlation between Young's modulus and the presence of modified

YMCAPs_Aut was observed, indicating that the use of YMCAPs_Aut reinforce the multi-YMCAPs_Aut/GelMA platform. For instance, GelMA-c-YMCAPs_Aut_5% is significantly stiffer than GelMA/YMCAPs_Aut with the same YMCAPs_Aut content. Moreover, the ultimate compressive strength of GelMA/YMCAPs_Aut_1%, GelMA/YMCAPs_Aut_5%, GelMA-c-YMCAPs_Aut_1% and GelMA-c-YMCAPs_Aut_5% was 164.6 kPa, 155.8 kPa, 141.1 kPa and 169.7 kPa, respectively, which further evidence that the chemical crosslinking improves the multi-YMCAPs_Aut/GelMA platform mechanical properties.

GelMA-c-YMCAPs_Aut_5% have a superior Young's modulus among all groups, demonstrating that the photopolymerization of methacrylate groups in YMCAPs_Aut with the GelMA polymeric chains, combined with a higher particle concentration, leads to a stronger binding of YMCAPs_Aut to the hydrogel matrix, reinforcing the mechanical strength of the fabricated composite hydrogels. However, the obtained values of Young's modulus of the prepared hydrogels are far lower when compared to human trabecular bone (1.8×10^5 - 3.3×10^5 kPa) and compact bone (1.7×10^7 - 1.9×10^7 kPa)¹¹². Due to the poor mechanical properties, these scaffolds should only be used in non-load bearing applications, whereupon their *in situ* photocrosslinkable and consequent ability to mould to the bone defect area might be advantageous. Furthermore, it is known that material stiffness influences the osteogenic stem cells fate and therefore, the commitment of MSCs to osteogenic lineage may be modulated through scaffolds elasticity tailoring¹⁶³. Although the optimum elasticity varies with the type of material, lower stiffness is generally associated with an increase of adipose cells, while higher stiffness is associated to their differentiation to osteoblastic cells¹⁶³. The MSCs sensibility to poly(acrylamide) substrate with an elastic modulus of 25-40 kPa, stimulates their osteogenic differentiation¹⁶³. Besides scaffolds stiffness, within covalently crosslinking hydrogels matrix, the mechanical forces exerted by cells also regulate their distribution, proliferation, and differentiation¹⁶⁴. For instance, the high traction mechanical forces generated by MSCs-mediated hydrogel degradation and subsequent mechanotransduction are propitious for osteogenic phenotype fate commintent¹⁶⁵.

In addition, from compressive stress-strain curves, it is possible to identify the stress at break (147.5 kPa for GelMA/YMCAPs_Aut_1%, 149.3 kPa for GelMA/YMCAPs_Aut_5%, 133.8 kPa for GelMA-c-YMCAPs_Aut_1% and 166.1 kPa for GelMA-c-YMCAPs_Aut_5%) and the respective strain at break (78 % for GelMA/YMCAPs_Aut_1%, 109 % for GelMA/YMCAPs_Aut_5%, 89 % for GelMA-c-YMCAPs_Aut_1% and 90 % for GelMA-c-YMCAPs_Aut_5%).

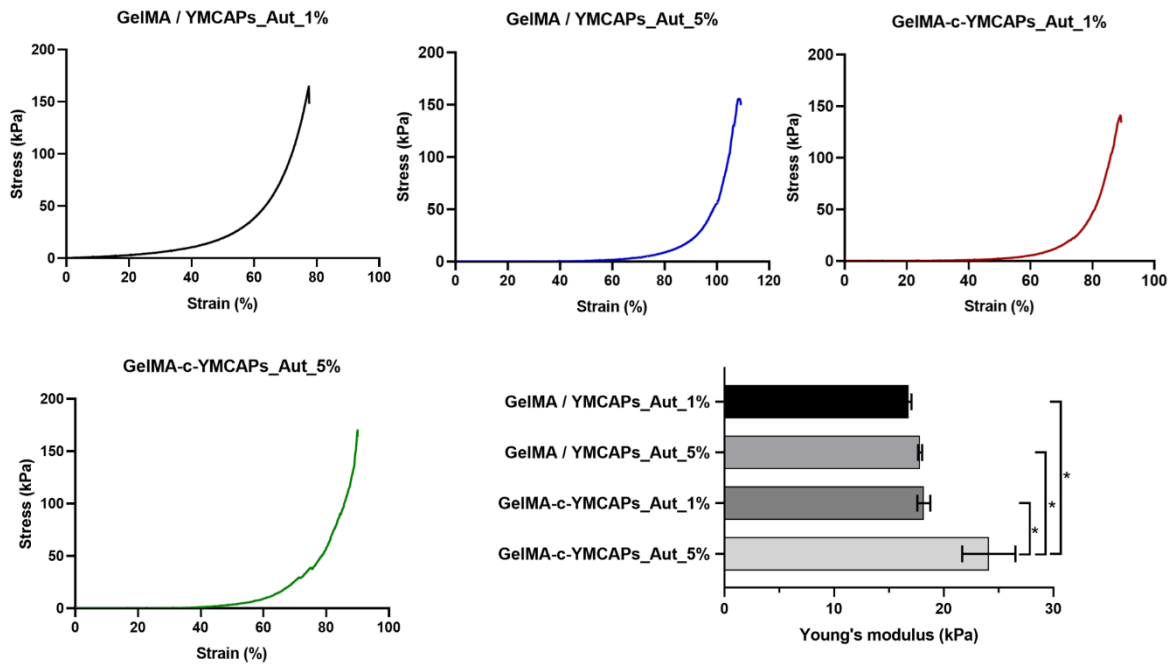


Figure 23: Compressive stress-strain curves and Young’s modulus representation of GelMA/YMCAPs_Aut and GelMA-c-YMCAPs_Aut. Data is represented as mean \pm standard deviation (n=3). * $p < 0.05$

4.3.2. Cytotoxicity evaluation

The results from metabolic activity evaluation of *h*ASCs exposure to stand-alone YMCAPs_Aut, indicate a noncytotoxic effect of the yeast capsules on the *h*ASCs cells’ metabolism (Figure 24). Although cell metabolic activity was decreased at 24 h, the cells were able to recover from the initial imposed stress, with a reversion of cell viability after 48 h (adaptation period) for the YMCAPs_Aut concentrations interval of 25 to 500 $\mu\text{g}/\text{mL}$. At 72 h, significant decreases of cell viability were found at concentrations of 500, 750 and 1000 $\mu\text{g}/\text{mL}$ compared to the control (0 $\mu\text{g}/\text{mL}$). However, none is below the cytotoxicity threshold of 75 % of viability¹⁶⁶. Altogether, *h*ASCs cells treated with stand-alone YMCAPs_Aut maintained a high cell viability, which was comprised between 80 % and 109 % at all the tested concentrations and time-points, with viability assay revealing that concentrations of 25, 50, 75, 100 and 250 $\mu\text{g}/\text{mL}$ support the cellular activity without changing the number of viable cells after 72 h of YMCAPs_Aut exposure.

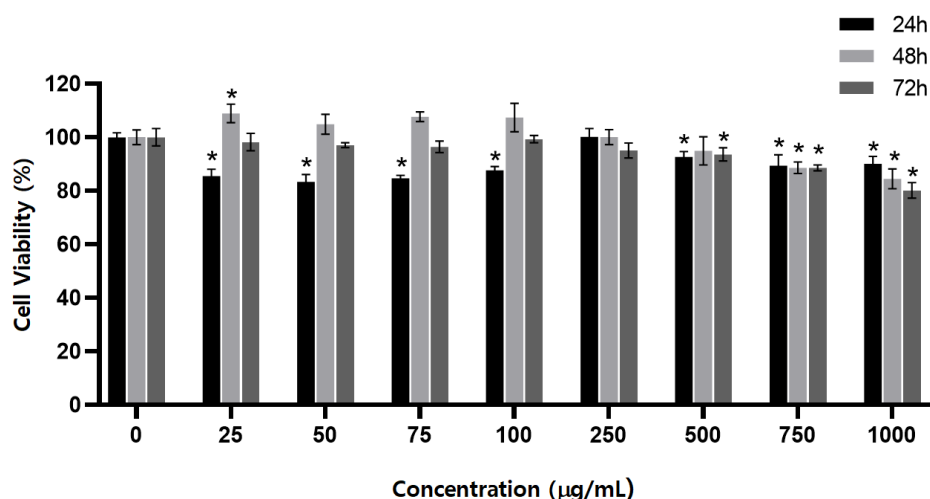


Figure 24: Stand-alone YMCAPs_Aut effect in *hASCs* cell viability. The cell viability is normalized with respect to the control (0 µg/mL, 100 %). Data is represented as mean \pm standard deviation (n=4). * $p < 0.05$ compare to the control group.

Considering 3D cell-laden cultures, not only noncytotoxic effect was observed in GelMA-c-YMCAPs_Aut_1%, but also a greater metabolic activity was prompted ($p > 0.05$), throughout the 7 days culture period (Figure 25). This result demonstrates that the multi-YMCAPs_Aut/GelMA platform with 1 % (w/v) of YMCAPs_Aut is biocompatible and provide the adequate 3D conditions for cellular activity.

Cell-laded hydrogel constructs with 5 % (w/v) of YMCAPs_Aut showed a lower cell metabolic activity at day 1, which was followed by a drastic decrease resulting in almost no cell viability after 7 days. The detrimental effect with the formulation with 5 % (w/v) of YMCAPs_Aut may be a result of: i) presence of YMCAPs_Aut in a toxic concentration to *hASCs*. In GelMA-c-YMCAPs_Aut_5%, 1×10^6 cells were exposure to 2850 µg of YMCAPs_Aut per hydrogel (~ 57 µL), which was much higher compared to the highest concentration tested in stand-alone YMCAPs_Aut assay, where 1000 µg/mL was responsible for the highest reduction in cell viability, compared to the other tested concentrations; ii) the increase of crosslinking points may reduce the platform pore size and consequently difficult the delivery of nutrients, the flow of oxygen and the diffusion of metabolic waste products^{27,31}. The lower permeability was already verified with the decrease of PBS uptake; iii) the denser structure may reduce the polymer chains mobility which in turn might not be adequate for cellular alignment and repositioning¹⁶⁵; iv) the presence of unreacted photoinitiator crosslinker within the hydrogel matrix¹⁶¹.

The results suggest that contrarily to GelMA-c-YMCAPs_Aut_5%, GelMA-c-YMCAPs_Aut_1% platform supports the encapsulated *hASCs* metabolic activity for at least 7 days. Given the

fabrication of multi-YMCAPs_Aut/GelMA platform for bone tissue regeneration, the biocompatibility of the formulation containing 1 % (w/v) of YMCAPs_Aut might be appreciated as a positive signal for its biomedical application.

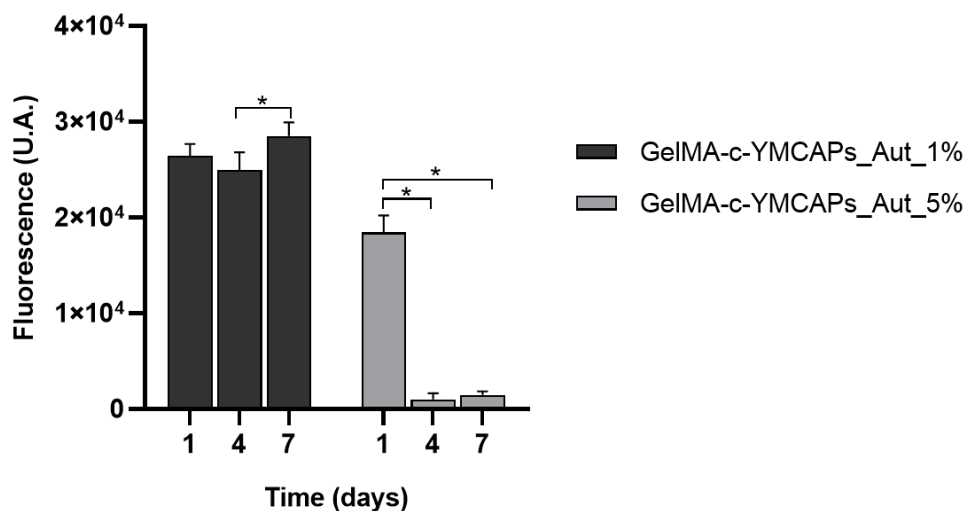


Figure 25: hASCs cell viability within 3D multi-YMCAPs_Aut/GelMA platform constructs. Data is represented as mean \pm standard deviation (n=4). * $p < 0.05$

4.4. Drug encapsulation and drug release profile

The drug encapsulation in YMCAPs was evaluated using different compounds with recognized osteogenic properties (naringin, naringenin and dexamethasone) (Figure 26). According to the literature, the methodology most frequently used is based on the passive diffusion of the drugs into the capsule structure, being processed by the combination of YMCAPs and drug in an aqueous or organic solution, under constant stirring and controlled temperature (ranging from RT to 60°C)¹⁶⁷.

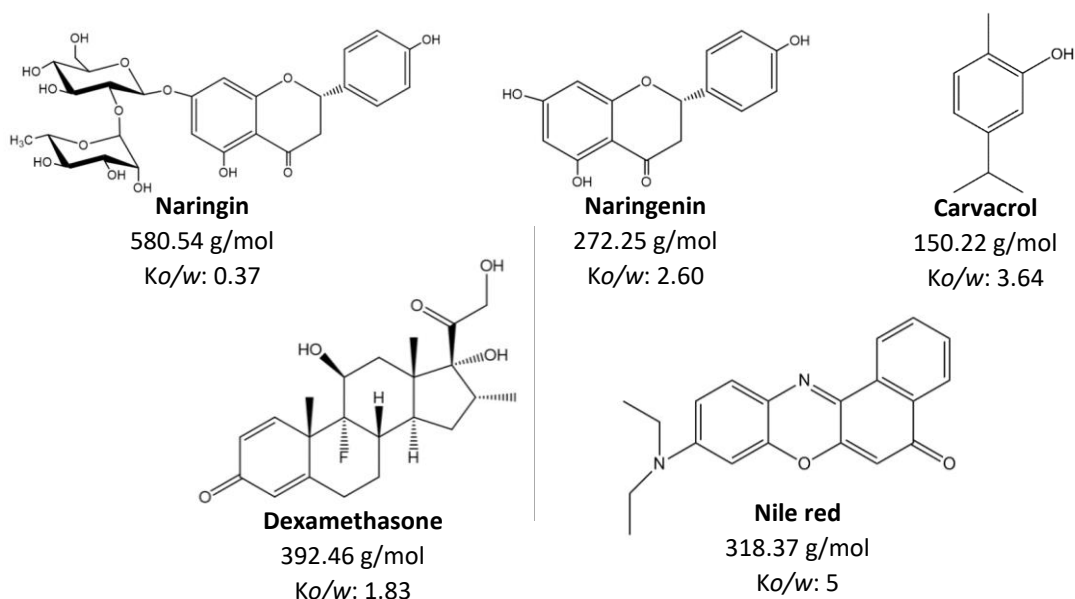


Figure 26: Chemical structure of encapsulated drugs and respective molar mass and *K_{o/w}* values.

Water has been considered essential to swell the yeasts cell wall through the interaction of water and the polar groups present in proteins and in cell wall constituent carbohydrates, thus facilitating the diffusion of drugs into yeasts cells which include remaining intracellular content¹⁶⁸. Based on this assumption, initially naringin was dissolved in EtOH being after added to freshly prepared aqueous encapsulation medium containing YMCAPs_Aut or 24 h after aqueous suspension of YMCAPs_Aut preparation. Other experimental conditions were evaluated in an attempt to encapsulate naringin, including the duration of the reaction, the type of stirring, and the mass ratio YMCAPs_Aut:drug. However, none of these conditions result in a successful naringin encapsulation. Naringin is a glycosylated flavanone formed from the glycosylation of naringenin with the disaccharide neohesperidose, composed of L-rhamnose ($\alpha\rightarrow2$)-linked to D-glucose^{169,170}. The sugars present in the naringin structure reduce the hydrophobicity of the molecule which may impede the entrapment of this drug in the hollow YMCAPs_Aut. Hence, similar encapsulation procedure was performed for naringenin and dexamethasone. Once more, the drugs were not effectively loaded in YMCAPs_Aut. Despite hydrophobic and hydrophilic compounds have already been encapsulated in yeast cells, the peculiar structure of YMCAPs_Aut restricts the loading of the tested compounds. In the produced material, the encapsulation seems to be determined by the solubility of the drug, in other words by the drug octane/water partition coefficient (K_o/w), since under identical conditions a highly hydrophobic lipophilic dye Nile red ($K_o/w = 5$) was successfully encapsulated in YMCAPs_Aut, reaching an EE of 90.9 % (Figure 27).

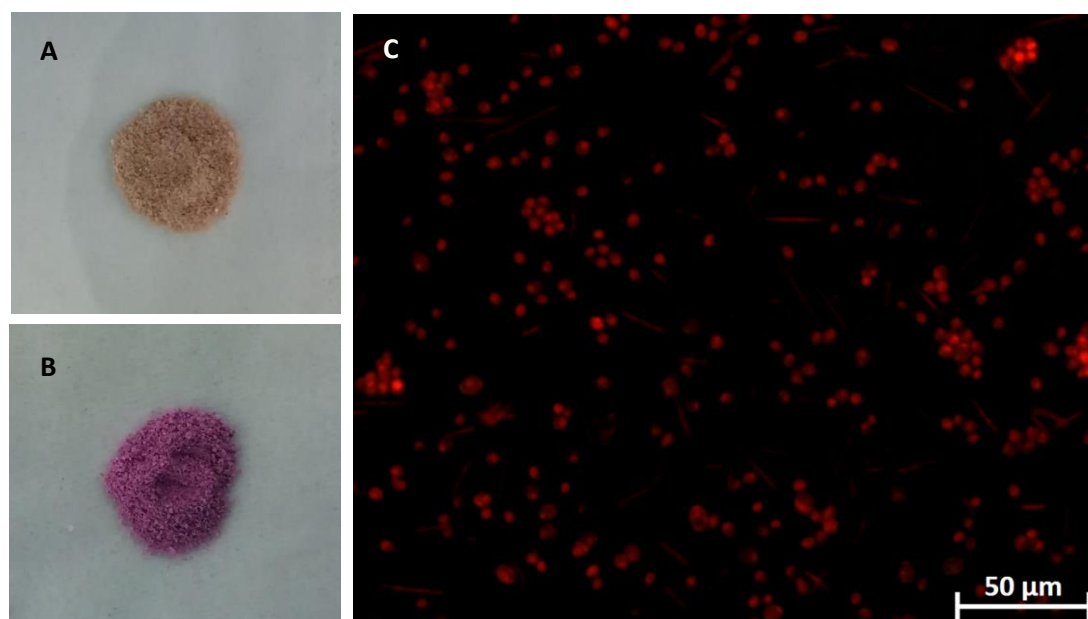


Figure 27: Freeze-dried YMCAPs_Aut before (A) and after (B) Nile red encapsulation. Microscope fluorescence images of YMCAPs_Aut with encapsulated Nile red (C).

For yeast cells, it was verified that the rate of compound uptake increases with the increase of the hydrophobic character of the compound¹⁷¹, and with a K_o/w superior to 2.0 was possible to reach an EE of 50 %¹⁶⁸. Similarly, EE in liposomes is also strongly positively correlated with drugs K_o/w ¹⁷². For this reason, carvacrol ($K_o/w = 3.64$) an antiosteoclastogenic monoterpenoid¹⁷³, was used as vehicle to entrap dexamethasone inside the hollow YMCAPs_Aut. The results demonstrate that unlike the previous outcome using ethanol as the encapsulation medium, this approach enabled the encapsulation of dexamethasone with an EE of 38.9 %, which supports the theory that the encapsulation in these microcarriers is dependent of the degree of drug hydrophobicity (higher K_o/w results in a higher EE). Synthesized YMCAPs_Aut possess the carrying ability of dexamethasone and probably of naringin and naringenin, nonetheless, as demonstrated with the use of carvacrol, a hydrophobic environment needs to be created and adjusted to prompt the passive diffusion of these drugs.

The controlled encapsulated drug release profile is of extremely importance in biomedical applications. The release of Nile red from GelMA-c-YMCAPs_5% and stand-alone YMCAPs (both formulations with methacrylic-chemically modified YMCAPs_Aut) were evaluated under physiological pH, at 37°C and quantified through fluorescence intensity measurement. Although the hydrogel delays the release profile of Nile red, non-substantial release was found for stand-alone YMCAPs_Aut after 10 days (Figure 28A). Similar results were obtained in other studies where an insignificant release of Nile red was observed without the use of an external release stimulator^{174–176}. The observed result might be explained by the insolubility of this dye in aqueous environment. The insolubility of drugs is known to be a critical factor in drug spontaneous release modulation, with higher insolubility in water associated¹⁷⁵ with a lower release of the cargo¹⁷⁵. Nonetheless, this prolonged release may be reverted *in vivo*. As previously referred, gelatin possess MMPs hydrolytic moieties which might accelerate the hydrogel degradability and promote the expose of YMCAPs_Aut to the action of macrophages and to the acidic environment resulting from cellular activity. These physiological conditions will prompt the release of the drug. In fact, the combination of lipase in PBS (pH 7.4) at 37°C triggers about 80 % release of Nile red from an amphiphilic capsule in 120 h¹⁷⁶.

However, the detected release behaviour of Nile red may be an underestimation of the real release profile. Due to the water insolubility of Nile red, the release of this dye into the PBS solution results not only in its precipitation, but also in this dye fluorescence quenching¹⁷⁷. Indeed, in aqueous environment, Nile red tends to self-assemble through supramolecular binding interactions (π - π stacking and hydrogen bonds), essentially leading to the formation of H-type

aggregates^{174,178,179}, which are characterized by a reduction of the dye fluorescence intensity¹⁷⁹. It is worth mentioning that during the different time points, the colour of PBS solution with Nile red became less intense (Figure 28B), which may justify the reduced fluorescence measured and therefore the reduced drug release, probably as a consequence of Nile red H-aggregates formation.

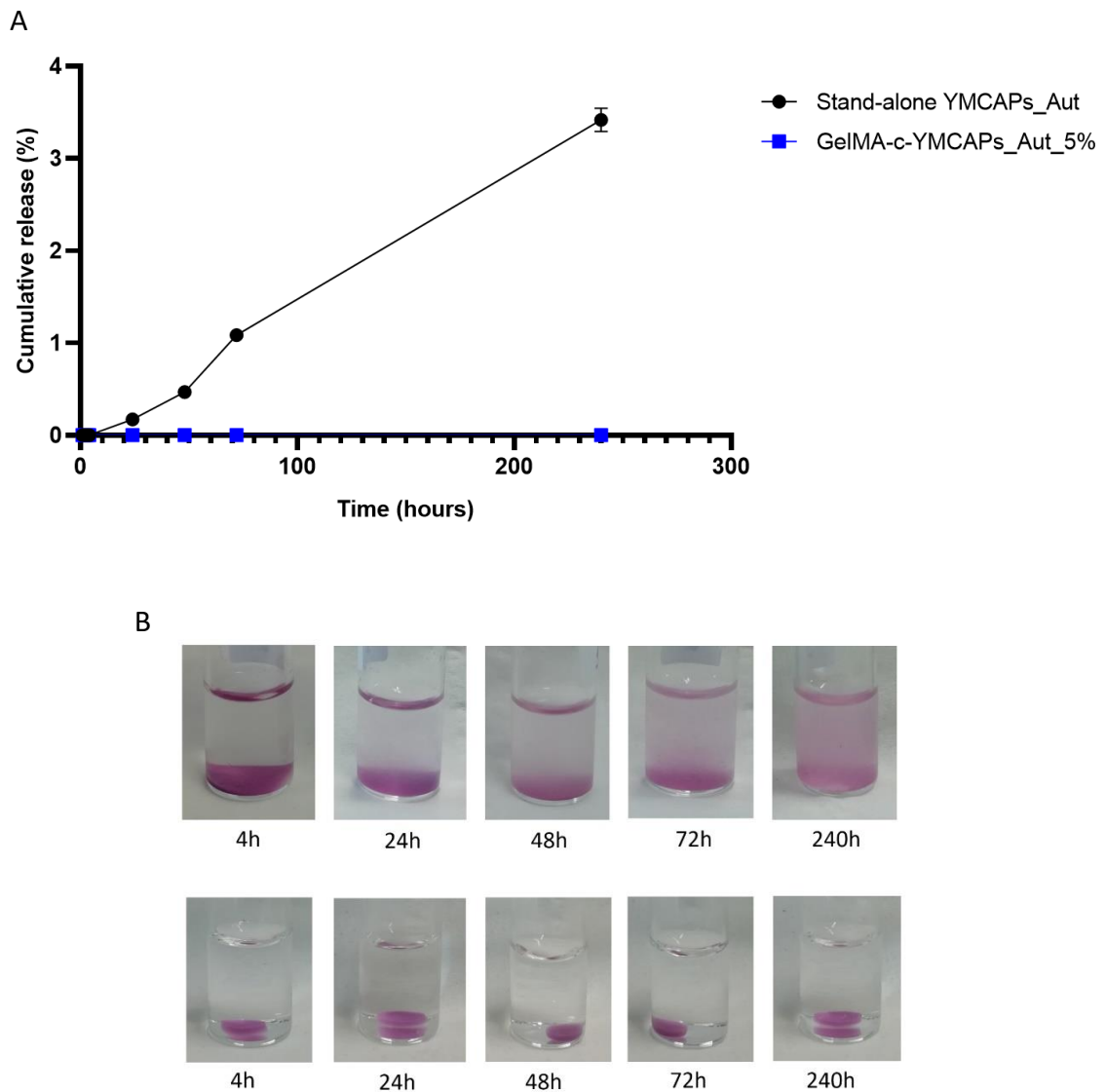


Figure 28: A) Nile red-loaded YMCAPs_Aut and GelMA-c-YMCAPs_Aut_5% *in vitro* release profile, expressed as cumulative release (%). B) Time related differences in PBS colour solution associated to the Nile red release. Data is represented as mean \pm standard deviation (n=3).

5. Conclusion and Future Perspectives

5.1. Conclusion and future perspectives

In this study, the isolation, chemical functionalization of YMCAPs and subsequent multi-YMCAPs/GelMA platform formation, to act as a delivery system for bone tissue engineering, was successfully achieved. YMCAPs were extracted from the BSY *S. pastorianus*, through thermal and alkali treatment. The application of these two extraction processes allowed the removal of the intracellular content and the isolation of the yeast cell wall. The isolated spherical to ellipsoid YMCAPs have distinct structural characteristics. Thermal autolysis allowed the obtention of YMCAPs_Aut with 41 % of carbohydrates (15 mol % Man and 85 mol % Glc) and 38 % of proteins. In addition, 4M KOH extraction allowed the extraction of 11.4 % of proteins and of alkali-soluble polysaccharides, purifying the polysaccharide component (54 % of carbohydrate with 4 mol % of Man and 96 mol % of Glc). Both presented similar proportion of linear [(1→3), (1→4) and (1→6)] and branched [(1→3,4), (1→3,6) and (1→4,6)] linkages between Glc residues. Regarding mannans, both have linear [(1→2), (1→3) and (1→6)] and branched (1→2,3)-Man; however, in YMCAPs_4M, these linkages are presented in a lower proportion and the (1→2,6) and (1→3,6) branching residues disappeared, demonstrating the removal of mannoproteins' external layer from YMCAPs_Aut. Although that extraction removed a large part of Man, the protein composition remained similar between the two capsules.

The better dispersion of YMCAPs_Aut in PBS and the presence of -OH and NH₂ chemical groups in their polysaccharide and protein components can be seen as an opportunity to chemically modify these yeast capsules. The functionalization of YMCAPs_Aut occurred in a greater extent in the presence of methacrylic anhydride instead of carbic anhydride, as confirmed by spectroscopic and glycosidic analysis. The introduction of methacrylate groups in YMCAPs_Aut (DS of 26.4 %) was more pronounced in the protein part, probably due to the higher accessibility of NH₂ groups associated to their external localization in the YMCAPs_Aut. Nonetheless, some modifications were identified in the sugar carbons, namely in C₁, C₂, C₃, C₄ and C₆ of Glc residues.

The modification resulted in the incorporation of groups that allowed the covalent crosslinking of the YMCAPs_Aut with GelMA, with the consequent formation of a hydrogel, also called multi-YMCAPs/GelMA platform. The effect of modification on physical properties of the hydrogel was evaluated through the comparison with hydrogels prepared with unmodified YMCAPs_Aut and varying the capsules concentration. The use of crosslinkable YMCAPs, combined with a higher YMCAPs concentration, synergistically decreases the swelling rate and water content of the platform, while significantly increments their mechanical properties (higher Young's modulus, ultimate tensile strength, and stress at break). Furthermore, the use of YMCAPs as crosslinking

points has a profound effect on the degradation rate of the formulation containing 5 % of YMCAPs, preventing its rapid mass loss.

Regarding cell culture, stand-alone YMCAPs_Aut revealed to be biocompatible with a cell viability ≥ 80 %, being the 25, 50, 75, 100 and 250 $\mu\text{g}/\text{mL}$ the concentrations that maintained a higher *hASCs* viability after 72 h. Considering the 3D cell scaffolds, the GelMA-c-YMCAPs_Aut_5% platform failed to maintain the cell metabolic activity. Contrarily, GelMA-c-YMCAPs_Aut_1% successfully supported cellular activity, highlighting their possible application in bone tissue engineering.

The peculiar structural features of YMCAPs_Aut allows the use of these capsules as encapsulating materials for highly hydrophobic drugs, as Nile red ($K_o/w = 5$). Therefore, the use of YMCAPs as delivery systems will be more advantageous for long-term drug release, thus being able to act in a more advanced bone regeneration stage (e.g., repair and/or remodeling stage), associated to the delayed release of highly hydrophobic drugs. Nonetheless, when dexamethasone with a K_o/w of 1.83 was solubilized in carvacrol (with a $K_o/w = 3.64$), it was satisfactorily encapsulated into YMCAPs. These results support the use of YMCAPs as a delivery system for bone regeneration.

In the future, other highly hydrophobic drugs [e.g. bazedoxifene ($K_o/w = 6$)] with osteogenic effects may be easily encapsulated into YMCAPs. Adding to this, further *in vitro* studies are needed to verify the multi-YMCAPs/GelMA platform effect on stem cells commitment into osteogenic lineage, through the evaluation of osteogenic markers secretion (e.g., ALP, OCN) and calcium deposition.

Overall, the hybrid platform comprised by naturally derived biomaterials has demonstrated potential to provide an added-value in comparison to stand-alone delivery systems or GelMA hydrogels and future validation of osteogenic markers *in vitro* and possibility *in vivo* may open new insights into its true potential for application in the context of bone tissue engineering and regenerative medicine.

6. References

- (1) Neto, A. S.; Ferreira, J. M. F. Synthetic and Marine-Derived Porous Scaffolds for Bone Tissue Engineering. *Materials (Basel)*. **2018**, *11*, 1702. <https://doi.org/10.3390/ma11091702>.
- (2) Oryan, A.; Monazzah, S.; Bigham-Sadegh, A. Bone Injury and Fracture Healing Biology. *Biomed. Environ. Sci.* **2015**, *28*, 57–71. <https://doi.org/10.3967/bes2015.006>.
- (3) VanPutte, C.; Regan, J.; Russo, A. *Seeley's Essentials of Anatomy & Physiology*, 9th ed.; New York, 2016; Vol. 9. <https://doi.org/10.21037/jtd.2017.07.86>.
- (4) Green, J.; Kleeman, C. R. Role of Bone in Regulation of Systemic Acid-Base Balance. *Kidney Int.* **1991**, *39*, 9–26. <https://doi.org/10.1038/ki.1991.2>.
- (5) Lavrador, P.; Gaspar, V. M.; Mano, J. F. Stimuli-Responsive Nanocarriers for Delivery of Bone Therapeutics – Barriers and Progresses. *J. Control. Release* **2018**, *273*, 51–67. <https://doi.org/10.1016/j.jconrel.2018.01.021>.
- (6) Henkel, J.; Woodruff, M. A.; Epari, D. R.; Steck, R.; Glatt, V.; Dickinson, I. C.; Choong, P. F. M.; Schuetz, M. A.; Hutmacher, D. W. Bone Regeneration Based on Tissue Engineering Conceptions-A 21st Century Perspective. *Bone Res.* **2013**, *3*, 216–248. <https://doi.org/10.4248/BR201303002>.
- (7) Junqueira, L. C.; Carneiro, J. *Histologia Básica*, 12th ed.; Rio de Janeiro, 2013.
- (8) Stewart, S.; Bryant, S. J.; Ahn, J.; Hankenson, K. D. Bone Regeneration. In *Translational Regenerative Medicine*; Atala, A., Allickson, J., Eds.; 2015; pp 313–333. <https://doi.org/10.1017/CBO9780511997839.031>.
- (9) Cashman, K. D.; Ginty, F. Bone. In *Encyclopedia of Food Sciences and Nutrition*; Caballero, B., Ed.; 2003; pp 557–565.
- (10) Ashrafi, M.; Gubaua, J. E.; Pereira, J. T.; Gahlich, F.; Doblaré, M. A Mechano-Chemo-Biological Model for Bone Remodeling With a New Mechano-Chemo-Transduction Approach. *Biomech. Model. Mechanobiol.* **2020**, *19*, 2499–2523. <https://doi.org/10.1007/s10237-020-01353-0>.
- (11) Rouhi, G. Biomechanics of Osteoporosis: The Importance of Bone Resorption and Remodeling Processes. In *Osteoporosis*; Dionyssiotis, Y., Ed.; 2012; pp 59–78. <https://doi.org/10.5772/29987>.
- (12) Kim, J. H.; Kim, N. Bone Cell Communication Factors Provide a New Therapeutic Strategy for Osteoporosis. *Chonnam Med. J.* **2020**, *56*, 94–98. <https://doi.org/10.4068/cmj.2020.56.2.94>.
- (13) Kameo, Y.; Miya, Y.; Hayashi, M.; Nakashima, T.; Adachi, T. *In silico* Experiments of Bone Remodeling Explore Metabolic Diseases and Their Drug Treatment. *Sci. Adv.* **2020**, *6*, eaax0938. <https://doi.org/10.1126/sciadv.aax0938>.
- (14) Baht, G. S.; Vi, L.; Alman, B. A. The Role of the Immune Cells in Fracture Healing. *Curr. Osteoporos. Rep.* **2018**, *16*, 138–145. <https://doi.org/10.1007/s11914-018-0423-2>.
- (15) Longoni, A.; Knežević, L.; Schepers, K.; Weinans, H.; Rosenberg, A. J. W. P.; Gawlitta, D. The Impact of Immune Response on Endochondral Bone Regeneration. *npj Regen. Med.* **2018**, *3*, 22. <https://doi.org/10.1038/s41536-018-0060-5>.
- (16) Maruyama, M.; Rhee, C.; Utsunomiya, T.; Zhang, N.; Ueno, M.; Yao, Z.; Goodman, S. B. Modulation of the Inflammatory Response and Bone Healing. *Front. Endocrinol. (Lausanne)*. **2020**, *11*, 386. <https://doi.org/10.3389/fendo.2020.00386>.
- (17) Muire, P. J.; Mangum, L. H.; Wenke, J. C. Time Course of Immune Response and Immunomodulation During Normal and Delayed Healing of Musculoskeletal Wounds. *Front. Immunol.* **2020**, *11*, 1056. <https://doi.org/10.3389/fimmu.2020.01056>.
- (18) Rucci, N. Molecular Biology of Bone Remodeling. *Clin. Cases Miner. Bone Metab.* **2008**, *5*, 49–56.
- (19) Yu, X.; Tang, X.; Gohil, S. V.; Laurencin, C. T. Biomaterials for Bone Regenerative Engineering. *Adv.*

- Healthc. Mater.* **2015**, *4*, 1268–1285. <https://doi.org/10.1002/adhm.201400760>.Biomaterials.
- (20) Qu, H.; Fu, H.; Han, Z.; Sun, Y. Biomaterials for Bone Tissue Engineering Scaffolds: A Review. *RSC Adv.* **2019**, *9*, 26252–26262. <https://doi.org/10.1039/c9ra05214c>.
- (21) Kazimierczak, P.; Przekora, A. Osteoconductive and Osteoinductive Surface Modifications of Biomaterials for Bone Regeneration: A Concise Review. *Coatings* **2020**, *10*, 971.
- (22) Alonzo, M.; Alvarez Primo, F.; Anil Kumar, S.; Mudloff, J. A.; Dominguez, E.; Fregoso, G.; Ortiz, N.; Weiss, W. M.; Joddar, B. Bone Tissue Engineering Techniques, Advances, and Scaffolds for Treatment of Bone Defects. *Curr. Opin. Biomed. Eng.* **2021**, *17*, 100248. <https://doi.org/10.1016/j.cobme.2020.100248>.
- (23) Koons, G. L.; Diba, M.; Mikos, A. G. Materials Design for Bone-Tissue Engineering. *Nat. Rev. Mater.* **2020**, *5*, 584–603. <https://doi.org/10.1038/s41578-020-0204-2>.
- (24) Bagde, A. D.; Kuthe, A. M.; Quazi, S.; Gupta, V.; Jaiswal, S.; Jyothilal, S.; Lande, N.; Nagdeve, S. State of the Art Technology for Bone Tissue Engineering and Drug Delivery. *Irbm* **2019**, *40*, 133–144. <https://doi.org/10.1016/j.irbm.2019.03.001>.
- (25) Mouriño, V.; Boccaccini, A. R. Bone Tissue Engineering Therapeutics: Controlled Drug Delivery in Three-Dimensional Scaffolds. *J. R. Soc. Interface* **2010**, *7*, 209–227. <https://doi.org/10.1098/rsif.2009.0379>.
- (26) Xu, C.; Thiruvadi, V. S.; Whitmore, R.; Liu, H. Delivery Systems for Biomedical Applications: Basic Introduction, Research Frontiers and Clinical Translations. In *Biomaterials in Translational Medicine: A Biomaterials Approach*; Yang, L., Bhaduri, S. B., Webster, T. J., Eds.; 2018; pp 93–116. <https://doi.org/10.1016/B978-0-12-813477-1.00005-0>.
- (27) Bai, X.; Gao, M.; Syed, S.; Zhuang, J.; Xu, X.; Zhang, X. Q. Bioactive Hydrogels for Bone Regeneration. *Bioact. Mater.* **2018**, *3*, 401–417. <https://doi.org/10.1016/j.bioactmat.2018.05.006>.
- (28) Zhang, Y.; Yu, T.; Peng, L.; Sun, Q.; Wei, Y.; Han, B. Advancements in Hydrogel-Based Drug Sustained Release Systems for Bone Tissue Engineering. *Front. Pharmacol.* **2020**, *11*, 622. <https://doi.org/10.3389/fphar.2020.00622>.
- (29) Sabu, C.; Mufeedha, P.; Pramod, K. Yeast-Inspired Drug Delivery: Biotechnology Meets Bioengineering and Synthetic Biology. *Expert Opin. Drug Deliv.* **2019**, *16*, 27–41. <https://doi.org/10.1080/17425247.2019.1551874>.
- (30) Agarwal, R.; García, A. J. Biomaterial Strategies for Engineering Implants for Enhanced Osseointegration and Bone Repair. *Adv. Drug Deliv. Rev.* **2015**, *94*, 53–62. <https://doi.org/10.1016/j.addr.2015.03.013>.
- (31) Turnbull, G.; Clarke, J.; Picard, F.; Riches, P.; Jia, L.; Han, F.; Li, B.; Shu, W. 3D Bioactive Composite Scaffolds for Bone Tissue Engineering. *Bioact. Mater.* **2018**, *3*, 278–314. <https://doi.org/10.1016/j.bioactmat.2017.10.001>.
- (32) Yue, K.; Trujillo-de Santiago, G.; Alvarez, M. M.; Tamayol, A.; Annabi, N.; Khademhosseini, A. Synthesis, Properties, and Biomedical Applications of Gelatin Methacryloyl (GelMA) Hydrogels. *Biomaterials* **2015**, *73*, 254–271. <https://doi.org/10.1016/j.biomaterials.2015.08.045>.
- (33) Klotz, B. J.; Gawlitta, D.; Rosenberg, A. J. W. P.; Malda, J.; Melchels, F. P. W. Gelatin-Methacryloyl Hydrogels: Towards Biofabrication-Based Tissue Repair. *Trends Biotechnol.* **2016**, *34*, 394–407. <https://doi.org/10.1016/j.tibtech.2016.01.002>.
- (34) Qiao, Y.; Liu, X.; Zhou, X.; Zhang, H.; Zhang, W.; Xiao, W.; Pan, G.; Cui, W.; Santos, H. A.; Shi, Q. Gelatin Templated Polypeptide Co-Cross-Linked Hydrogel for Bone Regeneration. *Adv. Healthc. Mater.* **2020**, *9*, 1901239. <https://doi.org/10.1002/adhm.201901239>.

- (35) Battista, E.; Causa, F.; Netti, P. Bioengineering Microgels and Hydrogel Microparticles for Sensing Biomolecular Targets. *Gels* **2017**, *3*, 20. <https://doi.org/10.3390/gels3020020>.
- (36) Mohammadinejad, R.; Maleki, H.; Larrañeta, E.; Fajardo, A. R.; Nik, A. B.; Shavandi, A.; Sheikhi, A.; Ghorbanpour, M.; Farokhi, M.; Govindh, P.; Cabane, E.; Azizi, S.; Aref, A. R.; Mozafari, M.; Mehrli, M.; Thomas, S.; Mano, J. F.; Mishra, Y. K.; Thakur, V. K. Status and Future Scope of Plant-Based Green Hydrogels in Biomedical Engineering. *Appl. Mater. Today* **2019**, *16*, 213–246. <https://doi.org/10.1016/j.apmt.2019.04.010>.
- (37) Kondiah, P. J.; Choonara, Y. E.; Kondiah, P. P. D.; Marimuthu, T.; Kumar, P.; Du Toit, L. C.; Pillay, V. A Review of Injectable Polymeric Hydrogel Systems for Application in Bone Tissue Engineering. *Molecules* **2016**, *21*, 1580. <https://doi.org/10.3390/molecules21111580>.
- (38) Daly, A. C.; Riley, L.; Segura, T.; Burdick, J. A. Hydrogel Microparticles for Biomedical Applications. *Nat. Rev. Mater.* **2020**, *5*, 20–43. <https://doi.org/10.1038/s41578-019-0148-6>.
- (39) Steele, A. N.; Stapleton, L. M.; Farry, J. M.; Lucian, H. J.; Paulsen, M. J.; Eskandari, A.; Hironaka, C. E.; Thakore, A. D.; Wang, H.; Yu, A. C.; Chan, D.; Appel, E. A.; Woo, Y. J. A Biocompatible Therapeutic Catheter-Deliverable Hydrogel for *In situ* Tissue Engineering. *Adv. Healthc. Mater.* **2019**, *8*, 1801147. <https://doi.org/10.1002/adhm.201801147>.
- (40) Zhao, X.; Liu, S.; Yildirim, L.; Zhao, H.; Ding, R.; Wang, H.; Cui, W.; Weitz, D. Injectable Stem Cell-Laden Photocrosslinkable Microspheres Fabricated Using Microfluidics for Rapid Generation of Osteogenic Tissue Constructs. *Adv. Funct. Mater.* **2016**, *26*, 2809–2819. <https://doi.org/10.1002/adfm.201504943>.
- (41) Safarova, Y.; Safarova, Y.; Umbayev, B.; Hortelano, G.; Askarova, S. Mesenchymal Stem Cells Modifications for Enhanced Bone Targeting and Bone Regeneration. *Regen. Med.* **2020**, *15*, 1579–1594. <https://doi.org/10.2217/rme-2019-0081>.
- (42) Liu, M.; Zeng, X.; Ma, C.; Yi, H.; Ali, Z.; Mou, X.; Li, S.; Deng, Y.; He, N. Injectable Hydrogels for Cartilage and Bone Tissue Engineering. *Bone Res.* **2017**, *5*, 17014. <https://doi.org/10.1038/boneres.2017.14>.
- (43) Lavanya, K.; Chandran, S. V.; Balagangadharan, K.; Selvamurugan, N. Temperature- and PH-Responsive Chitosan-Based Injectable Hydrogels for Bone Tissue Engineering. *Mater. Sci. Eng. C* **2020**, *111*, 110862. <https://doi.org/10.1016/j.msec.2020.110862>.
- (44) Gao, W.; Zhang, Y.; Zhang, Q.; Zhang, L. Nanoparticle-Hydrogel: A Hybrid Biomaterial System for Localized Drug Delivery. *Ann. Biomed. Eng.* **2016**, *44*, 2049–2061. <https://doi.org/10.1007/s10439-016-1583-9>. Nanoparticle-Hydrogel.
- (45) Chen, F. M.; Zhang, M.; Wu, Z. F. Toward Delivery of Multiple Growth Factors in Tissue Engineering. *Biomaterials* **2010**, *31*, 6279–6308. <https://doi.org/10.1016/j.biomaterials.2010.04.053>.
- (46) Costa, A. M. S.; Mano, J. F. Extremely Strong and Tough Hydrogels as Prospective Candidates for Tissue Repair - A Review. *Eur. Polym. J.* **2015**, *72*, 344–364. <https://doi.org/10.1016/j.eurpolymj.2015.07.053>.
- (47) Thoniyot, P.; Tan, M. J.; Karim, A. A.; Young, D. J.; Loh, X. J. Nanoparticle–Hydrogel Composites: Concept, Design, and Applications of These Promising, Multi-Functional Materials. *Adv. Sci.* **2015**, *2*, 1400010. <https://doi.org/10.1002/advs.201400010>.
- (48) Dannert, C.; Stokke, B. T.; Dias, R. S. Nanoparticle-Hydrogel Composites: From Molecular Interactions to Macroscopic Behavior. *Polymers (Basel)*. **2019**, *11*, 275. <https://doi.org/10.3390/polym11020275>.
- (49) Zhang, K.; Lin, S.; Feng, Q.; Dong, C.; Yang, Y.; Li, G.; Bian, L. Nanocomposite Hydrogels Stabilized by Self-Assembled Multivalent Bisphosphonate-Magnesium Nanoparticles Mediate Sustained Release of Magnesium Ion and Promote in-Situ Bone Regeneration. *Acta Biomater.* **2017**, *64*, 389–400. <https://doi.org/10.1016/j.actbio.2017.09.039>.

- (50) Shin, H.; Olsen, B. D.; Khademhosseini, A. Gellan Gum Microgel-Reinforced Cell-Laden Gelatin Hydrogels. *J. Mater. Chem. B* **2014**, *2*, 2508–2516. <https://doi.org/10.1039/c3tb20984a>.
- (51) Jiang, Y.; Krishnan, N.; Heo, J.; Fang, R. H.; Zhang, L. Nanoparticle–Hydrogel Superstructures for Biomedical Applications. *J. Control. Release* **2020**, *324*, 505–521. <https://doi.org/10.1016/j.jconrel.2020.05.041>.
- (52) Liu, X.; Fundora, K. A.; Zhou, Z.; Miller, A. L.; Lu, L. Composite Hydrogel Embedded with Porous Microspheres for Long-Term PH-Sensitive Drug Delivery. *Tissue Eng. - Part A* **2019**, *25*, 172–182. <https://doi.org/10.1089/ten.tea.2018.0071>.
- (53) Feldmann, H. *Yeast: Molecular and Cell Biology*, 2nd ed.; Feldmann, H., Ed.; 2012.
- (54) Huo, M.; Wang, L.; Chen, Y.; Shi, J. Nanomaterials/Microorganism-Integrated Microbiotic Nanomedicine. *Nano Today* **2020**, *32*, 100854. <https://doi.org/10.1016/j.nantod.2020.100854>.
- (55) Sabu, C.; Rejo, C.; Kotta, S.; Pramod, K. Bioinspired and Biomimetic Systems for Advanced Drug and Gene Delivery. *J. Control. Release* **2018**, *287*, 142–155. <https://doi.org/10.1016/j.jconrel.2018.08.033>.
- (56) Vaughan-Martini, A.; Martini, A. *Saccharomyces Meyen Ex Reess (1870)*. In *The Yeasts, a Taxonomic study*; Kurtzman, C. P., Fell, J. W., Boekhout, T., Eds.; 2011; pp 733–746. <https://doi.org/10.1016/B978-0-444-52149-1.00061-6>.
- (57) Pham-Hoang, B. N.; Romero-Guido, C.; Phan-Thi, H.; Waché, Y. Encapsulation in a Natural, Preformed, Multi-Component and Complex Capsule: Yeast Cells. *Appl. Microbiol. Biotechnol.* **2013**, *97*, 6635–6645. <https://doi.org/10.1007/s00253-013-5044-1>.
- (58) Alsteens, D.; Dupres, V.; Mc Evoy, K.; Wildling, L.; Gruber, H. J.; Dufrêne, Y. F. Structure, Cell Wall Elasticity and Polysaccharide Properties of Living Yeast Cells, as Probed by AFM. *Nanotechnology* **2008**, *19*, 384005. <https://doi.org/10.1088/0957-4484/19/38/384005>.
- (59) Teparić, R.; Mrša, V. Proteins Involved in Building, Maintaining and Remodeling of Yeast Cell Walls. *Curr. Genet.* **2013**, *59*, 171–185. <https://doi.org/10.1007/s00294-013-0403-0>.
- (60) Lipke, P. N.; Ovalle, R. Cell Wall Architecture in Yeast: New Structure and New Challenges. *J. Bacteriol.* **1998**, *180*, 3735–3740. <https://doi.org/10.1128/jb.180.15.3735-3740.1998>.
- (61) Kwiatkowski, S.; Thielen, U.; Glenney, P.; Moran, C. A Study of *Saccharomyces cerevisiae* Cell Wall Glucans. *J. Inst. Brew.* **2009**, *115*, 151–158. <https://doi.org/10.1002/j.2050-0416.2009.tb00361.x>.
- (62) Pinto, M.; Coelho, E.; Nunes, A.; Brandão, T.; Coimbra, M. A. Valuation of Brewers Spent Yeast Polysaccharides: A Structural Characterization Approach. *Carbohydr. Polym.* **2015**, *116*, 215–222. <https://doi.org/10.1016/j.carbpol.2014.03.010>.
- (63) Klis, F. M.; Mol, P.; Hellingwerf, K.; Brul, S. Dynamics of Cell Wall Structure in *Saccharomyces cerevisiae*. *FEMS Microbiol. Rev.* **2002**, *26*, 239–256. [https://doi.org/10.1016/S0168-6445\(02\)00087-6](https://doi.org/10.1016/S0168-6445(02)00087-6).
- (64) Klis, F. M.; Boorsma, A.; De Groot, P. W. J. Cell Wall Construction in *Saccharomyces cerevisiae*. *Yeast* **2006**, *23*, 185–202. <https://doi.org/10.1002/yea.1349>.
- (65) Bastos, R.; Coelho, E.; Coimbra, M. A. Modifications of *Saccharomyces pastorianus* Cell Wall Polysaccharides with Brewing Process. *Carbohydr. Polym.* **2015**, *124*, 322–330. <https://doi.org/10.1016/j.carbpol.2015.02.031>.
- (66) Lesage, G.; Bussey, H. Cell Wall Assembly in *Saccharomyces cerevisiae*. *Microbiol. Mol. Biol. Rev.* **2006**, *70*, 317–343. <https://doi.org/10.1128/mmlr.00038-05>.
- (67) Kwiatkowski, S.; Edgar, S. Yeast (*Saccharomyces cerevisiae*) Glucan Polysaccharides – Occurrence,

- Separation and Application in Food, Feed and Health Industries. In *The Complex World of Polysaccharides*; Karunaratne, D. N., Ed.; 2012; pp 47–70. <https://doi.org/10.5772/48100>.
- (68) Cabib, E.; Arroyo, J. How Carbohydrates Sculpt Cells: Chemical Control of Morphogenesis in the Yeast Cell Wall. *Nat. Rev. Microbiol.* **2013**, *11*, 648–655. <https://doi.org/10.1038/nrmicro3090>.
- (69) Lee, K.; Kwon, Y.; Hwang, J.; Choi, Y.; Kim, K.; Koo, H.; Seo, Y.; Jeon, H.; Choi, J. Synthesis and Functionalization of B-Glucan Particles for the Effective Delivery of Doxorubicin Molecules. *ACS Omega* **2019**, *4*, 668–674. <https://doi.org/10.1021/acsomega.8b02712>.
- (70) Soto, E. R.; Ostroff, G. R. Characterization of Multilayered Nanoparticles Encapsulated in Yeast Cell Wall Particles for DNA Delivery. *Bioconjug. Chem.* **2008**, *19*, 840–848. <https://doi.org/10.1021/bc700329p>.
- (71) Zhang, L.; Peng, H.; Zhang, W.; Li, Y.; Liu, L.; Leng, T. Yeast Cell Wall Particle Mediated Nanotube-RNA Delivery System Loaded with MiR365 Antagomir for Post-Traumatic Osteoarthritis Therapy via Oral Route. *Theranostics* **2020**, *10*, 8479–8493. <https://doi.org/10.7150/thno.46761>.
- (72) Rotrekl, D.; Devriendt, B.; Cox, E.; Kavanová, L.; Faldyna, M.; Šalamúnová, P.; Baďo, Z.; Prokopec, V.; Štěpánek, F.; Hanuš, J.; Hošek, J. Glucan Particles as Suitable Carriers for the Natural Anti-Inflammatory Compounds Curcumin and Dipsacone – Evaluation in an *ex vivo* Model. *Int. J. Pharm.* **2020**, *582*, 119318. <https://doi.org/10.1016/j.ijpharm.2020.119318>.
- (73) Sun, Y.; Duan, B.; Chen, H.; Xu, X. A Novel Strategy for Treating Inflammatory Bowel Disease by Targeting Delivery of Methotrexate Through Glucan Particles. *Adv. Healthc. Mater.* **2020**, *9*, e1901805. <https://doi.org/10.1002/adhm.201901805>.
- (74) Soto, E.; Kim, Y. S.; Lee, J.; Kornfeld, H.; Ostroff, G. Glucan Particle Encapsulated Rifampicin for Targeted Delivery to Macrophages. *Polymers (Basel)*. **2010**, *2*, 681–689. <https://doi.org/10.3390/polym2040681>.
- (75) James, S.; Ostroff, G. R.; Easson, D. Glucan Drug Delivery System and Adjuvant. 5,741,497, 1998.
- (76) Ostroff, G. R.; Easson, D. D.; Jamas, S. A New β -Glucan-Based Macrophage-Targeted Adjuvant. In *Polymeric drugs and drug delivery systems*; Dunn, R. L., Ottenbrite, R. M., Eds.; Washington, DC, 1991; pp 52–59.
- (77) Ren, T.; Gou, J.; Sun, W.; Tao, X.; Tan, X.; Wang, P.; Zhang, Y.; He, H.; Yin, T.; Tang, X. Entrapping of Nanoparticles in Yeast Cell Wall Microparticles for Macrophage-Targeted Oral Delivery of Cabazitaxel. *Mol. Pharm.* **2018**, *15*, 2870–2882. <https://doi.org/10.1021/acs.molpharmaceut.8b00357>.
- (78) Li, X.; Zhao, Z.; Yang, Y.; Liu, Z.; Wang, J.; Xu, Y.; Zhang, Y. Novel β -1,3-D-Glucan Porous Microcapsule Enveloped Folate-Functionalized Liposomes as a Trojan Horse for Facilitated Oral Tumor-Targeted Co-Delivery of Chemotherapeutic Drugs and Quantum Dots. *J. Mater. Chem. B* **2020**, *8*, 2307–2320. <https://doi.org/10.1039/c9tb02674f>.
- (79) Zhou, X.; Zhang, X.; Han, S.; Dou, Y.; Liu, M.; Zhang, L.; Guo, J.; Shi, Q.; Gong, G.; Wang, R.; Hu, J.; Li, X.; Zhang, J. Yeast Microcapsule-Mediated Targeted Delivery of Diverse Nanoparticles for Imaging and Therapy via the Oral Route. *Nano Lett.* **2017**, *17*, 1056–1064. <https://doi.org/10.1021/acs.nanolett.6b04523>.
- (80) De Jesus, M.; Ostroff, G. R.; Levitz, S. M.; Bartling, T. R.; Mantis, N. J. A Population of Langerin-Positive Dendritic Cells in Murine Peyer's Patches Involved in Sampling β -Glucan Microparticles. *PLoS One* **2014**, *9*, e91002. <https://doi.org/10.1371/journal.pone.0091002>.
- (81) Jamas, S.; Easson, D. D.; Ostroff, G. R. Method for Immune System Activation by Administration of a β (1,3) Glucan Which Is Produced by *Saccharomyces cerevisiae* Strain R4. 5,504,079, 1996.
- (82) Soto, E. R.; Kim, H. C.; Yagita, H.; De Jesus, M.; Ostroff, G. R. Polydopamine Coating of Glucan Particles Increases Uptake into Peyer's Patches. *ACS Appl. Bio Mater.* **2019**, *2*, 3748–3754.

- <https://doi.org/10.1021/acsabm.9b00379>.
- (83) Hong, F.; Yan, J.; Baran, J. T.; Allendorf, D. J.; Hansen, R. D.; Ostroff, G. R.; Xing, P. X.; Cheung, N.-K. V.; Ross, G. D. Mechanism by Which Orally Administered β -1,3-Glucans Enhance the Tumoricidal Activity of Antitumor Monoclonal Antibodies in Murine Tumor Models. *J. Immunol.* **2004**, *173*, 797–806. <https://doi.org/10.4049/jimmunol.173.2.797>.
- (84) Legentil, L.; Paris, F.; Ballet, C.; Trouvelot, S.; Daire, X.; Vetvicka, V.; Ferrières, V. Molecular Interactions of β -(1 \rightarrow 3)-Glucans With Their Receptors. *Molecules* **2015**, *20*, 9745–9766. <https://doi.org/10.3390/molecules20069745>.
- (85) Aouadi, M.; Tesz, G. J.; Nicoloso, S. M.; Wang, M.; Chouinard, M.; Soto, E.; Ostroff, G. R.; Czech, M. P. Orally Delivered siRNA Targeting Macrophage Map4k4 Suppresses Systemic Inflammation. *Nature* **2009**, *458*, 1180–1184. <https://doi.org/10.1038/nature07774>.
- (86) Huang, H.; Ostroff, G. R.; Lee, C. K.; Specht, C. A.; Levitz, S. M. Robust Stimulation of Humoral and Cellular Immune Responses Following Vaccination with Antigen-Loaded β -Glucan Particles. *MBio* **2010**, *1*, 1–7. <https://doi.org/10.1128/mBio.00164-10>.
- (87) Garello, F.; Arena, F.; Cutrin, J. C.; Esposito, G.; D'Angeli, L.; Cesano, F.; Filippi, M.; Figueiredo, S.; Terreno, E. Glucan Particles Loaded with a NIRF Agent for Imaging Monocytes/Macrophages Recruitment in a Mouse Model of Rheumatoid Arthritis. *RSC Adv.* **2015**, *5*, 34078–34087. <https://doi.org/10.1039/c5ra00720h>.
- (88) Yang, Z.; Sun, A.; Zhao, X.; Song, M.; Wei, J.; Wang, J.; Zhao, T.; Xie, Y.; Chen, Z.; Tian, Z.; Liu, H.; Huang, Z.; Song, X.; Feng, Z. Preparation and Application of a Beta-D-Glucan Microsphere Conjugated Protein A/G. *Int. J. Biol. Macromol.* **2020**, *151*, 878–884. <https://doi.org/10.1016/j.ijbiomac.2020.02.165>.
- (89) Chen, Z.; Klein, T.; Murray, R. Z.; Crawford, R.; Chang, J.; Wu, C.; Xiao, Y. Osteoimmunomodulation for the Development of Advanced Bone Biomaterials. *Mater. Today* **2016**, *19*, 304–321. <https://doi.org/10.1016/j.mattod.2015.11.004>.
- (90) Shi, Y.; Wang, L.; Niu, Y.; Yu, N.; Xing, P.; Dong, L.; Wang, C. Fungal Component Coating Enhances Titanium Implant-Bone Integration. *Adv. Funct. Mater.* **2018**, *28*, 1804483. <https://doi.org/10.1002/adfm.201804483>.
- (91) Liang, H.; Jin, C.; Ma, L.; Feng, X.; Deng, X.; Wu, S.; Liu, X.; Yang, C. Accelerated Bone Regeneration by Gold-Nanoparticle-Loaded Mesoporous Silica Through Stimulating Immunomodulation. *ACS Appl. Mater. Interfaces* **2019**, *11*, 41758–41769. <https://doi.org/10.1021/acsami.9b16848>.
- (92) Han, B.; Baruah, K.; Cox, E.; Vanrompay, D.; Bossier, P. Structure-Functional Activity Relationship of β -Glucans From the Perspective of Immunomodulation: A Mini-Review. *Front. Immunol.* **2020**, *11*, 658. <https://doi.org/10.3389/fimmu.2020.00658>.
- (93) Ataoğlu, S.; Ankaralı, H.; Ankaralı, S.; Ataoğlu, B. B.; Ölmez, S. B. Quality of Life in Fibromyalgia, Osteoarthritis and Rheumatoid Arthritis Patients: Comparison of Different Scales. *Egypt. Rheumatol.* **2018**, *40*, 203–208. <https://doi.org/10.1016/j.ejr.2017.09.007>.
- (94) Bauerová, K.; Paulovičová, E.; Mihalová, D.; Švík, K.; Poništ, S. Study of New Ways of Supplementary and Combinatory Therapy of Rheumatoid Arthritis with Immunomodulators. Glucomannan and Imunoglukan® in Adjuvant Arthritis. *Toxicol. Ind. Health* **2009**, *25*, 329–335. <https://doi.org/10.1177/0748233709102945>.
- (95) Rovenský, J.; Stančíková, M.; Švík, K.; Bauerová, K.; Jurčovičová, J. The Effects of β -Glucan Isolated from *Pleurotus ostreatus* on Methotrexate Treatment in Rats with Adjuvant Arthritis. *Rheumatol. Int.* **2011**, *31*, 507–511. <https://doi.org/10.1007/s00296-009-1258-z>.
- (96) Breivik, T.; Opstad, P. K.; Engstad, R.; Gundersen, G.; Gjermo, P.; Preus, H. Soluble β -1,3/1,6-Glucan From Yeast Inhibits Experimental Periodontal Disease in Wistar Rats. *J. Clin. Periodontol.* **2005**, *32*,

- 347–352. <https://doi.org/10.1111/j.1600-051X.2005.00672.x>.
- (97) Silva, V. D. O.; Lobato, R. V.; Andrade, E. F.; Macedo, C. G. de; Napimoga, J. T. C.; Napimoga, M. H.; Messoria, M. R.; Murata, R. M.; Pereira, L. J. β -Glucans (*Saccharomyces cerevisiae*) Reduce Glucose Levels and Attenuate Alveolar Bone Loss in Diabetic Rats with Periodontal Disease. *PLoS One* **2015**, *10*, e0134742. <https://doi.org/10.1371/journal.pone.0134742>.
- (98) Silva, V. D. O.; Lobato, R. V.; Andrade, E. F.; Orlando, D. R.; Borges, B. D. B.; Zangeronimo, M. Z.; Sousa, R. V. de; Pereira, L. J. Effects of β -Glucans Ingestion on Alveolar Bone Loss, Intestinal Morphology, Systemic Inflammatory Profile, and Pancreatic β -Cell Function in Rats with Periodontitis and Diabetes. *Nutrients* **2017**, *9*, 1016. <https://doi.org/10.3390/nu9091016>.
- (99) Duygulu, F.; Yakan, B.; Karaoglu, S.; Kutlubay, R.; Karahan, O. I.; Ozturk, A. The Effect of Zymosan and the Protective Effect of Various Antioxidants on Fracture Healing in Rats. *Arch. Orthop. Trauma Surg.* **2007**, *127*, 493–501. <https://doi.org/10.1007/s00402-007-0395-7>.
- (100) Ferreira, S. S.; Passos, C. P.; Madureira, P.; Vilanova, M.; Coimbra, M. A. Structure-Function Relationships of Immunostimulatory Polysaccharides: A Review. *Carbohydr. Polym.* **2015**, *132*, 378–396. <https://doi.org/10.1016/j.carbpol.2015.05.079>.
- (101) Barsanti, L.; Passarelli, V.; Evangelista, V.; Frassanito, A. M.; Gualtieri, P. Chemistry, Physico-Chemistry and Applications Linked to Biological Activities of β -Glucans. *Nat. Prod. Rep.* **2011**, *28*, 457–466. <https://doi.org/10.1039/c0np00018c>.
- (102) Lei, N.; Wang, M.; Zhang, L.; Xiao, S.; Fei, C. Z.; Wang, X.; Zhang, K.; Zheng, W.; Wang, C.; Yang, R.; Xue, F. Effects of Low Molecular Weight Yeast β -Glucan on Antioxidant and Immunological Activities in Mice. *Int. J. Mol. Sci.* **2015**, *16*, 21575–21590. <https://doi.org/10.3390/ijms160921575>.
- (103) Meng, X.; Liang, H.; Luo, L. Antitumor Polysaccharides From Mushrooms: A Review on the Structural Characteristics, Antitumor Mechanisms and Immunomodulating Activities. *Carbohydr. Res.* **2016**, *424*, 30–41. <https://doi.org/10.1016/j.carres.2016.02.008>.
- (104) Huang, W.; Deng, H.; Jin, S.; Yang, W.; Wang, H.; Meng, C.; Wang, H.; Yang, S. A Polysaccharide from Dried Aerial Parts of *Agrimonia pilosa*: Structural Characterization and Its Potential Therapeutic Activity for Steroid-Induced Necrosis of the Femoral Head (SANFH). *Carbohydr. Polym.* **2019**, *214*, 71–79. <https://doi.org/10.1016/j.carbpol.2019.03.004>.
- (105) Huang, W.; Jin, S.; Yang, W.; Tian, S.; Meng, C.; Deng, H.; Wang, H. Protective Effect of *Agrimonia pilosa* Polysaccharides on Dexamethasone-Treated MC3T3-E1 Cells via Wnt/ β -Catenin Pathway. *J. Cell. Mol. Med.* **2020**, *24*, 2169–2177. <https://doi.org/10.1111/jcmm.14868>.
- (106) Cui, D.; Zhao, D.; Huang, S. Structural Characterization of a Safflower Polysaccharide and Its Promotion Effect on Steroid-Induced Osteonecrosis *in vivo*. *Carbohydr. Polym.* **2020**, *233*, 115856. <https://doi.org/10.1016/j.carbpol.2020.115856>.
- (107) Yodthong, T.; Kedjarune-Leggat, U.; Smythe, C.; Sukprasirt, P.; Aroonkesorn, A.; Wititsuwannakul, R.; Pitakpornpreecha, T. Enhancing Activity of *Pleurotus sajor-caju* (Fr.) Sing β -1,3-Glucan oligosaccharide (Ps-GOS) on Proliferation, Differentiation, and Mineralization of MC3T3-E1 Cells Through the Involvement of BMP-2/Runx2/MAPK/Wnt/ β -Catenin Signaling Pathway. *Biomolecules* **2020**, *10*, 190. <https://doi.org/10.3390/biom10020190>.
- (108) Yamasaki, T.; Ariyoshi, W.; Okinaga, T.; Adachi, Y.; Hosokawa, R.; Mochizuki, S.; Sakurai, K.; Nishihara, T. The Dectin 1 Agonist Curdlan Regulates Osteoclastogenesis by Inhibiting Nuclear Factor of Activated T Cells Cytoplasmic 1 (NFATc1) Through Syk Kinase. *J. Biol. Chem.* **2014**, *289*, 19191–19203. <https://doi.org/10.1074/jbc.M114.551416>.
- (109) Souza, P. P. C.; Lerner, U. H. Finding a Toll on TheRroute: The Fate of Osteoclast Progenitors After Toll-like Receptor Activation. *Front. Immunol.* **2019**, *10*, 1663. <https://doi.org/10.3389/fimmu.2019.01663>.

- (110) Aizawa, M.; Watanabe, K.; Tominari, T.; Matsumoto, C.; Hirata, M.; Grundler, F. M. W.; Inada, M.; Miyaura, C. Low Molecular-Weight Curdlan, (1→3)- β -Glucan Suppresses TLR2-Induced RANKL-Dependent Bone Resorption. *Biol. Pharm. Bull.* **2018**, *41*, 1282–1285. <https://doi.org/10.1248/bpb.b18-00057>.
- (111) Przekora, A.; Ginalska, G. Addition of 1,3- β -D-Glucan to Chitosan-Based Composites Enhances Osteoblast Adhesion, Growth, and Proliferation. *Int. J. Biol. Macromol.* **2014**, *70*, 474–481. <https://doi.org/10.1016/j.ijbiomac.2014.07.035>.
- (112) Przekora, A.; Palka, K.; Ginalska, G. Biomedical Potential of Chitosan/HA and Chitosan/ β -1,3-Glucan/HA Biomaterials as Scaffolds for Bone Regeneration - A Comparative Study. *Mater. Sci. Eng. C* **2016**, *58*, 891–899. <https://doi.org/10.1016/j.msec.2015.09.046>.
- (113) Przekora, A.; Ginalska, G. Chitosan/ β -1,3-Glucan/Hydroxyapatite Bone Scaffold Enhances Osteogenic Differentiation Through TNF- α -Mediated Mechanism. *Mater. Sci. Eng. C* **2017**, *73*, 225–233. <https://doi.org/10.1016/j.msec.2016.12.081>.
- (114) Przekora, A.; Benko, A.; Blazewicz, M.; Ginalska, G. Hybrid Chitosan/ β -1,3-Glucan Matrix of Bone Scaffold Enhances Osteoblast Adhesion, Spreading and Proliferation Via Promotion of Serum Protein Adsorption. *Biomed. Mater.* **2016**, *11*, 045001. <https://doi.org/10.1088/1748-6041/11/4/045001>.
- (115) Lee, D. H.; Han, D. W.; Park, B. J.; Baek, H. S.; Takatori, K.; Aihara, M.; Tsubaki, K.; Park, J. C. The Influences of β -Glucan Associated with BMP-7 on MC3T3-E1 Proliferation and Osteogenic Differentiation. *Key Eng. Mater.* **2005**, *288–289*, 241–244. <https://doi.org/10.4028/www.scientific.net/kem.288-289.241>.
- (116) Jang, J. H.; Lee, J.; Kim, J. H.; Lee, Y. H.; Ju, Y. C.; Lee, J. S. Isolation and Identification of RANKL-Induced Osteoclast Differentiation Inhibitor From *Pleurotus citrinopileatus*. *Mycoscience* **2013**, *54*, 265–270. <https://doi.org/10.1016/j.myc.2012.08.009>.
- (117) Xu, H.-L.; Dai, J.-H.; Hu, T.; Liao, Y.-F. Lentinan Up-Regulates MicroRNA-340 to Promote Apoptosis and Autophagy of Human Osteosarcoma Cells. *Int. J. Clin. Exp. Pathol.* **2018**, *11*, 3876–3883.
- (118) Patel, D. K.; Seo, Y. R.; Dutta, S. D.; Lee, O. H.; Lim, K. T. Influence of Maitake (*Grifola frondosa*) Particle Sizes on Human Mesenchymal Stem Cells and *in vivo* Evaluation of Their Therapeutic Potential. *Biomed Res. Int.* **2020**, *2020*, 8193971. <https://doi.org/10.1155/2020/8193971>.
- (119) Rujanant, S.; Lee, W. K.; Kongruang, S. Promotion of Osteoblast Proliferation Activated by Betaglucan (BG) Derived from Yeast Sludge. *Key Eng. Mater.* **2019**, *824*, 8–15. <https://doi.org/10.4028/www.scientific.net/KEM.824.8>.
- (120) Sorgente, N.; Guenther, H. L.; Guenther, H. E.; Bahl, A. K. Use of Beta Glucans for the Treatment of Osteoporosis and Other Diseases of Bone Resorption. US7018986B2, 2006.
- (121) Meng, Y.; Lyu, F.; Xu, X.; Zhang, L. Recent Advances in Chain Conformation and Bioactivities of Triple-Helix Polysaccharides. *Biomacromolecules* **2020**, *21*, 1653–1677. <https://doi.org/10.1021/acs.biomac.9b01644>.
- (122) Guo, M. Q.; Hu, X.; Wang, C.; Ai, L. Polysaccharides: Structure and Solubility. In *Solubility of Polysaccharides*; IntechOpen, London, 2017; pp 7–21. <https://doi.org/10.5772/intechopen.71570>.
- (123) Ohno, N.; Miura, N. N.; Chiba, N.; Adachi, Y.; Yadomae, T. Comparison of the Immunopharmacological Activities of Triple and Single-Helical Schizophyllan in Mice. *Chem. Pharm. Bull.* **1995**, *18*, 1242–1247.
- (124) Zhang, R.; Edgar, K. J. Properties, Chemistry, and Applications of the Bioactive Polysaccharide Curdlan. *Biomacromolecules* **2014**, *15*, 1079–1096. <https://doi.org/10.1021/bm500038g>.
- (125) Bzducha-Wróbel, A.; Błazejak, S.; Kawarska, A.; Stasiak-Różańska, L.; Gientka, I.; Majewska, E. Evaluation of the Efficiency of Different Disruption Methods on Yeast Cell Wall Preparation for β -Glucan Isolation. *Molecules* **2014**, *19*, 20941–20961. <https://doi.org/10.3390/molecules191220941>.

- (126) Cui, S.; Brummer, Y. Understanding Carbohydrate Analysis. In *Food Carbohydrates*; Cui, S. W., Ed.; 2005. <https://doi.org/10.1201/9780203485286.ch2>.
- (127) Tester, R. F.; Karkalas, J. Carbohydrates | Classification and Properties. *Encyclopedia of Food Sciences and Nutrition*; Caballero, B., Finglas, P., Toldra, F., Eds.; 2003; pp 862–875. <https://doi.org/10.1016/b0-12-227055-x/00166-8>.
- (128) Soria, A. C.; Rodríguez-Sánchez, S.; Sanz, J.; Martínez-Castro, I. Gas Chromatographic Analysis of Food Bioactive Oligosaccharides. In *Food Oligosaccharides: Production, Analysis and Bioactivity*; Moreno, F. J., Sanz, M. L., Eds.; 2014; pp 370–398. <https://doi.org/10.1002/9781118817360.ch20>.
- (129) Ciucanu, I. Per-O-Methylation Reaction for Structural Analysis of Carbohydrates by Mass Spectrometry. *Anal. Chim. Acta* **2006**, *576*, 147–155. <https://doi.org/10.1016/j.aca.2006.06.009>.
- (130) Cui, S. Structural Analysis of Polysaccharides. In *Food Carbohydrates*; Cui, S. W., Ed.; 2005. <https://doi.org/10.1201/9780203485286.ch3>.
- (131) Pettolino, F. A.; Walsh, C.; Fincher, G. B.; Bacic, A. Determining the Polysaccharide Composition of Plant Cell Walls. *Nat. Protoc.* **2012**, *7*, 1590–1607. <https://doi.org/10.1038/nprot.2012.081>.
- (132) Monteiro, M. V.; Gaspar, V. M.; Ferreira, L. P.; Mano, J. F. Hydrogel 3D: *In vitro* Tumor Models for Screening Cell Aggregation Mediated Drug Response. *Biomater. Sci.* **2020**, *8*, 1855–1864. <https://doi.org/10.1039/c9bm02075f>.
- (133) Aslantürk, Ö. S. *In vitro* Cytotoxicity and Cell Viability Assays: Principles, Advantages, and Disadvantages. In *Genotoxicity - A Predictable Risk to Our Actual World*; Larramendy, M. L., Soloneski, S., Eds.; 2017; p 13.
- (134) Mukherjee, M.; Nandi, A.; Chandra, K.; Saikia, S. K.; Jana, C. K.; Das, N. Protein Extraction from *Saccharomyces cerevisiae* at Different Growth Phases. *J. Microbiol. Methods* **2020**, *172*, 105906. <https://doi.org/10.1016/j.mimet.2020.105906>.
- (135) Corbacho, I.; Olivero, I.; Hernández, L. M. A Genome-Wide Screen for *Saccharomyces cerevisiae* Nonessential Genes Involved in Mannosyl Phosphate Transfer to Mannoprotein-Linked Oligosaccharides. *Fungal Genet. Biol.* **2005**, *42*, 773–790. <https://doi.org/10.1016/j.fgb.2005.05.002>.
- (136) Marson, G. V.; de Castro, R. J. S.; Belleville, M. P.; Hubinger, M. D. Spent Brewer's Yeast as a Source of High Added Value Molecules: A Systematic Review on Its Characteristics, Processing and Potential Applications. *World J. Microbiol. Biotechnol.* **2020**, *36*, 1–22. <https://doi.org/10.1007/s11274-020-02866-7>.
- (137) Fountoulakis, M.; Lahm, H.-W. Hydrolysis and Amino Acid Composition Analysis of Proteins. *J. Chromatogr. A* **1998**, *826*, 109–134. <https://doi.org/10.1007/s10096-017-3055-z>.
- (138) Mustăţea, G.; Ungureanu, E. L.; Iorga, E. Protein Acidic Hydrolysis for Amino Acids Analysis in Food - Progress over Time: A Short Review. *J. Hyg. Eng. Des.* **2019**, *26*, 81–87.
- (139) Joseph, E.; Singhvi, G. Multifunctional Nanocrystals for Cancer Therapy: A Potential Nanocarrier. In *Nanomaterials for Drug Delivery and Therapy*; Grumezescu, A. M., Ed.; 2019; pp 91–116. <https://doi.org/10.1016/B978-0-12-816505-8.00007-2>.
- (140) Tsai, Y. T.; Chang, C. W.; Yeh, Y. C. Formation of Highly Elastomeric and Property-Tailorable Poly(Glycerol Sebacate)-Co -Poly(Ethylene Glycol) Hydrogels through Thiol-Norbornene Photochemistry. *Biomater. Sci.* **2020**, *8*, 4728–4738. <https://doi.org/10.1039/d0bm00632g>.
- (141) Sabu, C.; Raghav, D.; Jijith, U. S.; Mufeedha, P.; Naseef, P. P.; Rathinasamy, K.; Pramod, K. Bioinspired Oral Insulin Delivery System Using Yeast Microcapsules. *Mater. Sci. Eng. C* **2019**, *103*, 109753. <https://doi.org/10.1016/j.msec.2019.109753>.
- (142) Cavagna, M.; Dell'Anna, R.; Monti, F.; Rossi, F.; Torriani, S. Use of ATR-FTIR Microspectroscopy to

- Monitor Autolysis of *Saccharomyces cerevisiae* Cells in a Base Wine. *J. Agric. Food Chem.* **2010**, *58*, 39–45. <https://doi.org/10.1021/jf902369s>.
- (143) Burattini, E.; Cavagna, M.; Dell’Anna, R.; Malvezzi Campeggi, F.; Monti, F.; Rossi, F.; Torriani, S. A FTIR Microspectroscopy Study of Autolysis in Cells of the Wine Yeast *Saccharomyces cerevisiae*. *Vib. Spectrosc.* **2008**, *47*, 139–147. <https://doi.org/10.1016/j.vibspec.2008.04.007>.
- (144) Shi, G.; Rao, L.; Xie, Q.; Li, J.; Li, B.; Xiong, X. Characterization of Yeast Cells as a Microencapsulation Wall Material by Fourier-Transform Infrared Spectroscopy. *Vib. Spectrosc.* **2010**, *53*, 289–295. <https://doi.org/10.1016/j.vibspec.2010.04.007>.
- (145) Ishii, K.; Yoshihashi, S. S.; Chihara, K.; Awazu, K. FT-IR Analysis of Phosphorylated Protein. *Biophotonics New Front. From Genome to Proteome* **2004**, *5461*, 17–21. <https://doi.org/10.1117/12.541092>.
- (146) Galichet, A.; Sockalingum, G. D.; Belarbi, A.; Manfait, M. FTIR Spectroscopic Analysis of *Saccharomyces cerevisiae* Cell Walls: Study of an Anomalous Strain Exhibiting a Pink-Colored Cell Phenotype. *FEMS Microbiol. Lett.* **2001**, *197*, 179–186. [https://doi.org/10.1016/S0378-1097\(01\)00101-X](https://doi.org/10.1016/S0378-1097(01)00101-X).
- (147) Fein, K.; Bousfield, D. W.; Gramlich, W. M. The Influence of Versatile Thiol-Norbornene Modifications to Cellulose Nanofibers on Rheology and Film Properties. *Carbohydr. Polym.* **2020**, *230*, 115672. <https://doi.org/10.1016/j.carbpol.2019.115672>.
- (148) Stuart, B. H. *Infrared Spectroscopy: Fundamentals and Applications*; 2005. <https://doi.org/10.1002/0470011149>.
- (149) Agibayeva, L. E.; Kaldybekov, D. B.; Porfiryeva, N. N.; Garipova, V. R.; Mangazbayeva, R. A.; Moustafine, R. I.; Semina, I. I.; Mun, G. A.; Kudaibergenov, S. E.; Khutoryanskiy, V. V. Gellan Gum and Its Methacrylated Derivatives as *in situ* Gelling Mucoadhesive Formulations of Pilocarpine: *In vitro* and *in vivo* Studies. *Int. J. Pharm.* **2020**, *577*, 119093. <https://doi.org/10.1016/j.ijpharm.2020.119093>.
- (150) Liu, C. F.; Sun, R. C.; Zhang, A. P.; Ren, J. L. Preparation of Sugarcane Bagasse Cellulosic Phthalate Using an Ionic Liquid as Reaction Medium. *Carbohydr. Polym.* **2007**, *68*, 17–25. <https://doi.org/10.1016/j.carbpol.2006.07.002>.
- (151) McOscar, T. V. C.; Gramlich, W. M. Hydrogels from Norbornene-Functionalized Carboxymethyl Cellulose Using a UV-Initiated Thiol-Ene Click Reaction. *Cellulose* **2018**, *25*, 6531–6545. <https://doi.org/10.1007/s10570-018-2015-9>.
- (152) Mertz, G.; Fouquet, T.; Becker, C.; Ziarelli, F.; Ruch, D. A Methacrylic Anhydride Difunctional Precursor to Produce a Hydrolysis-Sensitive Coating by Aerosol-Assisted Atmospheric Plasma Process. *Plasma Process. Polym.* **2014**, *11* (8), 728–733. <https://doi.org/10.1002/ppap.201400050>.
- (153) Shie, M.-Y.; Lee, J.-J.; Ho, C.-C.; Yen, S.-Y.; Ng, H. Y.; Chen, Y.-W. Effects of Gelatin Methacrylate Bio-Ink Concentration on Mechano-Physical Properties and Human Dermal. *Polymers (Basel)*. **2020**, *12*, 1930.
- (154) Nichol, J. W.; Koshy, S. T.; Bae, H.; Hwang, C. M.; Yamanlar, S. Cell-Laden Microengineered Gelatin Methacrylate Hydrogels Biomaterials Cell-Laden Microengineered Gelatin Methacrylate Hydrogels. *Biomaterials* **2010**, *31* (11), 5536–5544. <https://doi.org/10.1016/j.biomaterials.2010.03.064>.
- (155) Maharjan, B.; Kumar, D.; Prasad, G.; Prasad, D.; Yeon, J.; Hee, C.; Sang, C. Synthesis and Characterization of Gold/Silica Hybrid Nanoparticles Incorporated Gelatin Methacrylate Conductive Hydrogels for H9C2 Cardiac Cell Compatibility Study. *Compos. Part B* **2019**, *177*, 107415. <https://doi.org/10.1016/j.compositesb.2019.107415>.
- (156) Domingues, R. M. A.; Silva, M.; Gershovich, P.; Betta, S.; Babo, P.; Motta, A.; Reis, R. L.; Gomes, M. E. Development of Injectable Hyaluronic Acid/Cellulose Nanocrystals Bionanocomposite Hydrogels for Tissue Engineering Applications. *Bioconjug. Chem.* **2015**, *26*, 1571–1581.

- <https://doi.org/10.1021/acs.bioconjchem.5b00209>.
- (157) Wang, Y.; Ma, M.; Wang, J.; Zhang, W.; Lu, W.; Gao, Y.; Zhang, B.; Guo, Y. Development of a Photo-Crosslinking, Biodegradable GelMA/PEGDA Hydrogel for Guided Bone Regeneration Materials. *Materials (Basel)*. **2018**, *11*, 1345. <https://doi.org/10.3390/ma11081345>.
- (158) Costa, A. M. S.; Mano, J. F. Highly Robust Hydrogels Via a Fast, Simple and Cytocompatible Dual Crosslinking-Based Process. *Chem. Commun.* **2015**, *51*, 15673–15676. <https://doi.org/10.1039/c5cc05564d>.
- (159) Kurzepa, J.; Baran, M.; Watroba, S.; Baruh, M.; Babula, D. Collagenases and Gelatinases in Bone Healing. The Focus on Mandibular Fractures. *Curr. Issues Pharm. Med. Sci.* **2014**, *27*, 121–126.
- (160) Paiva, K. B. S.; Granjeiro, J. M. Matrix Metalloproteinases in Bone Resorption, Remodeling, and Repair. In *Progress in Molecular Biology and Translational Science*; Khalil, R. A., Ed.; 2017; Vol. 148, pp 203–303. <https://doi.org/10.1016/bs.pmbts.2017.05.001>.
- (161) Athirasala, A.; Lins, F.; Tahayeri, A.; Hinds, M.; Smith, A. J.; Sedgley, C.; Ferracane, J.; Bertassoni, L. E. A Novel Strategy to Engineer Pre-Vascularized Full-Length Dental Pulp-like Tissue Constructs. *Sci. Rep.* **2017**, *7*, 3323. <https://doi.org/10.1038/s41598-017-02532-3>.
- (162) Zuo, Y.; Liu, X.; Wei, D.; Sun, J.; Xiao, W.; Zhao, H.; Guo, L.; Wei, Q.; Fan, H.; Zhang, X. Photo-Cross-Linkable Methacrylated Gelatin and Hydroxyapatite Hybrid Hydrogel for Modularly Engineering Biomimetic Osteon. *ACS Appl. Mater. Interfaces* **2015**, *7*, 10386–10394. <https://doi.org/10.1021/acsami.5b01433>.
- (163) Irawan, V.; Higuchi, A.; Ikoma, T. Physical Cues of Biomaterials Guide Stem Cell Fate of Differentiation: The Effect of Elasticity of Cell Culture Biomaterials. *Open Phys.* **2018**, *16*, 943–955. <https://doi.org/10.1515/phys-2018-0116>.
- (164) Polacheck, W. J.; Chen, C. S. Measuring Cell-Generated Forces: A Guide to the Available Tools. *Nat. Methods* **2016**, *13*, 415–423. <https://doi.org/10.1038/nmeth.3834>.
- (165) Khetan, S.; Guvendiren, M.; Legant, W. R.; Cohen, D. M.; Chen, C. S.; Burdick, J. A. Degradation-Mediated Cellular Traction Directs Stem Cell Fate in Covalently Crosslinked Three-Dimensional Hydrogels. *Nat. Mater.* **2013**, *12*, 458–465. <https://doi.org/10.1038/nmat3586>.
- (166) ISO 10993-5:2009 - Biological Evaluation of Medical Devices — Part 5: Tests for in Vitro Cytotoxicity.
- (167) Paramera, E. I.; Karathanos, V. T.; Konteles, S. J. Yeast Cells and Yeast-Based Materials for Microencapsulation. In *Microencapsulation in the Food Industry*; Gaonkar, A. G., Vasisht, N., Khare, A. R., Sobel, R., Eds.; 2014; pp 267–281. <https://doi.org/10.1016/b978-0-12-404568-2.00023-6>.
- (168) Dardelle, G.; Normand, V.; Steenhoudt, M.; Bouquerand, P. E.; Chevalier, M.; Baumgartner, P. Flavour-Encapsulation and Flavour-Release Performances of a Commercial Yeast-Based Delivery System. *Food Hydrocoll.* **2007**, *21*, 953–960. <https://doi.org/10.1016/j.foodhyd.2006.12.013>.
- (169) Bar-Peled, M.; Lewinsohn, E.; Fluhrig, R.; Gressell, J. UDP-Rhamnose:Flavanone-7-O-Glucoside-2''-O-Rhamnosyltransferase Purification and Characterization of an Enzyme Catalyzing the Production of Bitter Compounds in Citrus. *J. Biol. Chem.* **1991**, *266*, 20953–20959.
- (170) Chen, R.; Qi, Q. L.; Wang, M. T.; Li, Q. Y. Therapeutic Potential of Naringin: An Overview. *Pharm. Biol.* **2016**, *54*, 3203–3210. <https://doi.org/10.1080/13880209.2016.1216131>.
- (171) Ciamponi, F.; Duckham, C.; Tirelli, N. Yeast Cells as Microcapsules. Analytical Tools and Process Variables in the Encapsulation of Hydrophobes in *S. Cerevisiae*. *Appl. Microbiol. Biotechnol.* **2012**, *95*, 1445–1456. <https://doi.org/10.1007/s00253-012-4127-8>.
- (172) Nii, T.; Ishii, F. Encapsulation Efficiency of Water-Soluble and Insoluble Drugs in Liposomes Prepared by the Microencapsulation Vesicle Method. *Int. J. Pharm.* **2005**, *298*, 198–205.

- <https://doi.org/10.1016/j.ijpharm.2005.04.029>.
- (173) Deepak, V.; Kasonga, A.; Kruger, M. C.; Coetzee, M. Carvacrol Inhibits Osteoclastogenesis and Negatively Regulates the Survival of Mature Osteoclasts. *Biol. Pharm. Bull.* **2016**, *39*, 1150–1158. <https://doi.org/10.1248/bpb.b16-00117>.
- (174) Bhatia, S.; Mohr, A.; Mathur, D.; Parmar, V. S.; Haag, R.; Prasad, A. K. Biocatalytic Route to Sugar-PEG-Based Polymers for Drug Delivery Applications. *Biomacromolecules* **2011**, *12*, 3487–3498. <https://doi.org/10.1021/bm200647a>.
- (175) Steven, C. R.; Busby, G. A.; Mather, C.; Tariq, B.; Briuglia, M. L.; Lamprou, D. A.; Urquhart, A. J.; Grant, M. H.; Patwardhan, S. V. Bioinspired Silica as Drug Delivery Systems and Their Biocompatibility. *J. Mater. Chem. B* **2014**, *2*, 5028–5042. <https://doi.org/10.1039/c4tb00510d>.
- (176) Prasad, S.; Achazi, K.; Böttcher, C.; Haag, R.; Sharma, S. K. Fabrication of Nanostructures Through Self-Assembly of Non-Ionic Amphiphiles for Biomedical Applications. *RSC Adv.* **2017**, *7*, 22121–22132. <https://doi.org/10.1039/c6ra28654b>.
- (177) Zhang, H.; Xia, H.; Wang, J.; Li, Y. High Intensity Focused Ultrasound-Responsive Release Behavior of PLA-b-PEG Copolymer Micelles. *J. Control. Release* **2009**, *139*, 31–39. <https://doi.org/10.1016/j.jconrel.2009.05.037>.
- (178) Kurniasih, I. N.; Liang, H.; Kumar, S.; Mohr, A.; Sharma, S. K.; Rabe, J. P.; Haag, R. A Bifunctional Nanocarrier Based on Amphiphilic Hyperbranched Polyglycerol Derivatives. *J. Mater. Chem. B* **2013**, *1*, 3569–3577. <https://doi.org/10.1039/c3tb20366b>.
- (179) Ray, A.; Das, S.; Chattopadhyay, N. Aggregation of Nile Red in Water: Prevention through Encapsulation in β -Cyclodextrin. *ACS Omega* **2019**, *4*, 15–24. <https://doi.org/10.1021/acsomega.8b02503>.